REVIEW ARTICLE | JUNE 05 2024

Heterostructures enhance the absorption of lanthanides

Alasdair Tew ; Lars van Turnhout ; Yunzhou Deng ; Rakesh Arul ; Junzhi Ye ; Tianjun Liu ; Zhao Jiang ; Linjie Dai ; Huangtianzhi Zhu ; Yan Zhang ; Akshay Rao ; Zhongzheng Yu

Appl. Phys. Rev. 11, 021329 (2024)
https://doi.org/10.1063/5.0204199

Applied Physics Reviews REVIEW pubs.aip.org/aip/are

Heterostructures enhance the absorption of lanthanides

Cite as: Appl. Phys. Rev. **11**, 021329 (2024); doi: 10.1063/5.0204199
Submitted: 20 February 2024 · Accepted: 8 May 2024 ·
Published Online: 5 June 2024

Alasdair Tew,[1] Lars van Turnhout,[1] Yunzhou Deng,[1] Rakesh Arul,[1] Junzhi Ye,[1,2] Tianjun Liu,[1] Zhao Jiang,[1] Linjie Dai,[1] Huangtianzhi Zhu,[1] Yan Zhang,[3,a)] Akshay Rao,[1,a)] and Zhongzheng Yu[1,a)]

AFFILIATIONS

[1]Cavendish Laboratory, University of Cambridge, Cambridge CB3 0HE, United Kingdom
[2]Inorganic Chemistry Laboratory, University of Oxford, South Parks Road, Oxford OX1 3QR, United Kingdom
[3]College of Life Science and Technology, Huazhong University of Science and Technology, Wuhan 430074, China

[a)]**Authors to whom correspondence should be addressed:** yan_zhang@hust.edu.cn; ar525@cam.ac.uk; and yuzh0010@e.ntu.edu.sg

ABSTRACT

Lanthanide-doped nanoparticles (LnNPs) show unique optical properties and have been demonstrated in various applications, including imaging, optogenetics, photothermal therapy, photodynamic therapy, light-controlled release/cross-linking, anticounterfeiting, lasing, sensing, and super-resolution microscopy. One of the key and urgent limitations of LnNPs is the weak and narrow absorption of lanthanides. Fabrication of heterostructures will overcome this hurdle and enhance the performance of LnNPs. Developing novel heterostructures to enhance the absorption of lanthanides and studying the energy transfer pathways and efficiencies are of broad interest to the chemical and physical research community. There is currently no systematic review to summarize different types of LnNP heterostructures. Thus, this review will summarize five types of heterostructures combining LnNPs with organic and inorganic dyes, plasmonics, semiconducting quantum dots, and metal–organic frameworks. The enhancement of absorption and the improvement of light conversion performance are compared and discussed. This review also discusses the energy transfer pathways and efficiencies between LnNPs and other components and provides suggestions to form heterostructures with enhanced absorption and efficient energy transfer for future applications. We hope this review will further inspire active development and study of lanthanide-based heterostructures with stronger absorption, better light conversion performance, and ease of multifunctionality.

TABLE OF CONTENTS

I. INTRODUCTION

Lanthanides comprise 15 elements, ranging from lanthanum (La) to lutetium (Lu) with an increase in atomic number from 57 to 71 accompanied by the filling of the 4f electron shell. Inside lanthanide nanoparticles (LnNPs), the lanthanides almost exclusively exist as ions in the +3 oxidation state with a ground state electronic configuration [Xe] $4f^n$ with n = 0–14. The $4f^n$ electronic configurations of different lanthanide ions endow them with unique optical and magnetic properties. For optical properties, the f–f transitions lead to numerous energy levels from the ultraviolet (UV) to mid-infrared range.[1–3] However, these bands are narrow and comparatively weak as the f–f transitions are Laporte forbidden. The allowed 4f–5d transitions result in a broader and stronger absorption and emission in the UV region.[4] The 4f orbitals are well shielded by the 5s and 5p sub-shells and thus the absorption and emission of lanthanide ions are virtually unaffected by their environment.[5]

Owing to their unique electronic configuration and optical properties, inorganic LnNPs consisting of lanthanides doped into a host matrix show excellent chemical and photostability, no photobleaching or photoblinking, narrow and tunable emissions with large Stokes or anti-Stokes shifts, and long luminescence lifetimes. At the same time, LnNPs have low cytotoxicity and ease of multifunctionality.[6,7] In the recent decade, LnNPs have been demonstrated in bioimaging,[8,9] multiplexing,[10,11] diagnostics,[12] therapeutics,[13–15] optogenetics,[16,17] three-dimensional (3D) printing,[18] photo-controlled release,[19] single-particle spectroscopy,[20] anti-counterfeiting,[21] detection,[22] and lighting and lasing.[23,24]

The molar absorption coefficients of LnNPs are usually $<10\ M^{-1}\ cm^{-1}$, which is several orders of magnitude lower than for example organic dyes.[25] The fabrication of heterostructures will overcome the aforementioned limitation and enhance the performance of LnNPs.[26] Studying the underlying enhancement mechanism and corresponding energy transfer pathways and efficiencies is a research hot spot. Currently, there is no systematic review to summarize different types of lanthanide-based heterostructures.

In this review article, we will summarize five types of heterostructures for the absorption enhancement of LnNPs, including (i) organic dyes, (ii) inorganic dyes, (iii) plasmonics, (iv) semiconducting quantum dots (QDs), and (v) metal–organic frameworks (MOFs). The enhancement of absorption and the improvement of light conversion performance are compared and discussed. This review also discusses the energy transfer pathways and efficiencies between LnNPs and other components and provides suggestions to form heterostructures with enhanced absorption and efficient energy transfer with possible applications.

II. CLASSIFICATION OF LANTHANIDE-BASED HETEROSTRUCTURES

A. Organic dye-sensitized lanthanide nanoparticles

To overcome the innate low absorptivity of lanthanide ions, organic molecules can be employed as antennas. Organic molecules are exceptionally modifiable and so can be synthesized with properties designed for their intended applications. They are strongly absorbing, with absorption coefficients up to six orders of magnitude higher than lanthanides.[27] This makes them ideal for unlocking the potential of lanthanide emitters across a variety of fields, including optoelectronics,[28] biomedical,[29,30] and photocatalysis.[31]

For the energy absorbed by the organic to efficiently transfer to the lanthanide, they must be close in space and have strong energetic overlap. Förster resonance energy transfer (FRET) and Dexter energy transfer are two mechanisms of radiationless energy transfer. FRET occurs through dipolar coupling and Dexter involves the exchange of electrons between the two species. The rate of transfer is strongly dependent on the distance between donor and acceptor (d) for both mechanisms. The FRET rate is proportional to d^{-6} for dipole–dipole coupling; however, it can also occur through quadrupolar couplings that are proportional to d^{-8} (dipole–quadrupole) or d^{-10} (quadrupole–quadrupole) and can be important at distances under 2 nm.[5,32] Dexter energy transfer requires overlap of electron wavefunctions, resulting in a sharp, exponential distance dependence.[5]

Both FRET and Dexter can theoretically occur from either the singlet or triplet state of an organic molecule; however, FRET from a triplet state would require a forbidden electron spin flip and Dexter would not, so the latter is the favored mechanism for triplet energy transfer.[33] A schematic of a dye sensitization process is shown in Fig. 1(a) displaying both singlet energy transfer (SET) and triplet energy transfer (TET). Lanthanides have been shown to accelerate the intersystem crossing (ISC) rate in proximal organics through either spin–orbit coupling[34] or the interaction with unpaired 4f electrons, which can be exploited to maximize energy transfer efficiency.[35] A more detailed description of the energy transfer mechanism in these systems can be found in Sec. III A.

The ability of organic ligands, or chelates, to sensitize lanthanides has been studied since the 1940s.[38,39] LnNPs were first synthesized around the start of the 21st century,[40,41] and the first demonstration of ligand sensitization of LnNPs was in 2007 by Zhang *et al.*[42] The advantages LnNPs offer over traditional lanthanide chelate compounds are the tunable interaction of multiple lanthanides in a single particle and the protection from environmental deactivation offered by the host lattice. The specific lanthanide composition can be tuned to optimize properties including upconversion[43] or downconversion.[44,45] It was shown by Auzel in 1966 that the most efficient form of lanthanide upconversion, energy transfer upconversion (ETU), requires multiple different lanthanides in close proximity.[46] This process usually uses Yb^{3+}, with only one excited state energy level, as a lanthanide sensitizer to donate energy to a lanthanide acceptor with a more complex energy level structure that will then emit. Figure 1(a) shows a schematic of the ETU process, and Fig. 1(b) shows the different emission colors of various lanthanide acceptors: Er, Tm, and Ho. The host material of the nanoparticle protects most lanthanides from non-radiative relaxation due to overtones of C–H, O–H, and N–H vibrations of the solvents or ligands.[42] Another benefit of LnNPs is their increased refractive index that decreases the radiative lifetime of lanthanides and increases their photoluminescence quantum efficiency (PLQE).[47] LnNPs are solution processable and, therefore, are industrially scalable[48] and applicable in biological environments.

As mentioned, the first example of dye-sensitized LnNPs was shown in 2007 using a UV-absorbing tropolonate ligand previously

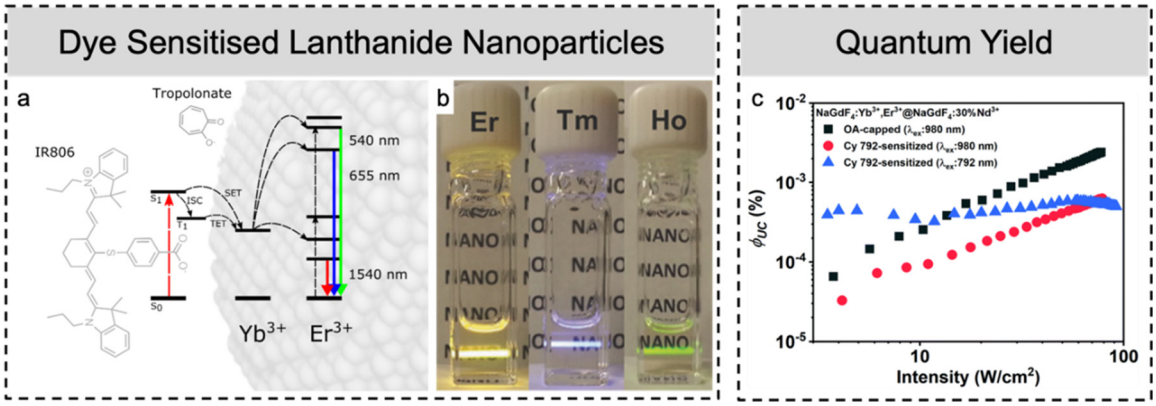

FIG. 1. (a) Schematic of energy transfer from either the singlet (SET) or the triplet level (TET) of dye to lanthanide that can then undergo energy transfer upconversion (ETU). (b) Images of various dye sensitized upconverting nanoparticles showing different emission colors. Reproduced with permission from Adv. Opt. Mater. **4**, 1760 (2016).[36] Copyright 2016 John Wiley & Sons. (c) Power dependence of upconversion quantum yield showing an increased quantum yield of dye sensitization at low (but not high) excitation power. Reproduced with permission from J. Mater. Chem. C **9**, 16313 (2021).[37] Copyright 2021 Royal Society of Chemistry.

used to sensitize lanthanide chelates.[42,49] The ligand was capable of transferring energy to Yb^{3+} and Nd^{3+}, despite the energy gap of 6600 cm^{-1} between the ligand triplet level and the Yb^{3+} $^2F_{5/2}$ excited state. The authors deemed this possible due to phonon assisted transfer or a Dexter mechanism. The lifetimes of the lanthanides in the nanoparticles were roughly five times longer than those in the respective molecular lanthanide tropolonate chelates, demonstrating the advantageous protection nanoparticles offer. Subsequently, the first near-infrared (NIR) organic sensitization of upconversion LnNPs was demonstrated in 2012 by Zou *et al.*, using a cyanine dye modified with a carboxylic acid to enable binding to lanthanides.[27] The dye itself (IR806) possesses an absorption coefficient 5×10^6 higher than that of Yb^{3+}, and it produced a 3300-fold enhancement of upconversion brightness calculated using the dye and lanthanide contributions in the upconversion excitation spectra. Since then, sensitization in the UV and visible part of the spectrum has reached unity efficiency with ligands such as FITC and CPPOA, although unity transfer efficiency from an organic dye has not yet been reported in the near infrared.

It is important to briefly touch on brightness enhancements and upconversion yields. First, brightness (B) is the product of molar absorption coefficient (ε) and quantum yield (ϕ):[50]

$$B = \varepsilon \times \phi. \tag{1}$$

Upon direct excitation of the LnNP, this becomes:

$$B_{Ln}^{Ln} = \varepsilon_{Ln} \times \phi_{Ln}^{Ln}, \tag{2}$$

in which the superscript indicates which species is being excited and the subscript indicates which is emitting. Upon excitation of an organic sensitizer, this equation transforms into

$$B_{Ln}^{L} = \varepsilon_{L} \times \phi_{ET} \times \phi_{Ln}^{Ln}, \tag{3}$$

in which the subscript "L" represents the ligand and ϕ_{ET} is the quantum efficiency of energy transfer from the ligand to the lanthanide. Therefore, the brightness enhancement is equal to the absorption ratio (of the whole nanoparticle construct) multiplied by the energy transfer efficiency from the ligand to the lanthanide, which is given as

$$\frac{B_{Ln}^{L}}{B_{Ln}^{Ln}} = \frac{\varepsilon_{L}}{\varepsilon_{Ln}} \times \phi_{ET}. \tag{4}$$

This neglects any changes to intrinsic lanthanide quantum yield upon ligand binding that may occur, for example, due to energy back transfer (EBT) to the ligand or passivation effects. By measuring the intrinsic lanthanide quantum yield after ligand association and using this value in the equation for B_{Ln}^{L}. The full form of ϕ_{ET} is

$$\phi_{ET} = \phi_{ET,singlet} + \phi_{ISC} \times \phi_{ET,triplet} = \frac{\phi_{Ln}^{L}}{\phi_{Ln}^{Ln}}. \tag{5}$$

Efficient transfer may occur from either the ligand singlet or triplet state; however, for triplet mediated transfer to predominate, there must also be efficient ISC.

The upconversion quantum yield (UCQY) is not linearly dependent on excitation power. As upconversion is a multi-photon process, the relationship is a power law of roughly the number of excitation photons required to produce a higher energy emitted photon. As the power increases, lower energy states involved in upconversion become saturated and, eventually, the quantum yield should reach a plateau.[51] It is possible for a particular lanthanide emission wavelength to decrease in QY with power due to the increased utilization of the energy level by higher order upconversion processes.[51] In reality, samples may degrade or even improve due to annealing at high powers.[52] Jones *et al.* cover the measurement procedure for determining reliable upconversion quantum yields in their review on the subject.[53]

Given this, dye antenna ligands have the effect of "boosting" the effective excitation power experienced by the lanthanide due to the higher absorption of the excitation light. This has the effect of horizontally shifting the power dependence graph so that the quantum yield of the sensitized system may be higher than the unsensitized particles at lower excitation powers. However, the saturated UCQY of a sensitized system should be less than (or equal to) the quantum yield when the lanthanide is directly excited, as the energy transfer efficiency cannot be more than 100% ($\phi_{Ln}^{L} = \phi_{ET} \times \phi_{Ln}^{Ln}$). This is untrue if the ligand also passivates the lanthanide, increasing its intrinsic quantum yield. Figure 1(c) shows the decreased intrinsic

quantum yield of sensitized nanoparticles at all powers (red circles), likely due to back transfer from the lanthanide to the ligand. However, the sensitized particles (blue triangles) show a higher quantum yield at low powers upon ligand excitation.

1. Near-infrared sensitization of lanthanide nanoparticles

This section discusses the NIR organic dye sensitization of LnNPs, which are mainly studied for upconversion,[27,34,37,54] bioimaging,[55–59] and energy harvesting applications,[60–62] and comprise most of the work in this field. For upconversion, the dyes must absorb only at wavelengths longer than the visible to prevent quenching and reabsorption of the upconverted emission. They must also bind well and transfer energy efficiently to the lanthanide. For bioimaging, the windows of the highest penetration depth are between 650 and 1350 nm, and longer wavelength excitation is beneficial for the reduction of autofluorescence.[63] The lanthanides commonly sensitized by organic dyes in this region of the spectrum are Yb^{3+}, with an energy level at 980 nm, and Nd^{3+}, with levels at 808 and 880 nm.[64]

The development of this field began with the first demonstration by Zou *et al.* in 2012.[27] Figure 2 shows the timeline of NIR dye photoactive backbones that have successfully demonstrated sensitization since then. Many of the dyes produced have utilized the same backbone but added extra functionality through different binding, protective, or analyte sensing groups. Binding is mostly achieved through carboxylate or sulfonate groups, often more than one per molecule. Surface treatments to remove native oleic acid stabilizing ligands and improve dye binding are popular. This can be done with $NOBF_4$,[65] HCl,[37] or amino β-cyclodextrin[66] treatment.

The suffix "(2)" was added to various dyes in Fig. 2 due to dyes being published or sold under the same name as a previously published dye with a different structure. The full structures of all dyes referred to in Fig. 2 can be found in the supplementary material. Notably, there is confusion around IR806, the first NIR dye sensitizer used by Zou *et al.*,[27] which can be mistaken for a commercially available dye by the same name but different structure, herein referred to as IR806 (2).

Sections II A 2–II A 5 will cover examples that have made progress in some of the main research areas for NIR dye sensitization: energy transfer mechanisms, compositional optimizations, stability, and binding.

2. Energy transfer mechanism

Discerning whether energy transfer is mediated by the singlet or triplet level of the organic, and by which mechanism: FRET or Dexter, can guide molecular design to achieve highly efficient antennae. The mechanisms are discussed in further detail in Sec. III A and Fig. 11. Efficient transfer may be achieved from either state;[39] however, the triplet state has certain advantages. Dexter energy transfer is the only spin allowed deactivation process for the triplet state. As the transfer efficiency is equal to the energy transfer rate divided by the sum of all other deactivation rates, this can lead to high transfer efficiencies. However, the triplet can be quenched by oxygen, and Dexter transfer can only occur over short distances.

Increasing the triplet yield can, therefore, increase the efficiency of energy transfer. This can be achieved via enhanced spin–orbit coupling by substituting heavier atoms into the commonly used $NaYF_4$, for example, Cs^+ for Na^+[67] or Gd^{3+} for Y^{3+}.[34]

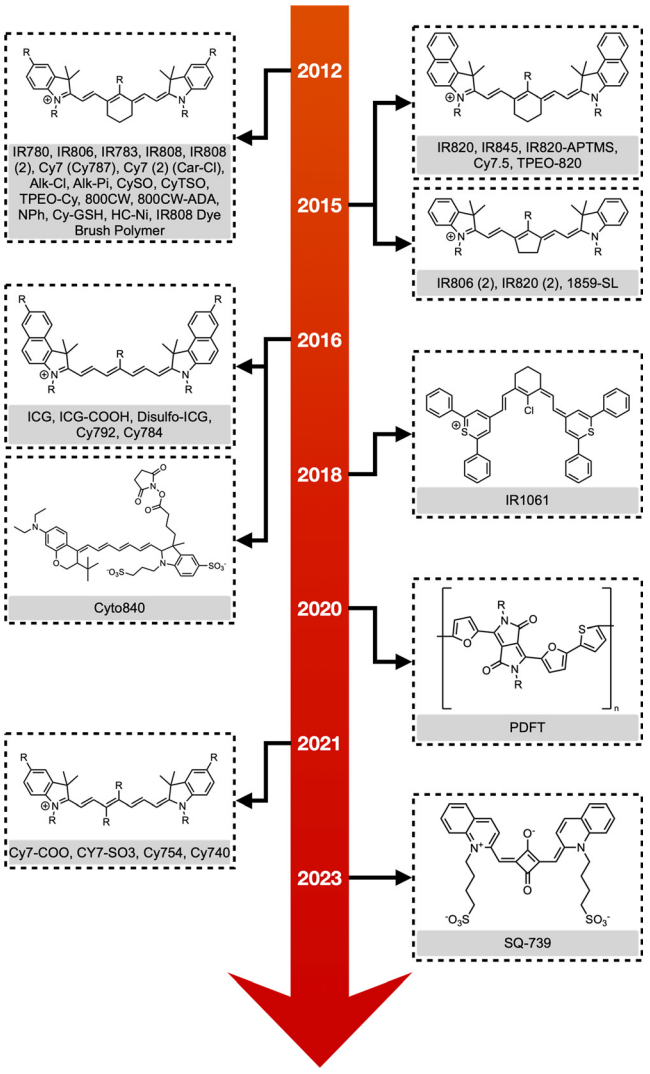

FIG. 2. Timeline of photoactive backbones of near-infrared dye sensitizers for LnNPs. Dyes with suffix "(2)" and dyes in brackets are those either with different structures but the same name as another, or a different name but the same structure as another dye. Full structures can be found in the supplementary material.

In 2018, Garfield *et al.* found that the phosphorescence of IR806 overlapped strongly with the absorption of Yb^{3+}.[34] They were only able to detect a phosphorescence spectrum by combining the dye with $NaGdF_4$ nanoparticles that enhanced the ISC rate. By including 30% Gd in the upconversion LnNPs, the UCQY was increased 68-fold; however, at higher doping concentrations, the UCQY decreased. They also showed that the upconversion luminescence (UCL) was reduced upon introduction of the triplet quencher cyclooctatetraene (COT). This was corroborated subsequently with other dyes and other authors.[34,68]

Zhang *et al.* demonstrated that $CsLn_2F_7$ increased ISC in a cyanine dye sensitizer, reaching unity efficiency.[67] This resulted in a 13-fold higher UCL enhancement, compared to $NaLnF_4$ particles sensitized by the same dye. Figures 3(a)–3(e) display the increase in ISC

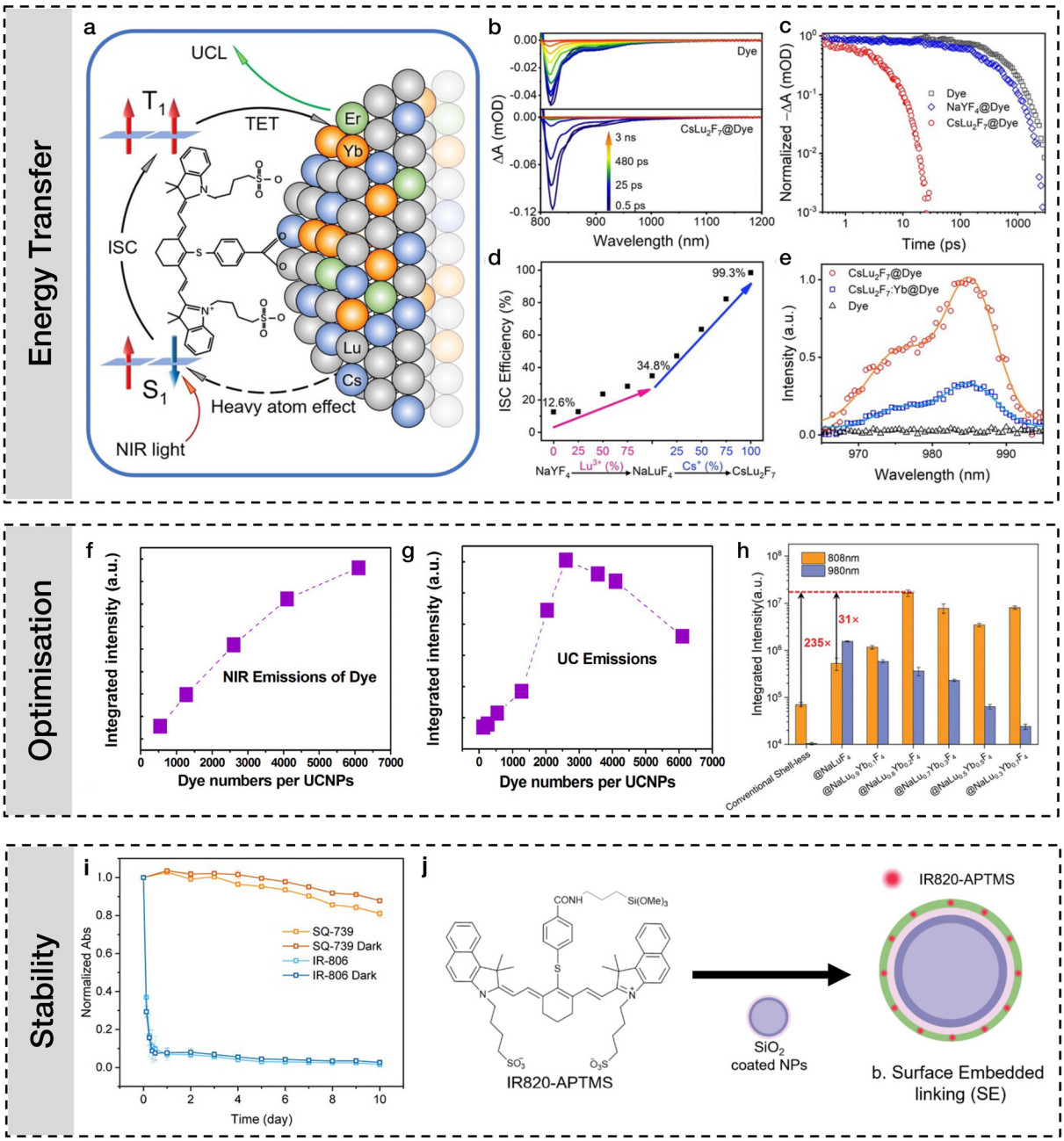

FIG. 3. (a)–(e) Increased ISC due to heavy atom effect of Cs based nanoparticles. Reproduced with permission from Angew. Chem. Int. Ed. **61**, e202112125 (2022).[67] Copyright 2022 John Wiley & Sons. (f) and (g) Dye and upconversion luminescence as a function of dye concentration. Reproduced with permission from J. Phys. Chem. Lett. **9**, 4625 (2018).[77] Copyright 2018 American Chemical Society. (h) Relative emission intensity from IR806 (2) sensitized upconversion LnNPs with varying concentrations of Yb^{3+} in the outer shell. Reproduced with permission from Adv. Opt. Mater. **10**, 2101763 (2022).[78] Copyright 2022 John Wiley and Sons. (i) Squaraine dye stability compared to IR806 (2). Reproduced with permission from Nano Lett. **23**, 5209 (2023).[54] Copyright 2023 American Chemical Society. (j). Strategy to embed a cyanine dye within a silica shell on LnNPs. Reproduced with permission from Nanoscale **15**, 13583 (2023).[31] Copyright 2023 Royal Society of Chemistry.

efficiency upon Cs inclusion and phosphorescence quenching of the cyanine dye in the presence of Yb^{3+}. Recently, Tan *et al.* enhanced the ISC rate of an antenna cyanine dye embedded in a MOF shell by decorating it with platinum.[29] Although no direct evidence for triplet state formation was found in the transient-absorption spectroscopy (TAS) study, it did result in increased UCL emission.

Liu *et al.* studied the interaction of three molecules spanning the visible and NIR with lanthanide doped CaF_2 via TAS.[69] For all three

molecules they saw no evidence of a triplet state, even with highly Gd^{3+} doped LnNPs, and therefore concluded that the energy transfer to lanthanides was singlet mediated. For the visible absorbing molecule, FITC, they found near unity energy transfer efficiency, which they deemed to be due to the molecular configuration on the surface constraining the frontier orbitals to be proximal to the lanthanides. Huang *et al.* included a TAS study on ICG, finding no evidence for a triplet state and concluding SET was dominant at an efficiency of 61%.[70] Liang *et al.* found both dyes they studied were not sensitive to oxygen and, therefore, concluded the triplet state did not play a major role in the energy transfer.[71]

Evidence for SET or TET from NIR antenna dyes is mixed as no direct evidence of the triplet state production and subsequent quenching has been demonstrated thus far. Indirect evidence of triplet state involvement includes phosphorescence spectra,[34] singlet oxygen production,[55] and oxygen/COT quenching of sensitization,[34] although care must be taken to ensure oxygen quenching is not due to degradation of the dyes or quenching of singlet states.[72]

3. Optimization

In 2015, Chen *et al.* introduced the concept of "energy cascaded upconversion" by assembling a core–shell (CS) structure to optimize the brightness of dye-sensitized LnNPs.[64] The outer shell contained Nd^{3+} that then cascaded the energy down to Yb^{3+} in the core for upconversion. They measured the UCQY of the sensitized particles to be 4.8%, which the authors increased to 9.2% the next year by co-doping Yb^{3+} in the outer shell.[36] Both Wu *et al.*[73] and Chen *et al.*[64] showed that co-sensitizing LnNPs with different dyes could enhance the sensitization effect by broadening the excitation wavelength range and increasing the maximum achievable sensitization effect. Wei *et al.* showed that due to dye sensitization, the optimal nanoparticle composition must be adjusted to contain a larger amount of acceptor lanthanide in the shell, which would usually reduce brightness due to surface quenching and cross-relaxation (CR).[25] They referred to this as alleviating luminescence concentration quenching and a similar effect has been seen by many other authors.[68,70,74–76]

In 2018, Xue *et al.* found that IR806 can quench both Nd^{3+} and Er^{3+} through EBT, which limits the brightness of upconversion LnNPs.[77] They also found that the commonly witnessed quenching of upconversion emission does not correspond to a quenching of dye emission [Figs. 3(f) and 3(g)], which may indicate that the aggregation induced quenching is occurring only for the surface bound dyes and not for free dyes in solution. Hu *et al.* clearly demonstrated LnNP compositional optimization: As the Yb^{3+} concentration in the outer shell was increased, the relative sensitization enhancement also increased.[78] However, the overall brightest particles were achieved with 20% Yb^{3+} doping [Fig. 3(h)]. To achieve maximum brightness, nanoparticle compositions and heterostructures must be re-optimized to account for the antenna effect.

4. Stability

Garfield *et al.* noted the instability of IR806 in the presence of oxygen in 2018.[34] This was further elucidated in 2023 by Wang *et al.*, which showed evidence of singlet oxygen production upon photoexcitation of IR806, accelerated in the presence of LnNPs.[55] The singlet oxygen then cleaves the three exposed double bonds along the backbone of IR806.

Kaur *et al.* modified a cyanine dye with nitrophenyl group and found it to increase the stability twofold, which they deem to be due to the steric protection and electron withdrawing properties reducing electrophilic attack on the heptamethine backbone.[79] Even with the improvements, the upconverting dye–LnNP hybrid was completely degraded after 1.5 h under a 2.1 W cm^{-2} illumination. A year later, Kaur *et al.* embedded an alkoxysilane modified cyanine dye within a silica shell, which demonstrated excellent stability and sensitization, a schematic is shown in Fig. 3(k).[31] The dye was sufficiently protected from the environment that it could be utilized in a reactive oxygen species (ROS) producing photocatalytic assembly designed to decompose Rhodamine B. This appears to be a promising method to enhance the stability of dyes and the brightness of particles without too much disruption of the organic–lanthanide interface. Zhang *et al.* showed low concentrations of triethylamine (TEA) can improve UCL intensity of cyanine dye sensitized LnNPs and improve the stability by up to 10.4 times in heptanol.[80] Liang *et al.* similarly found sensitization improvements by using TEA to reduce aggregation.[71] In 2021, Bao *et al.* introduced a bulky moiety "TPEO" to a cyanine dye to suppress bond rotation.[81] The modification improved PLQE threefold and stability sevenfold.

In 2020, Ji *et al.* published the first non-cyanine polymer-based NIR sensitization of LnNPs.[82] The sensitization effect was weak, with a 0.3-fold enhancement of UCL intensity when exciting the polymer over Yb^{3+}. Importantly however, the polymer showed higher photostability when compared with ICG (although only shown over 20 min). Recently, Hu *et al.* demonstrated the first use of a squaraine dye for Yb^{3+} and Nd^{3+} LnNP sensitization called SQ-739.[54] The dye had reduced concentration quenching compared to a cyanine dye and higher stability as shown in Fig. 3(j). The transfer rate was much higher for Nd^{3+} compared to Yb^{3+}, and no phosphorescence could be detected so it appeared that the transfer was singlet mediated. However, the triplet quencher COT reduced UCL intensity by 50%, evidencing TET. Due to the high photostability, they were able to capture single particle images.

5. Binding

In 2023, Zhao *et al.* investigated the role of bonding distance and strength, using commercially available dyes with additional sulfonate binding groups positioned closer to the photoactive cyanine backbone than previously studied dyes.[68] The new dyes demonstrated a large upconversion enhancement, however, they also showed stronger quenching of the upconversion lifetime of the particles due to EBT.

In 2016, LaBoda and Dwyer modeled the adsorption of dye Cyto840 using a Langmuir process based on quenching lanthanide lifetimes due to EBT, allowing them to extract a fractional occupancy of the dye.[83] They found that 50% of the lanthanide sites were occupied by the dye but also a large amount of dye remained in the solution. The study utilized a two-dye system whereby one dye (Cyto840) sensitized the upconversion LnNPs, and another dye (Atto488) accepted the upconverted energy, leading to dye emission in the visible region. Nasrabadi *et al.* compared six new cyanine dyes to understand the binding mechanism, stability, strength, and involvement of triplet states in the energy transfer process.[37] They compared the dyes' binding strength using a centrifugation based binding assay. The binding

strength of the dye had a larger impact on sensitization than the spectral overlap with the lanthanide absorption. The dyes that bound the strongest had the most marked sensitivity to oxygen, which was evidence for a triplet mediated transfer. Yin *et al.* added a carboxylic acid to a dye that contained two sulfonate binding groups and found a large UCL enhancement which demonstrates the strength of multi-dentate binding.[84]

6. Biological

A prerequisite of bioimaging applications is that the dye–LnNP system can be dispersed in aqueous environments and retain strong sensitization and luminescence. However, most studies are performed in organic solvents as water quenches the dye and LnNP emission.

Liang *et al.* investigated this by modifying a cyanine dye that forms deleterious H-aggregates, which cause emission quenching in water.[85] By using amphiphilic DSPE-PEG to coat the particles, maintaining a hydrophobic local environment on the particle surface, H-aggregation was reduced (although remained present at higher concentrations). The removal of carboxylic acid binding groups further reduced H-aggregation and the dyes remained "bound" to the particles through hydrophobic interactions. Blue shifting the absorption of the dye by central piperazine substitution reduced back transfer from Nd^{3+} to the dyes, further increasing the brightness. In 2021, Wang *et al.* used the final optimized dye (Alk-Pi) to dynamically image vascular disorders via monitoring of the downshifted 1530 nm Er^{3+} emission.[86]

Sensing of hypochlorite, glutathione, and pH has been achieved in biological environments through both turn-off and turn-on sensitization.[57,58,87–89] Turn-off sensing is caused by the destruction of the dye sensitizer and turn-on sensing is achieved with dye sensitizers modified with recognition groups that quench emission (and therefore sensitization ability) until reacting with the target analyte. Zhu *et al.* produced a sensitized LnNP for both downconversion imaging and controlled nitric oxide release *in vivo*.[30] Wu *et al.* demonstrated optogenetic triggering by NIR light using IR806 sensitized CS nanoparticles that stimulated channelrhodopsin from the upconversion emission.[59] The enhanced penetration depth this system demonstrated is of great utility for *in vivo* applications.

7. UV-visible dye sensitization

This section will discuss the findings of dye sensitization in the UV and visible parts of the spectrum. Due to the higher energy of antenna absorption, these systems are employed in applications of downconversion (akin to quantum cutting) and downshifting luminescence with large Stokes shift. They have been shown to have a much higher efficiency of energy transfer and benefit from 80 years of lanthanide chelate sensitization literature that has traditionally focused on small molecule ligands that bind strongly to lanthanide ions and form stable complexes. Due to the higher stability, increased PLQE, and lower steric hindrance upon binding, they are often favorable for fundamental studies.

As has been well understood in lanthanide chelate literature, the triplet lanthanide energy gap is very important for antenna optimization and is optimally around 3000 cm^{-1} above the lanthanide level.[5,39] Zhao *et al.* applied this when optimizing UV-sensitized LnNPs for an invisible ink application.[90] They found dipicolinic acid sensitized Eu^{3+} and Tb^{3+} most strongly out of the six antennas tested and had suitable triplet energy gap from phosphorescence measurements of the Gd^{3+} complexes. However, the authors found the triplet energy gap law not to be true in all circumstances, as coordination affinity is also important. Other authors have found dipicolinic acid to coordinate so strongly that it was able to leach lanthanides from LaF_3 based nanoparticles.[91]

Our group's previous work clearly elucidated that the interaction of unpaired 4f electrons was dominant over spin–orbit coupling for ISC enhancement.[35] For the first time, we showed direct triplet absorption at room temperature of organics bound to LnNPs. This only occurred when the lanthanide had unpaired electrons. We also demonstrated unity energy transfer efficiency from an antenna ligand, CPPOA, to both Eu^{3+} and Tb^{3+} via the triplet state of the ligand monitored with TAS as shown in Fig. 4(d). Near unity transfer efficiency has also been found for another fluorescein-based molecule, FITC; however, Liu *et al.* saw no evidence of a triplet mediated transfer in their TAS study.[69,92] Recently, Xu *et al.* sensitized Nd^{3+}, Yb^{3+}, and Er^{3+} using an iridium complex.[93] They found phosphonate to bind more strongly than carboxylate and the molecule was more stable than tropolonate (the first LnNP antenna ligand) under prolonged irradiation. Additionally, they had evidence for triplet mediated energy transfer via a TAS study.

Shao *et al.* sensitized the Tb^{3+}–Yb^{3+} quantum cutting pair with an aggregation induced enhanced emission dye as shown in Figs. 4(e) and 4(f).[28] This allowed for maximum dye loading onto the particles without suffering aggregation induced quenching. The evidence for quantum cutting came from a power dependence exponent of 0.69 for the Yb^{3+} emission, which lies within the expected dependence between 0.5 and 1 depending on whether the process is non-linear (utilizing a virtual state) or linear. Different lanthanide hosts or cutting pairs have shown both linear and sub-linear power dependences.[94] Dye sensitized downconversion has also been reported by Wang *et al.* using a coumarin dye to sensitize the Pr^{3+}–Yb^{3+} cutting pair; however, the paper does not show direct evidence for downconversion.[45]

8. Discussion

Much research has taken place in the field of NIR sensitization with an abundance of dyes reported. Most of these dyes are of the same or similar heptamethine cyanine dye backbone, and therefore, many suffer from the same issues, including non-unity energy transfer efficiency, low stability, and weak binding.

Some studies have helped enlighten these areas. Regarding stability, advances have been made such as by adding bulky groups in the center of the backbone to protect from singlet oxygen attack,[30,81] embedding a cyanine dye within a silica shell,[31] or using other dyes such as polymers[82] and, recently, squaraines.[54] The mechanism of singlet oxygen degradation was elucidated clearly by Wang *et al.* recently.[55] Regarding ligand coordination, reports have highlighted how binding strength and distance are of the utmost importance for facilitating efficient triplet energy transfer.[37,68] It is often not recognized that a large proportion of the dyes in the sample may not be interacting with the LnNPs at any one time; care must be employed to take this into account when making ensemble photophysical measurements.[83]

Studies regarding how the act of sensitization changes the way the LnNP is designed are abundant and have demonstrated how active

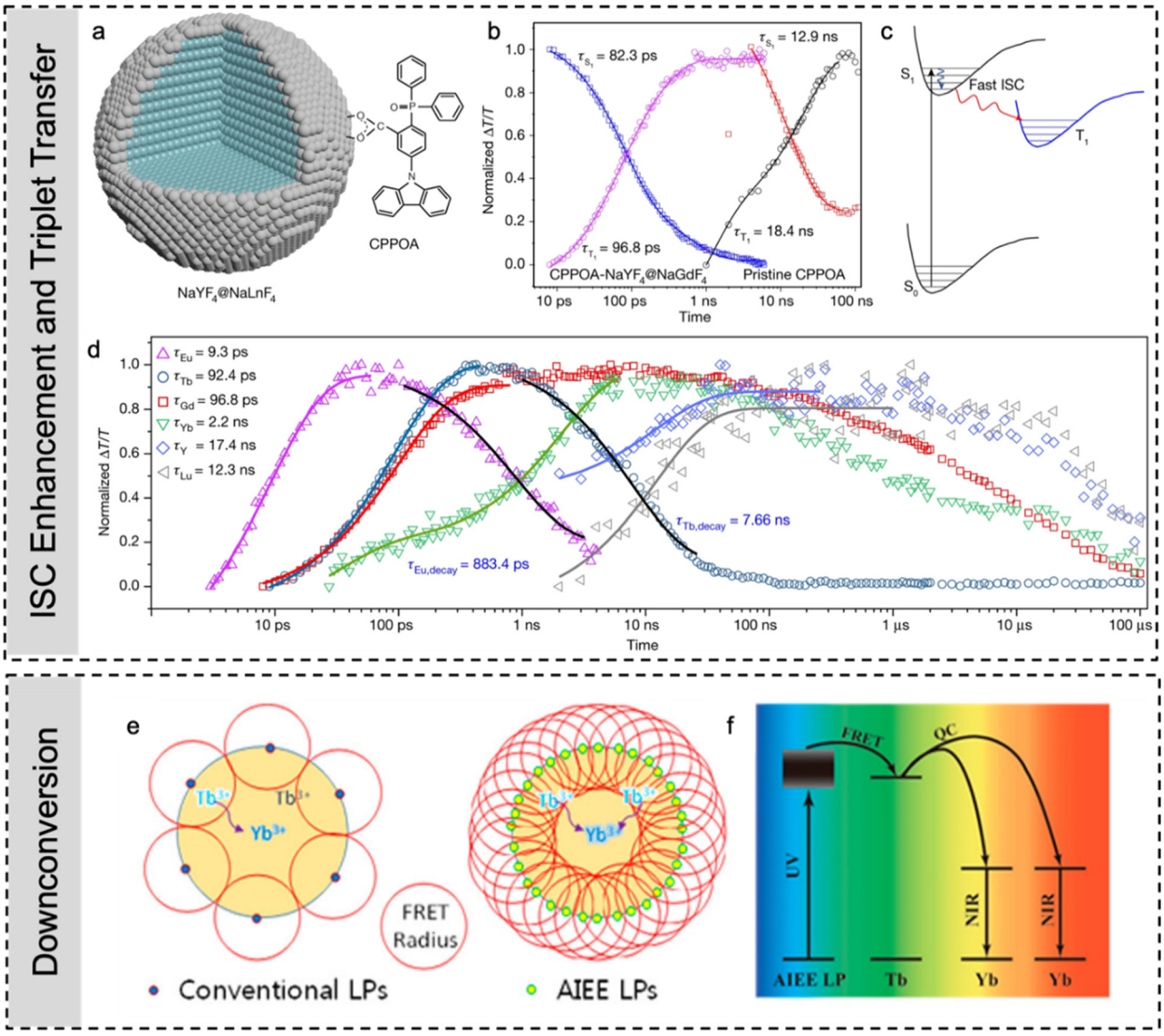

FIG. 4. (a)–(d) Triplet state rise and quenching as a function of lanthanide dopant for the molecule CPPOA. Reproduced with permission from Nature **587**, 594 (2020).[35] Copyright 2020 Springer Nature. (e) and (f) Downconversion using an aggregation induced enhanced emission (AIEE) dye with Tb^{3+}–Yb^{3+} quantum cutting pair. Reproduced with permission from Nano Lett. **18**, 4922 (2018).[28] Copyright 2018 American Chemical Society.

shells can be used to cascade[64] or concentrate[95] energy. The concentration of lanthanide dopants will change when using dye sensitisation[25,78] and when designing particles for applications such as single particle imaging that occurs under intense excitation power.[78] Surface treatment with $NOBF_4$ to aid the binding of organic ligands and allow nanoparticles to be transferred to polar phases has proved popular.[65,85] The use of phosphatidylcholines,[96] DSPE-PEG,[97] and cyclodextrin[66] has also been shown to transfer the nanoparticles to aqueous phases. A plethora of applications have been demonstrated using dye sensitized LnNPs including, but not limited to, activatable invisible ink,[90] photothermal therapy,[98–102] memory,[103] optogenetics,[59] lymphatic imaging,[96] glutathione sensing,[104] hypochlorite sensing,[87,105] water detection,[106] bioimaging,[30,56–59,70,85,105,107–109] ROS production,[107] photocatalysis,[31] wavelength selective imaging,[73] security printing,[71] computational energy transfer networks,[83] mercury detection,[95] and, finally, single particle imaging.[68,78]

Regarding whether NIR dyes sensitize via singlet[69,71] or triplet[34,67,68,71] pathways, the literature is divided. There is clear evidence that UV–visible dyes sensitize via singlet and triplet pathways.[35,39,110] Theoretically, triplet transfer can be more efficient due to long excited state lifetimes and Dexter transfer being the only spin allowed deactivation process. However, this type of energy transfer is more harshly distance dependent than FRET so tight binding is required.[47] Direct evidence via TAS has detected the involvement of a triplet state in energy transfer for UV–visible dyes;[35] however, this direct evidence has not been found for NIR dyes.[69,71] Indirect evidence such as

phosphorescence energy matching and the influence of triplet quenchers such as oxygen or COT (cyclooctatetraene) have been shown for NIR dyes;[34,68] however, oxygen sensitivity may be due to degradation of the dye.

Additionally, we are unable to compare these dyes due to a lack of reliable standardized measurements or reference materials. Regarding measurement methodologies, there are a few points that are important to stress. Due to the known ISC acceleration that lanthanides have on organic molecules,[35,39] the photoluminescence (singlet) lifetime quenching cannot be used to estimate energy transfer efficiency (ϕ_{ET}) using equation:

$$\phi_{ET} = 1 - \frac{\tau_{DA}}{\tau_D}, \tag{6}$$

in which τ is the measured lifetime of the donor (D) with or without the acceptor (DA).[111] This is because although triplets may form rapidly and quench the singlet photoluminescence lifetime, they may or may not be subsequently transferred to the lanthanide. For the correct treatment of ϕ_{ET}, see Eq. (5) in Sec. II A. For the lanthanide PLQEs used in Eq. (5), upconversion quantum yields cannot be used as they are power dependent. Therefore, a normal downshifted emission quantum yield under a low excitation power must be used in order to guarantee a linear regime. These measurements can be difficult due to the often low PLQE of lanthanides, the part of the spectrum they emit (IR), and the strong overlap between absorption and emission.[5]

Frequently, the only metric provided in papers to compare dye-sensitization ability are relative upconversion measurements. These are error prone as they are affected by many parameters, including excitation power and power density, excitation wavelength, in-coupling, out-coupling, organic dye to LnNP ratio, concentration, inner filter effects, detector sensitivity, LnNP batch, LnNP dopant concentration, organic photobleaching, oxygen concentration; water concentration, ligand exchange time, solvent, LnNP stabilizing ligands, washing procedure, and many more. At the minimum, dye sensitization enhancements should be calculated in reference to the intrinsic emission of the LnNPs at the same excitation power at an excitation wavelength that the particle absorbs at. For example, this could be achieved with an excitation scan of lanthanide emission by comparison of the dye absorption peak with the lanthanide absorption peak.

Future research should focus on maximizing the potential of dye-sensitized lanthanide systems by reaching unity energy transfer efficiency across the spectrum with minimal energy loss between donor and acceptor. If possible, this would allow for high efficiency solar energy harvesting and increased usability across all current applications. This will require combining knowledge gained across the areas of stability,[79] aggregation,[28,54] passivation,[112] absorption,[113] singlet-triplet splitting,[114,115] transfer efficiency,[35] and quantum yield[81] into a bespoke dye and possibly embedding strategy.[116]

Development of reliable and accurate measurement methods for quantifying the binding efficiency and energy transfer efficiency is still lacking, which would enable accurate comparisons to be drawn between dyes, further guiding the design. For example, inspiration can be drawn from areas such as biology in order to analyze the binding of ligands,[117] which would enable distinguishing advances in binding strength and energy transfer efficiency that both contribute to total brightness enhancement.

Stability is an often overlooked but vital characteristic for any future application. It has been well documented that the accelerated triplet generation on the dyes leads to singlet oxygen production, subsequently cleaving the commonly used cyanine dyes. Squaraine dyes[54] and polymers[82] have shown encouraging stability alongside the promising demonstration by Kaur *et al.*[31] of embedded dyes in silica shells, which showed stability even in a system designed to photodegrade organic molecules. Another important factor to consider for organic sensitizers is environmental tolerance, as dyes are often sensitive to water and oxygen,[85] which hampers their biological applicability.

A trade-off always exists with sensitized systems between maximizing energy transfer from the organic and minimizing energy losses from the particle, which currently hampers the maximum quantum yield of the particles. A promising area of further study would be in novel encapsulation methods that prevent surface losses (as with inert shells) while still enabling organic sensitization interaction, such as the recent demonstration of aluminum oxide encapsulation by Green *et al.*[11,57,116]

Dye sensitization offers one of the strongest and most versatile absorption enhancements for lanthanides, not without associated hurdles yet to be overcome. The successfully commercialized organic light-emitting diode (OLED) field has shown a path to how similar issues can be surmounted, such as regarding long-term stability.[118]

B. Inorganic dye-coated core–shell heterostructures

Inorganic dyes are coloring agents derived from inorganic compounds, distinct from organic dyes due to their composition of elements other than carbon and hydrogen, such as metals. Unlike organic dyes, they are chosen for their properties such as heat resistance, photostability, and chemical stability. At the same time, inorganic dyes normally possess crystal structures and are difficult to combine with LnNPs due to the possible lattice mismatch. Thus, it is very challenging to form an LnNP@inorganic dye CS heterostructure and reports of them are scarce.

Our work has demonstrated the first combination of Nd^{3+} nanoparticles (NdNP in the form of $NaNdF_4$) with a typical inorganic dye, Prussian blue (PB) to form a CS heterostructure [Fig. 5(a)]. To overcome the lattice mismatch, we have first performed a surface modification by replacing oleic acid with citric acid, which will provide growth sites for PB on the surface of NdNP. Thus, a PB shell with an average thickness of about 3 nm has been successfully fabricated.

The absorption of the CS heterostructures has been significantly enhanced and broadened due to the involvement of PB, compared with that of NdNPs. The PB shell layer is designed to generate new cross-relaxation (CR) pathways between the NdNPs and PB [Fig. 5(b)]. Nd^{3+} ions have ladder-like energy levels. CR between the $^4F_{3/2}$ to $^4I_{5/2}$ and $^4I_{9/2}$ to $^4I_{15/2}$ states of Nd^{3+} ions as well as other non-radiative transitions to the ground state generates the photothermal effect. The exceptionally high photothermal conversion of 60.8% (higher than 8.7% for NdNPs and 19.8% for PB) was attributed to the interaction of NdNPs and PB from the newly formed CR2 pathway. This has been proved by the decreased NIR fluorescence of NdNPs and a shortened lifetime of the 1058 nm emission [Figs. 5(c) and 5(d)]. Another work by Wang *et al.* further combined core–shell–shell (CSS) LnNPs ($NaErF_4$@$NaYF_4$@$NaNdF_4$) with PB.[119] Here, the ErNP core was incorporated as an imaging agent emitting at 1525 nm for NIR-II fluorescent imaging. The PB coating was found to enhance the

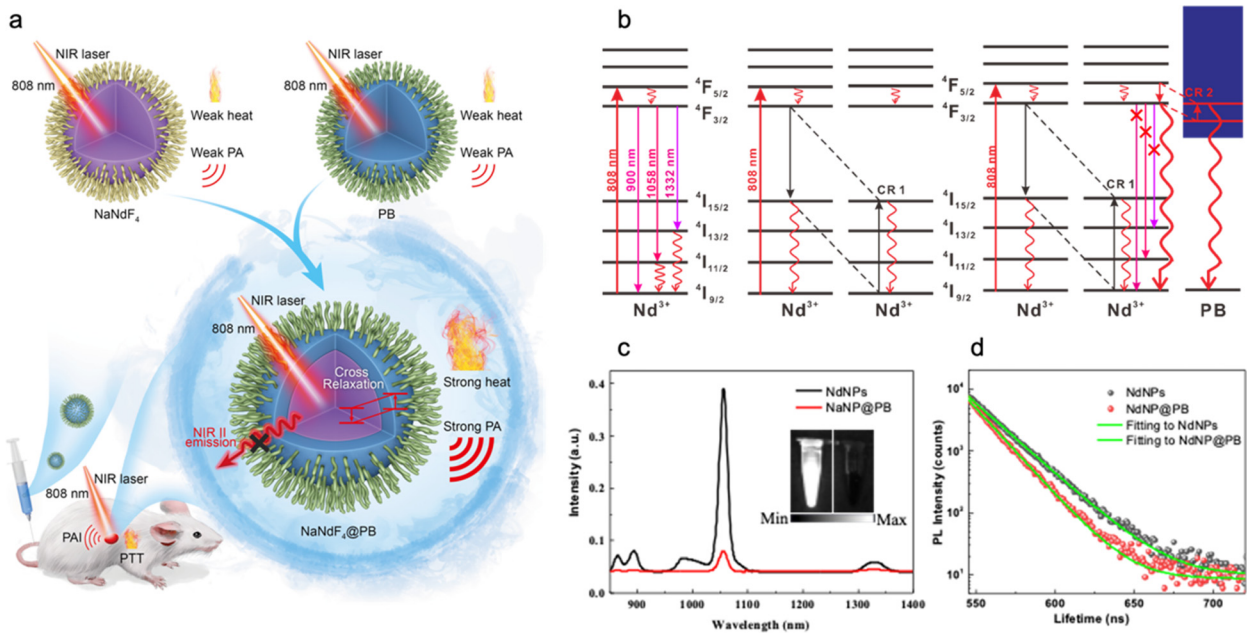

FIG. 5. The fabrication of NdNP@PB CS heterostructures. (a) Schematic illustration of the energy transfer and biomedical applications of these heterostructures.[120] (b) Detailed energy transfer pathways and cross-relaxation in pure NdNPs and NdNP@PB CS heterostructures.[120] The comparison of (c) NIR fluorescence and (d) lifetime decay at 1058 nm of NdNPs before and after coating of PB shell.[120] Reproduced with permission from Angew. Chem. Int. Ed. **58**, 8536 (2019). Copyright 2019 John Wiley and Sons.[120]

absorption of this system by tenfold and increase the photothermal conversion efficiency three times in comparison to the CSS particles without PB, which is a decent demonstration for multifunctional biomedicines.

Overall, the combination of inorganic dyes and LnNPs is limited and worthy of further studies to form more novel all-inorganic heterostructures with enhanced performance and new functionalities.

C. Plasmonic-enhanced lanthanide-based heterostructures

A radically different approach to design higher effective absorption coefficients of LnNPs, increasing their luminescence efficiency, and reducing the lifetime is by engineering the nanophotonic environment around an emitter. Placing emitters within a cavity resonant with an emissive transition can enhance the rate of emission through the Purcell effect.[121] An emitter never emits in isolation, it emits via a spontaneous probabilistic process into the vacuum. Such a probability is controlled not just by intrinsic emitter properties but also by the available density-of-states (DOS) of the vacuum into which a photon is emitted. By engineering the environment into which an emitter releases photons, the local photonic DOS can be increased, enhancing the likelihood of light emission and the PLQE. The reverse process of enhanced absorption of light is also possible, as the volume of space, which a light field occupies (the optical mode volume), can also be controlled.

Engineering the local photonic DOS can be achieved through placing emitters within dielectric optical microcavities[123] or nanoscale optical nanocavities[124] using plasmonics. Dielectric microcavities confine light through the formation of standing waves, either simply by having two mirrors spaced apart or through whispering gallery mode resonances.[125] In contrast, plasmonic nanocavities confine light by hybridization of light with electron oscillations in a plasma within metal surfaces. Such hybridization between light and plasma creates a surface plasmon polariton, which confines light to sub-wavelength scales, as it acquires the character of electron waves that have a smaller wavelength than light. A detailed introduction to the physics of plasmonic systems can be found in Ref. 126.

Dielectric optical microcavities possess higher quality factors [Fig. 6(a) showing the ratio of emission energy to its linewidth] matching the narrow linewidth of lanthanide ion emission, however, suffer from lower DOS and optical mode volume [Fig. 6(b)]. In contrast, nanoscale cavities, often made using plasmonic metal nanostructures, have low quality factors but exceptionally compressed optical mode volumes.

Dielectric microcavities have been shown to enable dynamic modulation of the emission lifetime properties by placing lanthanides in tunable spacing Fabry–Pérot microcavities.[127] Whispering gallery mode microresonators have also demonstrated lasing action.[24] Placing lanthanides inside electro-optically tunable dielectric cavities also allows for emission wavelength tuning and integration into on-chip CMOS-compatible optoelectronic devices.[128] More exotic proposals for the use of lanthanides in bulk host matrices have been demonstrated for quantum transduction from microwave to optical frequencies.[129,130] Such approaches may benefit from the use of brighter, more tunable LnNPs.

Plasmonic structures have been used to demonstrate the Purcell effect and light enhancement since the earliest days of nano-optics,

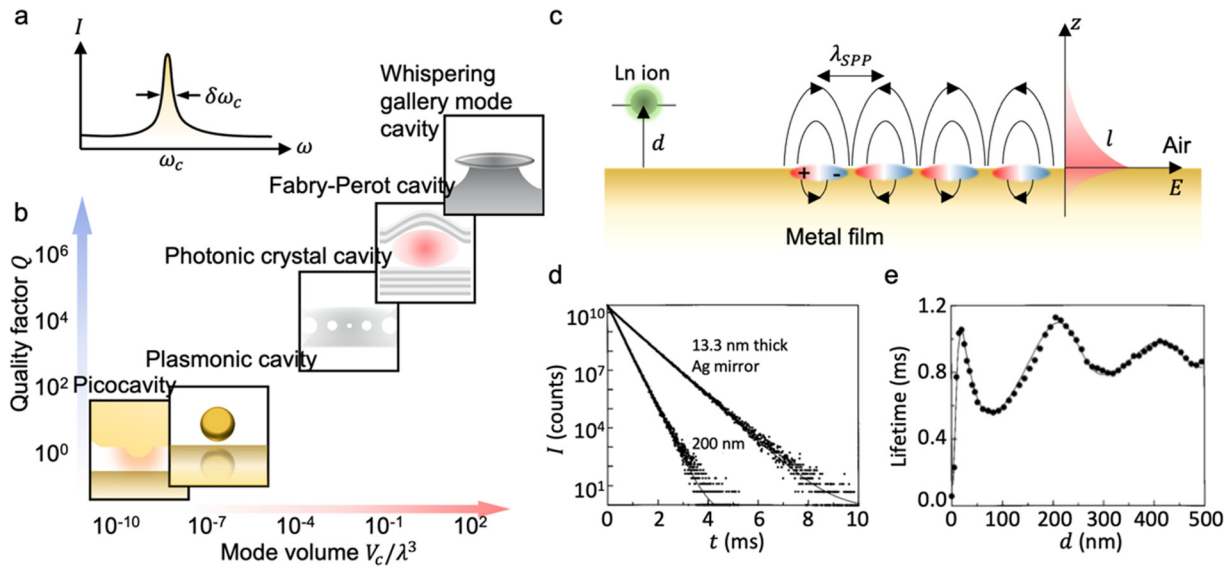

FIG. 6. (a) Schematic of resonance of an optical cavity with resonant frequency (ωc) and linewidth ($\delta\omega c$).[122] (b) Quality factor (Q) vs mode volume (V_c) relative to volume occupied by the wavelength (λ^3) for different cavity geometries.[122] (c) Lanthanide ion at distance (d) from a metallic surface interacting with surface plasmon polaritons (SPP, wavelength SPP) generated by light interacting with electron oscillations (positive and negative charge indicated with electric field lines connecting them). Electric field (E) of the SPP decays exponentially from the surface with length (l).[122] (d) Time resolved emission for an Eu^{3+} ion on a 13.3 nm vs 200 nm thick Ag film. (e) Lifetime vs distance (d) of a Eu^{3+} from a 200 nm thick Ag film.[122] Reproduced with permission from Nat. Mater. **18**, 668 (2019).[122] Copyright 2019 Springer Nature.

with the pioneering experiments of Drexhage.[131] Placing an emitter on top of an Ag film of different thickness reduces the emission lifetime due to the coupling of the emitter with SPP. By varying the distance between an Eu^{3+} emitter and a silver mirror [Fig. 6(e)], the emission lifetime can be clearly shown to oscillate as predicted by theory in Figs. 6(d) and 6(e), and once the emitter is very close to the mirror, its emission is quenched as the energy is coupled to loss surface plasmon waves that do not emit to the far-field. We can overcome this disadvantage by using other plasmonic geometries such as the nanoparticle-on-a-mirror[122] (NPoM) or nanoparticle-dimers, where the radiative rate is increased to such a degree that it out-competes the non-radiative decay even when the emitter is within 1 nm of a metallic surface. Within such structures, light is squeezed into the nanogap between a nanoparticle and a mirror or between two nanoparticles, within which lanthanides may be placed. Plasmonic nanogap structures can be fabricated with poor reproducibility via top-down fabrication (ion-beam milling or electron beam lithography to form metallic gratings[132,133]) or with high reproducibility in the case of NPoMs using solution-based processing[134] and gap-cleaning/re-definition methods.[135]

The overall design requirement when making plasmonic structures/optical microcavities to enhance emission is to ensure that the plasmonic/optical resonance wavelength overlaps with the lanthanide's absorption or emission bands. The geometry of these structures such as the general morphology, spacing, and size can be tuned to achieve the desired resonance wavelength from the visible to the mid-infrared.[136,137] Once that is achieved, further considerations such as the emission angles, polarization, and outcoupling efficiency can be designed. For example, the NPoM geometry emits resonant light at high angles when out-coupled into the fundamental plasmonic mode, while other structures may emit light at normal incidence. This allows for tuning of emissive display angles. Furthermore, plasmonic structures may be used to enhance forbidden transitions, either through confinement of light in multi-polar local modes in NPoM structures[138] or via proximity of an emitter to a heavy metal such as Ag or Au.

A related concept is photon-recycling,[139,140] which is more trivial as the multiple-bounces of light within a structure enhance the effective path length which light propagates in a material. While photon-recycling is used in perovskite systems and photovoltaics, its utility remains to be seen. However, increasing the path length of light through lanthanides to enhance its interaction and increase photon conversion or emission is a well-known method and used with incredible success in the field of fiber optics. The erbium-doped fiber amplifier[141] and use of lanthanides as emissive centers in optical fiber lasers[142] is one of the clear technological successes of lanthanides and is ubiquitous in modern telecommunications.

We will also introduce applications that directly relate to plasmonic enhanced absorption and luminescence of the LnNPs, including UCL,[143–146] upconversion lasing,[147–149] emission from single particles,[150,151] and sensing related applications[152–154] (Fig. 7). As introduced previously, the mechanism of plasmonic enhancement of LnNPs absorption and emission is to overlap the plasmon spectra of the plasmonic nanoparticles such as Au or Ag nanorods, nanoparticles, or other nanostructures with the absorption or emission spectra of the lanthanides. For example, Wu *et al.* sandwiched the LnNPs between gold thin film and Ag nanocubes as shown in Figs. 7(a) and 7(b).[143] They tuned the gap of the plasmon mode so that its spectrum is overlapped with the emission spectra of the LnNPs [Fig. 7(c)]. By doing that, the emission intensity of the LnNPs increased by four to five orders of magnitude compared with LnNPs on bare glass substrates without coupling to plasmon modes [Fig. 7(d)].[143] Figure 7(d) presents typical luminescence spectra of the three different samples [LnNPs on

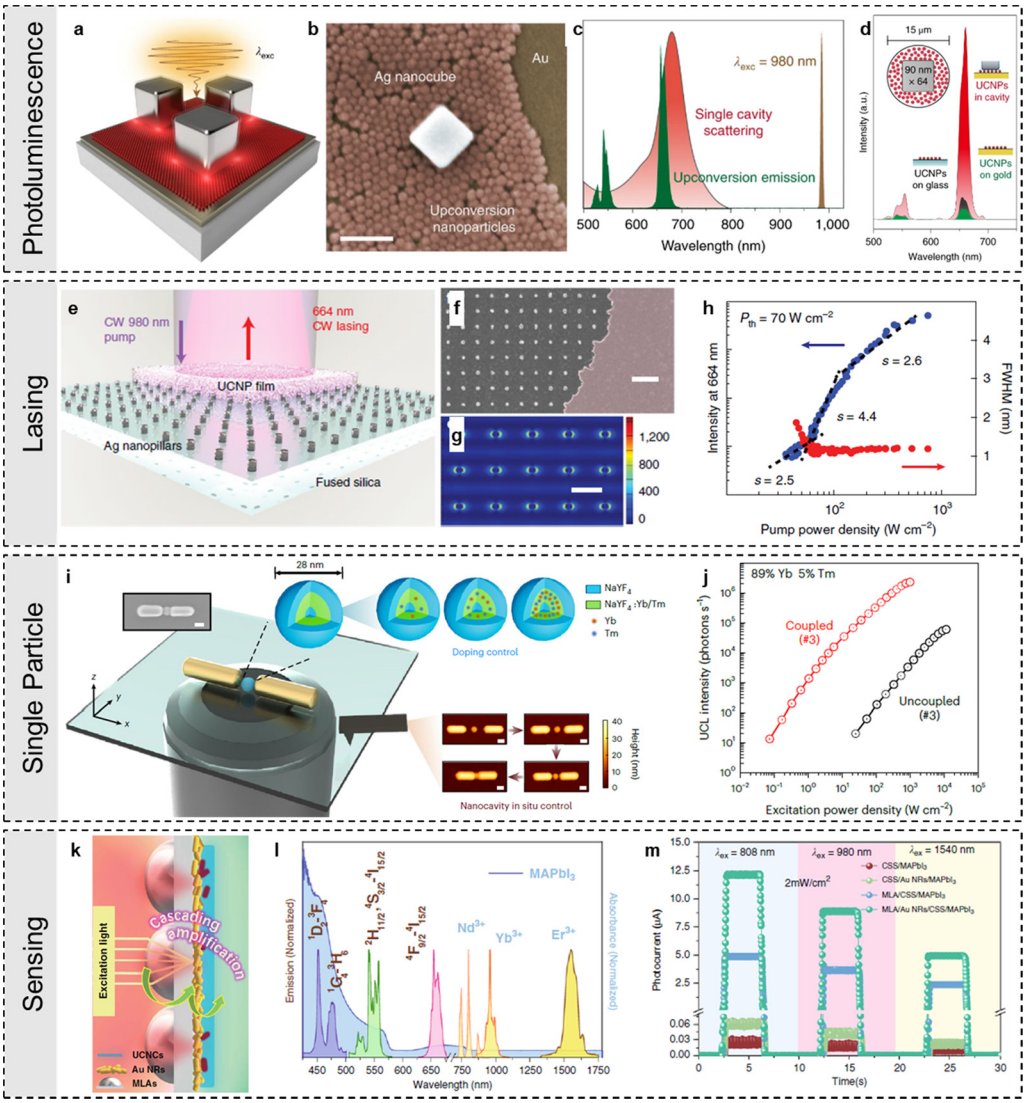

FIG. 7. (a) Rationally designed plasmonic cavity coupled of upconversion LnNPs composed of a gold thin film, a silver nanocube, and a monolayer of LnNPs embedded in the sub-20 nm wide gap.[143] (b) Scanning electron microscopy (SEM) image of a typical plasmonic cavity. Scale bar, 100 nm.[143] (c) Photoluminescence spectrum of the Er^{3+}-activated LnNPs and simulated scattering spectrum of a single nanocavity. The red upconversion emission spectrum under 980 nm laser excitation overlaps with the plasmonic resonance wavelength at 660 nm.[143] (d) Photoluminescence spectra of an upconversion LnNP monolayer deposited on the glass substrate (black) and gold film (green) or in the nanocavity (red). Top left: Schematic of the experimental condition applied for the photoluminescence measurement in the nanocavity mode.[143] (a)–(d) Reproduced with permission from Nat. Nanotechnol. **14**, 1110 (2019). Copyright 2019 Springer Nature.[143] (e) Schematic of the upconversion LnNP coating on top of Ag arrays with spacing of 450 nm. Ag nanopillars are with 80 nm diameter, 50 nm height, and the arrays are scalable over square centimeters areas. The upconversion LnNP film is roughly 150 nm thick.[147] (f) Scanning electron micrograph showing the Ag nanopillar array with a partial conformal coating (right) with a film of 14 nm CS LnNPs ($NaYF_4$:Yb^{3+}, Er^{3+}). Scale bar, 1 μm.[147] (g) Representative near-field $|E|^2$ plot for the 450 nm spaced Ag nanopillars at resonance (n = 1.46) from an FDTD method simulation. Scale bar, 500 nm.[147] (h) Input–output curves in log–log scale with emission linewidth narrowing showing a low lasing threshold P_{th} of 70 W cm^{-2}. FWHM, full width half maximum.[147] (e)–(h) Reproduced with permission from Nat. Mater. **18**, 1172 (2019).[147] Copyright 2019 Springer Nature. (i) The experimental platform for investigating single nanocrystal upconversion coupled to a single plasmonic nanocavity mode. An SEM image of a typical coupled composite is displayed at the top left (scale bar, 50 nm). The plasmonic nanocavity field is tunable through the use of an atomic force microscopy (AFM) tip, as shown by the series of AFM topographic images of the coupled system (scale bars, 50 nm). The sample is situated on an inverted microscope. Laser light at 980 nm is launched to excite the sample through the microscope objective, and the UCL is collected through the same objective.[150] (j) Excitation power dependent UCL intensity curves for the same upconversion LnNP (#3) before and after coupling with the nanocavity. The polarization of the excitation is along the x direction. The UCL intensity represents the detected count rate with background and dark count rates subtracted.[150] (i) and (j) Reproduced with permission from Nat. Photonics **17**, 73 (2022).[150] Copyright 2022 Springer Nature. (k) Schematic illustration of the cascading amplification strategy for LnNPs with microlens arrays (MLA), plasmonic Au nanorods, and LnNPs.[152] (l) Absorption of $MAPbI_3$ films, Nd^{3+}, Yb^{3+}, and Er^{3+} and emission spectra from $^1D_2 \rightarrow {}^3F_4$, $^1G_4 \rightarrow {}^3H_6$, $^2H1_{1/2}$, $^4S_{3/2} \rightarrow {}^4I1_{5/2}$, and $^4F_{9/2} \rightarrow {}^4I_{15/2}$ transitions in CSS LnNPs.[152] (m) On–off switching currents of CSS/$MAPbI_3$, Au NR/CSS/$MAPbI_3$, MLA/CSS/$MAPbI_3$, and MLA/Au NR/CSS/$MAPbI_3$ under 808, 980, and 1540 nm excitation at a power density of 2 mW cm^{-2}.[152] (k)–(m) Reproduced with permission from Light Sci. Appl. **9**, 184 (2020).[152] Copyright 2020 Springer Nature.

bare glass, on gold films, and on gold films with Ag nanocubes (with cavity)] at an excitation power of 7.5 mW. The luminescence intensity from LnNPs coupled to plasmonic nanocavities is substantially larger than that of the nanoparticles deposited on either a gold film or a glass slide. Apart from the increase in emission intensity for the LnNPs in the nanocavity, they also reported a 166-fold rate increase in spontaneous emission as the PL lifetime decreased to below 2 μs when LnNPs were inside the nanocavity.[143] This emission enhancement effect is widely observed with other plasmonic systems such as Au pyramids[144] or Au nanorods,[146] but the reduction of emission lifetime to such extent is difficult to achieve with only the presence of plasmonic metals. The advantage of having a plasmonic nanocavity is that it enables manipulation of the nanoparticle local DOS through the Purcell effects. As a result, the emission rate can be increased since it is proportional to the local density of optical states based on the Fermi's golden rule. The rapid emission and higher emission intensity from the plasmon nanocavity enhanced LnNPs provide future development of rapid nonlinear image scanning nanoscopy and open up the possibility of constructing high frequency, single-photon emitters driven by telecommunication wavelengths.

Lasing is another important emission application for LnNPs. Continuous-wave (CW) lasing at room temperature is critical for integration with optoelectronic devices. Plasmonic nanocavities integrated with gain can generate coherent light at subwavelength scales. Lowering the lasing threshold and improving the material stability are the key focuses. Odom *et al.* developed an ultralow-threshold, CW upconverting lasing from subwavelength plasmons by integrating LnNPs on Ag nanopillar arrays [Fig. 7(e)].[147] Figures 7(e) and 7(g) demonstrate the schematic diagram, scanning electron microscopy (SEM), and simulation of the LnNPs on Ag nanopillar arrays. The CW 664 nm upconverting lasing is achieved by pumping the substrates with 980 nm CW laser. The presence of Ag nanopillar arrays reduced the lasing threshold to 70 W cm^{-2} due to the intense electromagnetic near-field enhancement from the plasmonic metal [Fig. 7(h)].[147] The reported plasmon-nanoarray upconverting lasers provide directional, ultra-stable output at visible frequencies under NIR pumping, even after 6 h of constant operation, which offers prospects in previously unrealizable applications of coherent nanoscale light. Other plasmonic metals such as Au nanoparticles shelled with LnNPs can also achieve a relatively low upconversion lasing threshold (360 W cm^{-2} for 545 nm and 500 W cm^{-2} for 658 nm) when pumping with a 980 nm laser.[148] Future directions include further reducing the lasing threshold and improving stability by improving the integration between densely packed quantum emitters (LnNPs) and plasmonic nanocavities. Also, integrating these lasing platforms on chips is important to realize quantum-optical technologies and commercial lab-on-a-chip photonic devices.

Considering on-chip applications, achieving bright emission at the single particle level is critical. Meng *et al.* reported bright single LnNP upconversion at sub 0.5 W cm^{-2} irradiance by coupling the single upconversion LnNP to a single nanocavity mode (Au nanorod dimer) [Fig. 7(i)].[150] They used a single Yb^{3+}/Tm^{3+} doped LnNP in a nanocavity for single particle emission with 2.3×10^5 fold enhancement of UCL. For a single sub-30 nm upconversion LnNP, it can provide up to 560 detected photons per second at an ultralow excitation intensity of 0.45 W cm^{-2}.[150] The findings provide possibilities for advanced investigation of light–matter interactions and quantum optical phenomena down to the single-photon level.

Another common application for plasmonic enhanced LnNPs is sensing. Figures 7(k)–7(m) demonstrate an LnNP integrated perovskite photodetector for sensing narrow band NIR light.[152] Ji *et al.* designed a cascade optical field modulation, which consists of microlensing arrays (MLAs) with superlensing effect, a layer of Au nanorods with plasmonic effect, and upconversion LnNP films [Fig. 7(k)] for improving the upconversion efficiency when absorbing narrow band NIR light, including 808, 980, and 1540 nm.[152] The adaption of this cascading strategy was motivated by the consideration that MLAs can effectively confine far-field propagating incident light to a highly localized hotspot at the micrometer scale, while the Au NRs can tailor the photoelectric field spatially more precisely at the nanometer scale. Such a synergistic field tuning effect cannot be achieved solely using routine MLAs or Au NRs. By combining the superlensing and plasmonic effect, the upconversion enhancement factor can reach 2.4×10^4, 2.2×10^4, and 1.6×10^4-fold for 808, 980, and 1540 nm illumination, respectively. As a result, the photocurrents reached 12, 9, and 4.6 μA in MLA/Au NR/CSS photodetectors for 808, 980, and 1540 nm, while they were 0.03, 0.023, and 0.01 μA in pristine perovskite/LnNP photodetectors under corresponding excitations. The amplification factors of the photocurrent were estimated to be 410-fold for 808 nm, 390-fold for 980 nm, and 460-fold for 1540 nm light detection.[152]

To summarize this section, the application of plasmonic enhanced LnNP UCL has made great progress. Using the plasmonic effect of nano-metallic materials to enhance the luminescence of lanthanide elements by designing the structure, size, and shape of nanostructures has become a research trend. The local surface plasmon resonance (LSPR) effect of plasmonic NPs can influence the luminescence of materials in different aspects, including excitation enhancement induced by enhanced local field, emission enhancement induced by the Purcell effect, and quenching induced by energy transfer from Ln^{3+} to metals non-radiatively. Plasmonic NPs can also be used to modulate FRET between an excited donor and an acceptor. Though great progress has been made, there are still some unsolved shortcomings. In future studies, seeking for well-designed new constructions of plasmonic NPs, hybrid nanostructures, and coupling systems may be the ideal platform and the future trend to greatly enhance the absorption and luminescence of lanthanides.

D. Semiconducting quantum dots shelled heterostructures

1. Lanthanide nanoparticles–quantum dots

The integration of LnNPs with semiconducting QDs has been recently reported. Chu *et al.* prepared LnNP@$AgBiS_2$ CS heterostructures through ion exchange to improve the photothermal conversion efficiency of $AgBiS_2$ from 14.7% to 45% [Figs. 8(a) and 8(b)].[155] The $NaYF_4$:Yb/Er/Nd@$NaYF_4$:Nd with 1% Nd^{3+} doping concentration can excite the $AgBiS_2$ shell to produce ROS for photodynamic therapy of cancer cells. As a result, the CS heterostructure exhibits combined photothermal/photodynamic therapy against malignant tumors.[155] QDs can also sensitize lanthanides. Swabeck *et al.* coat the InP QD with a shell of Yb^{3+}-doped yttrium trifluoride ($Y_{1-x}Yb_xF_3$), and grow a final passivating shell of LnF_3 (Ln is Y or Lu). These CSS InP/$Ln_xY_{1-x}F_3$/ShF_3 (Ln = Yb, Nd; Sh = Lu, Y) nanocrystals exhibit a

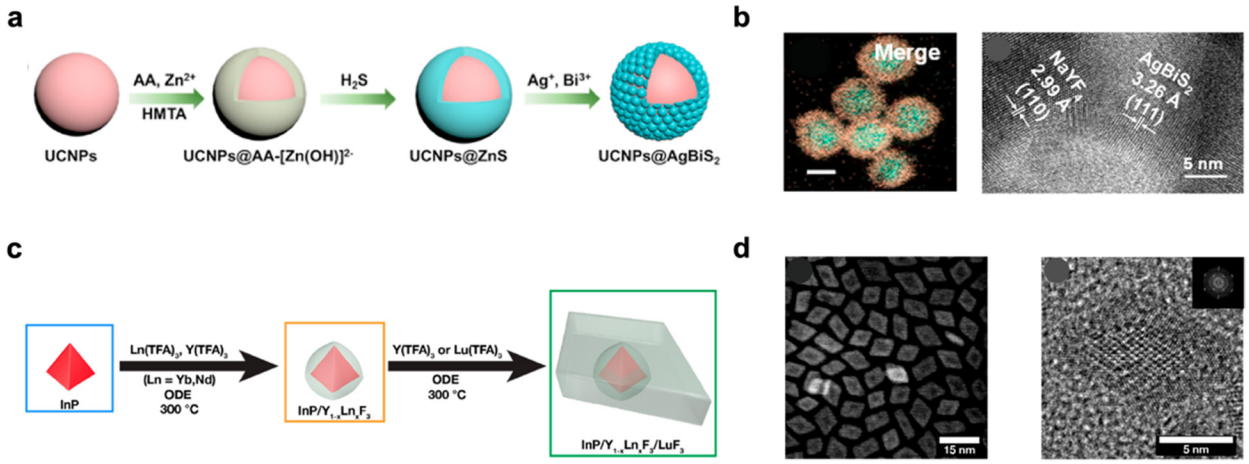

FIG. 8. Heterostructures formed by combining LnNPs with quantum dots. (a) Schematics of the synthesis of LnNP@$AgBiS_2$ CS heterostructures.[155] (b) Element distributions and TEM images of individual LnNP@$AgBiS_2$ CS heterostructures. (a) and (b) Reproduced with permission from Bioact. Mater. **17**, 71 (2022).[155] Copyright 2022 Elsevier. (c) Schematics of the synthesis of CSS InP/$Ln_xY_{1-x}F_3$/ShF_3 NPs.[156] (d) TEM images of the InP/$Ln_xY_{1-x}F_3$/ShF_3 NPs. (c) and (d) Reproduced with permission from J. Am. Chem. Soc. **140**, 9120 (2018).[156] Copyright 2018 American Chemical Society.

broadband absorption from InP core and a sharp absorption from Yb at 976 nm [Figs. 8(c) and 8(d)].[156]

2. Lanthanide nanoparticles–perovskites

Over the past decade, metal halide perovskites have gained significant attention, emerging as a leading material for photovoltaic applications and LEDs.[157–159] As a result, numerous researchers are exploring the integration of LnNPs with perovskites, aiming to optimize their optical performance.[160–162] Four strategies are listed below classified based on material structure.

The most straightforward method involves direct physical blending. For light harvesting, Guo *et al.* introduced β-$NaYF_4$:Yb^{3+}/Er^{3+}/Sc^{3+}@$NaYF_4$ upconversion LnNPs as a spectral converter into a TiO_2 mesoporous layer of perovskite solar cells to harvest and convert NIR photons to red and green ones.[62] The upconversion LnNPs broaden the absorption range of solar irradiation and generate extra photocurrent in the solar cells, leading to an increased power conversion efficiency (PCE) of 20.19% compared to the pristine device with an efficiency of 17.44%.[62] For light emission applications, Zhang *et al.* physically mixed $LiYbF_4$:Tm^{3+}@$LiYF_4$ nanoparticles with $CsPbX_3$ (X = Cl, Br, I) perovskite nanocrystals to fine-tune the upconversion luminescence in perovskite nanocrystals.[163] The perovskite nanocrystals are excited by radiation from energy transfer upconversion process in LnNPs [Figs. 9(a) and 9(b)].[163] Progressing toward organized nanostructures, the second approach can be realized by the design of superlattices. Cherniukh *et al.* demonstrated long-range-ordered perovskite-type superlattices containing $NaGdF_4$ LnNPs and $CsPbBr_3$ perovskite nanocrystals [Fig. 9(c)].[164] This was achieved by using the shortest-chain capping ligand, which maintained the colloidal stability and emissive properties of the perovskite nanocrystals. The resulting superlattices exhibited the collective behavior of superfluorescence, with great potential in ultrabright quantum light sources [Fig. 9(d)].[164] The third strategy employs an intermediary "adhesive" to combine LnNPs with perovskite nanocrystals. Francés-Soriano *et al.* developed an innovative strategy consisting of using cucurbituril to anchor the perovskite nanoparticles to the $NaYF_4$:Yb^{3+},Tm^{3+} upconversion LnNPs, leading to lanthanide-to-perovskite energy transfer efficiency approaching 100% under 975 nm excitation.[165] Estébanez *et al.* demonstrated the first 1D-ordered linear co-assemblies of perovskite nanocrystals and upconversion LnNPs, within an open peapod-like shell provided by a $PbSO_4$ polymer.[166] The perovskite PL lifetime controlled by the energy transfer rate can be adapted to the technological application desired.[166] Using mesoporous silica as the adhesive, Xie *et al.* achieved broadband photon detection covering x-ray, UV, visible, and NIR using an upconversion LnNP–perovskite nano-transducer, with the structure $NaYF_4$:Yb^{3+}/Tm^{3+}@$NaYF_4$ nanoparticles@$mSiO_2$@$MAPbX_3$ (X = Cl, Br, or I).[167]

The final method is the design of heterostructures with direct contact between semiconductors and lanthanides. LnNPs may be coated with perovskite shells by minimizing lattice mismatch by growing cubic phase α-$NaYF_4$:Yb,Tm onto cubic phase $CsPbBr_3$ NCs,[168] or hexagonal phase $NaYF_4$:Er,Yb onto hexagonal phase $CsMnCl_3$.[169] The cubic phase α-$NaYF_4$:Yb,Tm can be converted into hexagonal β-$NaYF_4$:Yb,Tm [Figs. 9(g) and 9(h)], where FRET may not occur between the perovskite and lanthanide systems.[168] Recently, our group demonstrated a mixed-phase LnNP@$CsPbBr_3$ CS heterostructure and successfully overcome the lattice mismatch between the β-phase core and α-phase shell by seeding ultrasmall LnNPs.[170]

E. Metal–organic framework combined heterostructures

Metal–organic frameworks (MOFs) are a class of crystalline materials that consist of coordination bonds between metal cations and multidentate organic linkers. The characteristic structure of MOFs features an open framework with high porosity, which can be modified to produce multifunctional materials with large surface areas, such as for loading of functional cargo in the pores. These characteristics nurture the integration of LnNPs with MOFs to form LnNP–MOF heterostructures with Janus,[171–175] core–satellite,[176–178] and core–shell[172,179–183] architectures

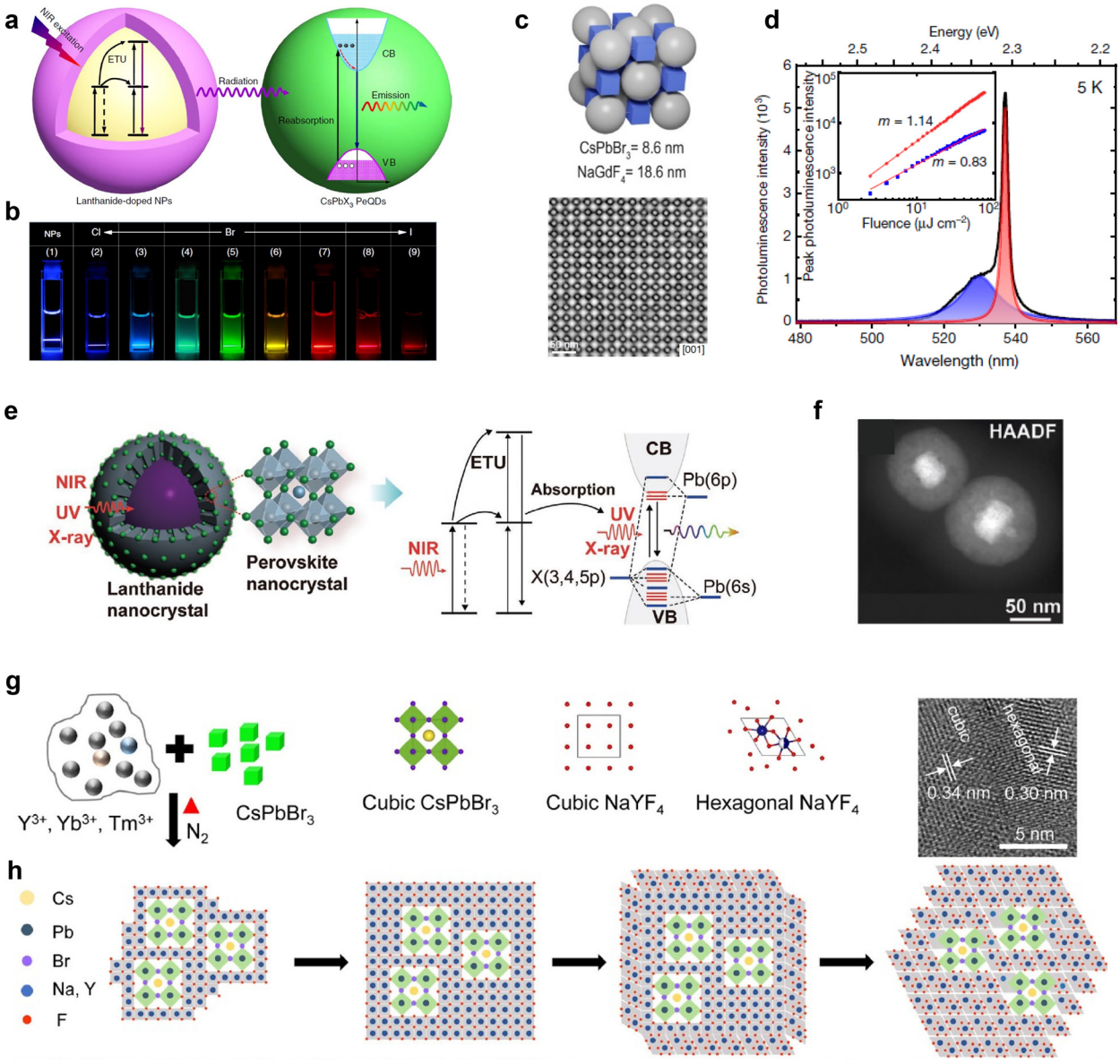

FIG. 9. Heterostructures formed by combining LnNPs with perovskites. (a) Schematics of the upconversion process in LnNPs blended with $CsPbX_3$ perovskite quantum dots.[163] (b) Photographs of the visible emission of the LnNP–$CsPbX_3$ mixtures under NIR excitations.[163] (a) and (b) Reproduced with permission from Nat. Commun. **9**, 3462 (2018).[163] Copyright 2018 Springer Nature. (c) Schematics (top) and high-resolution TEM image (bottom) of the perovskite-type superlattices containing $NaGdF_4$ and $CsPbBr_3$ perovskite nanocrystals.[164] (d) Superfluorescence spectrum from the $NaGdF_4$–$CsPbBr_3$ superlattices.[164] (c) and (d) Reproduced with permission from Nature **593**, 535 (2021).[171] Copyright 2021 Springer Nature. (e) Schematics and (f) HADDF image of the upconversion processes of the LnNP@$mSiO_2$@$MAPbX_3$ heterostructure. Reproduced with permission from Adv. Funct. Mater. **26**, 5131 (2016).[165] Copyright 2016 John Wiley and Sons. (g) Schematics of growing cubic phase α-$NaYF_4$:Yb,Tm onto cubic phase $CsPbBr_3$ NCs.[168] (h) Schematics of the CS watermelon-like nanostructures consisting of $CsPbBr_3$ quantum dots (watermelon seeds) embedded in hexagonal $NaYF_4$:Yb,Tm nanoparticles (watermelon pulp). Reproduced with permission from Nat. Commun. **12**, 219 (2021).[168] Copyright 2021 Springer Nature.

[Fig. 10(a)]. LnNP–MOF heterostructures have displayed a wide range of applications such as therapy,[182] imaging,[184] drug delivery and release,[181] detection of pH[185] and ROS,[179] photocatalysis,[177] and anti-counterfeiting.[186] Generally, the pores of MOFs are capable of loading photosensitizers, therapeutic drugs, and imaging probes; and stimuli-responsive ligands can be designed for the MOF skeleton to achieve pH-sensitivity or photo-sensitivity of the heterostructure. The energy interaction between LnNPs and MOFs is multifaceted. For example, the absorption of low energy photons by the LnNPs can be upconverted and then transferred to MOFs to activate the skeleton to generate ROS[173,180] [Figs. 10(b) and 10(c)]. Or the upconversion of LnNPs can activate the photoacid generator (pHP) encapsulated in MOFs cavities to trigger local pH

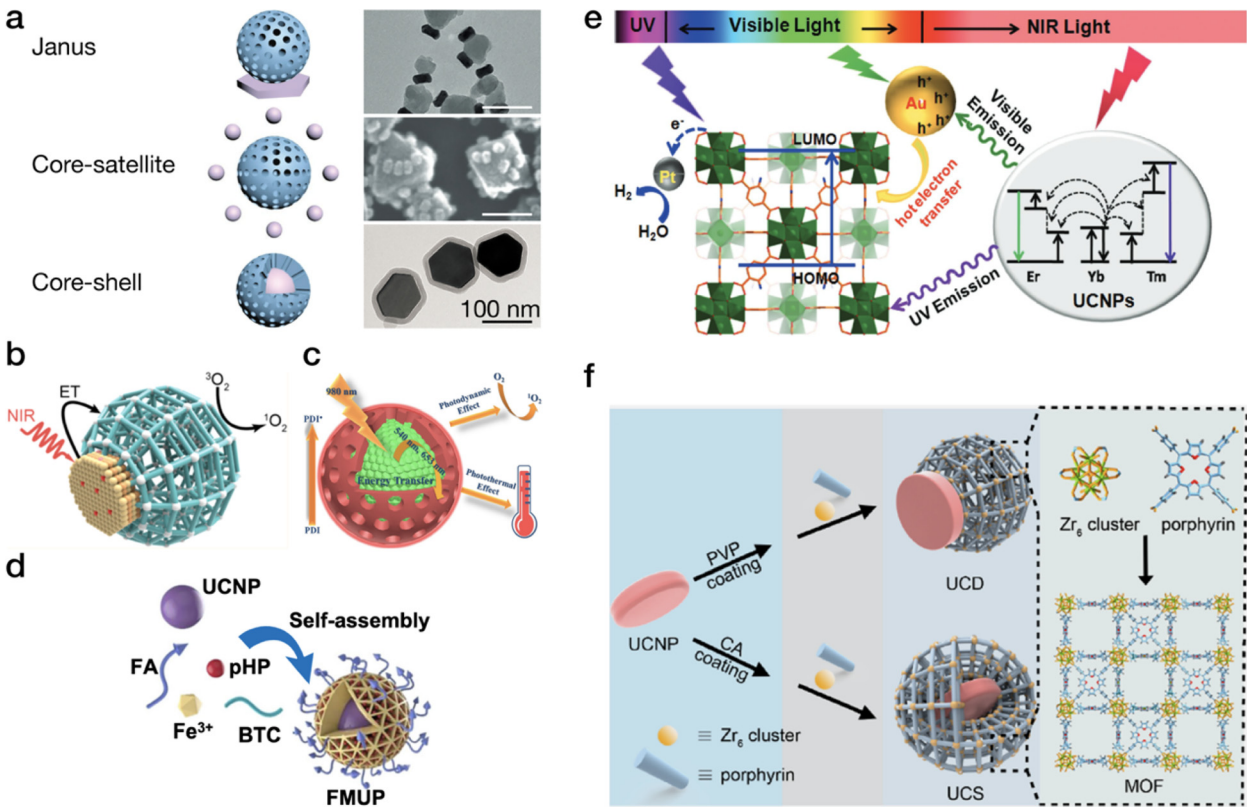

FIG. 10. (a) Schematic illustration of the LnNP–MOF heterostructures with Janus, core–satellite, and core–shell architectures. Reproduced with permission from Angew. Chem. Int. Ed. **59**, 2634 (2020).[174] Copyright 2020 John Wiley and Sons. Reproduced with permission from Nano Res. **15**, 7533 (2022).[178] Copyright 2022 Springer Nature. Reproduced with permission from J. Am. Chem. Soc. **141**, 19373 (2019).[179] Copyright 2019 American Chemical Society. (b) and (c) LnNP–MOF with energy transfer from LnNP to MOF skeleton to activate the generation of ROS. Reproduced with permission from J. Am. Chem. Soc. **139**, 13804 (2017).[173] Copyright 2017 American Chemical Society. Reproduced with permission from Angew. Chem. Int. Ed. **60**, 25701 (2021).[180] Copyright 2021 John Wiley and Sons. (d) CS LnNP–MOF with energy transfer from LnNP to photoacid generator that encapsulated in MOFs. Reproduced with permission from Nat. Commun. **12**, 6399 (2021).[182] Copyright 2021 Springer Nature. (e) Core–satellite LnNP–MOF with energy transfer from LnNP to both MOF and the anchored Au NPs. Reproduced with permission from Adv. Mater. **30**, 1707377 (2018).[177] Copyright 2018 John Wiley and Sons. (f) Comparison of energy transfer between Janus and CS LnNP-MOF heterostructures. Reproduced with permission from J. Am. Chem. Soc. **142**, 3939 (2020).[172] Copyright 2020 American Chemical Society.

changes and the secondary intracellular microenvironment adjustment[182] [Fig. 10(d)]. Alternatively, the energy can be transferred to both the MOFs and the loaded cargoes. In an Au NP loaded LnNP-Pt@MOF, the NIR light can be converted to UV and visible light and then transferred to UV-responsive MOF and visible light-responsive plasmonic Au NPs, achieving photocatalytic H_2 production by light harvesting in all UV, visible, and NIR regions[177] [Fig. 10(e)].

Typically, the smart control and intelligent response of LnNP–MOF heterostructures to analytes rely on energy transfer from LnNP to MOF to activate specific photochemical processes. An asymmetric Janus architecture [Fig. 10(a)] supports directional energy transfer from LnNP to MOF but is limited by low interfacial contact area. A core–satellite[187] and core–shell[172] structure with large contact areas provide better FRET efficiency [Fig. 10(f)]. The enhancement of absorption of lanthanides by forming LnNP–MOF heterostructures has been limited due to the misalignment of the absorption ranges of LnNP and MOF; however, this could be further studied to unlock new application scenarios.

III. ABSORPTION ENHANCEMENTS AND ENERGY TRANSFER IN LANTHANIDE-BASED HETEROSTRUCTURES

As mentioned previously, LnNPs suffer from low absorption cross sections and hence the formation of heterostructures comprised of a light absorbing unit to sensitize the LnNPs is the first key requirement to enhance the absorption of lanthanides. The light harvesting unit can be an organic dye, inorganic dye, semiconductor QD, or plasmonics, as summarized before. Table I gives a comparison and summary of the absorption enhancements in different heterostructures with some typical examples for each type.

Efficient energy transfer from the sensitizing unit to the LnNPs is another key requirement to create bright heterostructures. An LnNP contains many Ln^{3+} ions acting as individual energy centers, making energy transfer significantly more complicated than for conventional systems such as QDs or organic chromophores that generally are only able to host one excitation per particle. In this section, the key energy transfer or

TABLE I. Absorption enhancements comparison.

Category	LnNP	Heterostructure	Excitation wavelength (nm)	Emission enhancement factor	Reference
Organic dye	$NaYF_4$:Yb,Er	IR806	800	3300×	27
	$NaYF_4$:Gd,Yb@$NaErF_4$	IR806	808	33 000×	34
	$NaYF_4$:20%Yb,2%Er@$NaYF_4$:10%Yb	IR806	800	7×	59
	$NaYF_4$@NaYb F_4:12%Lu,8%Er@ $NaLuF_4$: y%Yb (y = 0, 0.1, 0.2, 0.3, 0.5, and 0.7)	IR806 (2)	808	0.3–70×	78
	$CsLu_2F_7$:Yb/Er	IR808	808	13.3×	67
	Li(Gd,Y)F_4:Yb,Tm@$LiYF_4$:Nd,Yb	IR808	800	87×	188
	$NaGdF_4$:Yb,Ho,Ce@$NaYF_4$:Nd,Yb	IR808	800	110×	188
	$NaErF_4$:2.5%Ce@$NaYbF_4$@$NaLuF_4$	IR808 dye brush polymer	808	675×	189
	$NaLuF_4$: Gd,Yb,Er@$NaLuF_4$:Yb,Pr	IR820 (2)	820	800×	84
	$NaLuF_4$:Gd,Yb, Tm@$NaLuF_4$:Gd,Yb@$NaLuF_4$:Yb	IR820 (2)	808	10×	84
	$NaYF_4$:Yb,Er@$NaYbF_4$@$NaYF_4$:Nd30%	ICG	700–860	4×	9
	$NaGdF_4$:20%Yb,25%Er@$NaYbF_4$: 10%Gd@$NaGdF_4$:20%Nd	ICG	808	23.5×	22
	$NaYF_4$:Nd20%	ICG	800	34×	93
	$NaYF_4$:20%Yb,2%Er@ $NaYF_4$:20%Nd	Alk-Pi	808	638×	85
	$NaYF_4$:Yb/Er/Ce@$NaYF_4$:Nd	AlkPi	808	40×	86
	$NaYF_4$:20%Yb,0.5%Tm@$NaYF_4$:20%Nd, 10%Yb	TPEO-820	808	102× UC, 8.5× DS	30
	$NaYF_4$:20%Yb, 2%Er	TPEO-Cy	793	800 000×	81
	$NaGdF_4$:Yb,Er@$NaGdF_4$:10%Yb,30%Nd	Cy754	754	680×	37
	$NaYF_4$:Yb,Nd,Er@$NaYF_4$:Nd	Cy7	808	17×	96
	$NaYF_4$:20%Yb,2%Er	Cy7.5	808	4820×	66
	$NaYF_4$:Yb20%,2%Er	1859-SL	808	21×	190
	$NaYF_4$:Yb, Er@$NaYF_4$: Yb	PDFT	808	0.3×	82
	$NaYbF_4$:8%Er@$NaLuF_4$:10%Yb@ $NaLuF_4$:30%Nd,10%Yb	SQ-739	730	51×	54
	$NaYF_4$:20%Yb,0.5%Tm	BODIPY-FL, Cy3.5, IR806	488, 517, 800, 980	100×	74
	CaF_2:30%Er	FITC	467	28×	191
	CaF_2:30%Yb@CaF_2:30%Nd	FITC	467	2100×	192
	$NaYF_4$:1%Pr20%Yb	Coumarin	397	30×	45
	$NaYF_4$:20%Nd	Ir1	300–550	130×	93
	$NaYF_4$:50%Yb, 12%Tb	DCDCS	405	2260×	28
	YbF_3, EuF_3	2,6-Naphtalenedicarboxylate	337	100×	193
	$NaYF_4$:15%Tb,10%Yb	Tripyridine dicarboxylic acid	320	330×	194
	La95%Eu5%F_3	$bipyCOO^-$	305	100×	195
Plasmonic	$NaYF_4$:Nd,Yb,Ho	Ag nanosphere	808, 980	15×	196
	$NaYF_4$:Yb,Tm	Au nanorods	980	27×	197
	$NaGdF_4$:Yb,Nd@$NaGdF_4$: Yb,Er@$NaGdF_4$	Au nanorods	808, 980	20×	198
	$NaYF_4$:Yb,Tm	Au shell	975	9×	199
	NaY_4:Yb,Er,Tm	Au and Ag shells	980	20×	200
	Lu_2O_3:Gd,Yb, Er	Ag nanospheres	980	30×	201
	$NaYF_4$:Yb,Er	Au disks	980	>1000×	202
	$NaYF_4$:Yb,Er	Au cap	980	>100×	203

TABLE I. (*Continued.*)

Category	LnNP	Heterostructure	Excitation wavelength (nm)	Emission enhancement factor	Reference
Semiconductor	YF_3:Yb/LuF_3	InP	440	Not reported, PLQE 0.1%–0.5%	156
	$NaYF_4$:Yb,Er	Ag_2S	808	17× (1550 nm)	204
	$NaYF_4$:Yb,Gd,Er@$NaYF_4$:Yb,Nd	Ag_2Se	808	18× (green)	205
Inorganic dye	$NaNdF_4$	PB	800	NA	120
	$NaErF_4$@$NaYF_4$@$NaNdF_4$	PB	800	NA	119

absorption enhancement pathways in LnNP@chromophore heterostructures will be discussed.

A. Organic dyes

LnNP@organic nanohybrids benefit from the high absorption cross section of the organic chromophore to sensitize the lanthanide luminescence. While enhancing the LnNP brightness, this process is furthermore advantageous as excited organic chromophores are prone to photoblinking and photobleaching, the latter causing irreversible damage to the chromophore. When connected to the Ln^{3+} ions, the excited state energy can be transferred onto the LnNP, which has high photostability and is considered free from photo-blinking and photobleaching.[206–208]

Upon excitation of the organic chromophore, the dye is generally excited from the singlet electronic ground state (S_0) to the singlet excited state manifold (S_n) after which rapid internal conversion and vibrational relaxation produce the first singlet excited electronic state (S_1) in its vibrational ground state according to Kasha's rules.[209] Several competing processes can deactivate the S_1 state: (i) fluorescence, $S_1 \rightarrow S_0 + hv$; (ii) internal conversion, $S_1 \rightarrow S_0$; (iii) ISC, $S_1 \rightarrow T_1$; and (iv) energy transfer to the LnNP, $S_1 + Ln^{3+} \rightarrow S_0 + (Ln^{3+})^*$. When the triplet excited state is produced, it can similarly undergo various deactivation processes back to the S_0 state: (i) ISC, $T_1 \rightarrow S_0$; (ii) phosphorescence, $T_1 \rightarrow S_0 + hv$; and (iii) energy transfer to the LnNP, $T_1 + Ln^{3+} \rightarrow S_0 + (Ln^{3+})^*$.[210]

The energy transfer in these organic–inorganic systems can occur via radiative [Fig. 11(a)] and non-radiative [FRET, Fig. 11(b)/Dexter, Figs. 11(c) and 11(d)] mechanisms,[211,212] both from the singlet and triplet excited state manifold of the organic chromophore. Discriminating between the exact sensitization mechanism is challenging as this is usually done on the basis of distance dependence studies, and such studies on LnNP@organic systems are rare. It is, however, of large importance to elucidate the mechanism(s) via which the energy transfer proceeds as the different mechanisms possess their own set of criteria that need to be optimized. We will briefly describe the fundamental principles of the main energy transfer mechanisms, followed by a discussion on the current consensus and debates in this field.

Radiative energy transfer corresponds to the donor, here the organic chromophore, emitting a photon that is subsequently absorbed by the acceptor, i.e., the Ln^{3+} ion in the LnNP [Fig. 11(a)]. The rate of radiative energy transfer $k_{DA,rad}$ is inversely proportional to the donor–acceptor distance R squared and hence can occur over long distances:[46]

$$k_{DA,rad} = \frac{\delta_A}{4\pi R^2 \tau_S} J. \tag{7}$$

Here, δ_A is the acceptor absorption coefficient, τ_S is the donor lifetime, and J is the spectral overlap term. Since the efficiency of this "reabsorption" process is correlated with the acceptor absorption coefficient δ_A, this energy transfer mechanism is generally inefficient for the systems discussed here due to the low absorption cross sections of the energy accepting Ln^{3+} ions.

Non-radiative energy transfer, on the other hand, can occur through Coulombic multipolar interactions in an FRET mechanism [Fig. 11(b)]. Here the organic chromophore donor releases its excited state energy to the ground state while the Ln^{3+} ion simultaneously gets excited. The rate of this type of energy transfer $k_{DA,FRET}$ has been shown to have a shallow distance dependence and can be described as[206]

$$k_{DA,FRET} = \frac{1}{\tau_D}\left(\frac{R_0}{R}\right)^s. \tag{8}$$

Here, τ_D is the donor excited state lifetime, R is the average distance between donor and acceptor, and R_0 is the Förster radius at which the energy transfer is 50% efficient. The coefficient s changes depending on the type of multipolar interaction: for the most common dipole–dipole interaction $s = 6$, for dipole–quadrupole interactions $s = 8$, and for quadrupole–quadrupole interactions $s = 10$. Electrostatic interactions beyond the most common dipole–dipole interactions were found to only have a minor contribution to the energy transfer and hence will not be discussed further. For the dipole-dipole transitions, R_0 can be described as[206]

$$R_0^6 = \frac{9\ln 10}{128\pi^5 N_A}\frac{k^2\Phi_D}{n^4} J. \tag{9}$$

Here, N_A is the Avogadro's number, k is the orientation factor, Φ_D is the quantum yield of the donor in the absence of FRET (i.e., acceptor), and n is the refractive index of the medium. The shallow distance dependence for dipole–dipole interactions allows FRET to efficiently occur over distances up to approximately 10 nm for most systems. J in this equation corresponds to the spectral overlap:[206]

$$J = \int F_D(\lambda)\varepsilon_A(\lambda)\lambda^4 d\lambda, \tag{10}$$

in which $F_D(\lambda)$ is the normalized emission spectrum of the donor and $\varepsilon_A(\lambda)$ is the molar absorption coefficient spectrum of the acceptor.

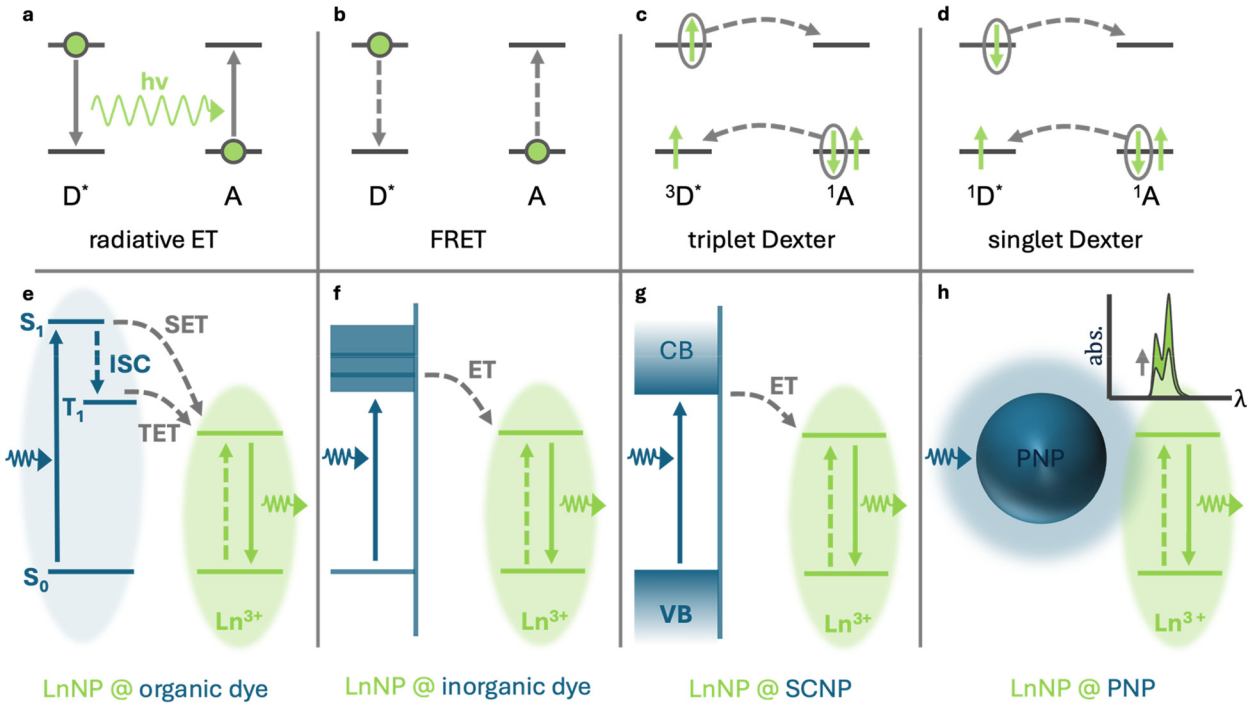

FIG. 11. Schematic illustration of (a) radiative energy transfer mechanism, (b) FRET energy transfer mechanism, (c) triplet-mediated Dexter energy transfer mechanism, and (d) singlet-mediated Dexter energy transfer mechanism. (e) Schematic illustration of the non-radiative energy transfer processes occurring from organic dyes to Ln^{3+} ions. Following excitation of the organic chromophore, singlet energy transfer (SET) to the Ln^{3+} ion or ISC can occur from the S_1 state. Triplet energy transfer (TET) can occur from the T_1 state to the Ln^{3+} ion. (f) Schematic illustration of the energy transfer process occurring from inorganic dyes to Ln^{3+} ions. Energy transfer (ET) from the continuous energy band of the inorganic dye to the ladder-like energy levels from the Ln^{3+} ion can occur. (g) Schematic illustration of the energy transfer processes occurring from semiconducting nanoparticles (SCNP) to Ln^{3+} ions. Energy transfer occurs from the conduction band (CB) of the SCNP and generally proceeds via a radiative or FRET mechanism. (h) Schematic illustration of the plasmon-enhanced absorption of Ln^{3+} ions. Upon excitation of the plasmonic nanoparticle (PNP) the local electric field is enhanced resulting in increased absorption of the Ln^{3+} ions as illustrated in the inset.

Despite the low absorption cross section of the Ln^{3+} ions, a simple calculation can show that FRET has the potential to occur with relatively large efficiencies even in LnNP@organic nanohybrid systems. Since FRET involves deexcitation of the organic excited state to the ground state through an electric–dipole transition, FRET is usually associated with singlet energy transfer as the transition from the triplet excited state manifold to the (usually) spin-singlet ground state is spin-forbidden. One could imagine that due to the heavy-atom effect or spin–exchange coupling, this triplet to singlet ground state transition might gain oscillator strength. However, to the best of our knowledge, no papers have investigated or observed FRET from triplet excited state to LnNPs.

Non-radiative energy transfer can also be governed by exchange interactions involving a double electron transfer mechanism, i.e., a Dexter mechanism. This consists of an excited electron from the organic chromophore donor transferring to the Ln^{3+} acceptor ion while, either in a concerted or in a two-step process, an electron from the Ln^{3+} ground state is transferred back to the organic donor [Figs. 11(c) and 11(d)]. As this process involves the actual exchange of electrons, wavefunction overlap between the donor and the acceptor is required and as such the rate of such non-radiative energy transfer $k_{DA,Dexter}$ has been found to have a strong, exponential distance dependence on the donor–acceptor distance (R):[206]

$$k_{DA,Dexter} = \frac{2\pi}{h} D J' \exp\left(\frac{-2R}{L}\right). \quad (11)$$

In this equation, D is the Dexter parameter, and L is the sum of the van der Waals radii of the donor and acceptor. This rate equation contains a spectral overlap term J' in which the acceptor absorption coefficient is also normalized, hence overcoming the bottleneck of the weak Ln^{3+} absorption. This energy transfer mechanism has predominantly been reported for triplet energy transfer. However, singlet energy transfer can occur through a Dexter mechanism too and has been reported in some systems to be dominant over an FRET mechanism at short donor–acceptor distances up to 1 nm.

While radiative energy transfer in LnNP@organic systems is unlikely, a straightforward method to differentiate between a radiative and non-radiative energy transfer mechanism is by studying the lifetime of the organic chromophore emission using readily available techniques such as time-correlated single photon counting (TCSPC) to measure the time-resolved photoluminescence. In the case of non-radiative energy transfer, an additional deactivation channel is activated for the organic chromophore, which will accelerate its decay and result in a shortening of the observed fluorescence lifetime. In the case of radiative energy transfer, this extra deactivation channel is absent.

Hence, a shortening of the observed fluorescence lifetime of the organic dye is indicative of non-radiative energy transfer.

Oftentimes, the energy transfer efficiency is quantified as $\phi_{ET} = 1 - \frac{\tau_{DA}}{\tau_D}$,[206,213] where τ_{DA} is the observed donor lifetime in the presence of the acceptor and τ_D is the observed lifetime in the absence of the acceptor, i.e., the Ln^{3+} ion. Most often when this equation is employed, τ_D is taken as the fluorescence lifetime of the uncoordinated donor, i.e., the uncoordinated organic dye. While this might seem valid at first glance, it does not consider the fact that coordination of an organic chromophore onto an LnNP is expected to result in changes to its intrinsic excited state dynamics. Thus, it is crucial to fairly compare the observed lifetime τ_{DA}, for example, by defining τ_D as the observed donor fluorescence lifetime upon coordination to an "inert" LnNP, i.e., an LnNP to which no energy transfer can occur. The equation must be used with caution, as changes to other non-energy transfer related pathways, such as ISC, will also affect lifetimes.

Non-radiative energy transfer can occur from either the singlet or triplet excited state [Fig. 11(e)]. The dominant energy transfer mechanism is usually highly distance dependent and hence can be hard to elucidate due to for example the lack of comparable molecules to carry out a distance-dependence energy transfer study with. A trend can be seen across many papers that the terms FRET and singlet energy transfer, as well as Dexter and triplet energy transfer, are used interchangeably. This is, however, not necessarily correct and the claims of an FRET/Dexter mechanism are generally not supported by proper distance dependence measurements, leaving the true nature of the energy transfer process elusive.

Although a topic of debate,[214] many initial reports in this field claimed that a Förster model alone is sufficient to describe energy transfer between organic dyes and Ln^{3+} ions due to the larger rate of energy transfer from the S_1 state in comparison to the ISC rate producing T_1 states.[27,210] This approach does, however, make the underlying assumption that singlet excitons are transferred primarily via an FRET type mechanism. Although this assumption might be correct, distance dependence measurements supporting this mechanism are generally lacking. Most papers that followed these seminal publications focused on optimizing the "FRET" rate, i.e., the singlet energy transfer process from the organic dye to the (often upconversion) LnNPs. Due to the requirement of spectral overlap for efficient FRET, only a limited number of dyes in the NIR spectral region have been reported, as described before.

Thus, overcoming the challenge of low absorption in LnNPs through the formation of LnNP@organic heterostructures shows great promise due to the high absorption cross section of most conjugated organic dyes as well as the high organic tunability. However, several key limitations remain that need to be taken care of. First, core-only LnNPs often suffer from high surface quenching, which is often overcome through the formation of CS structures where the emitter ions are doped in the LnNP core to prevent surface quenching.[26] A shelled structure, however, introduces a spatial gap between the organic chromophore and the LnNP. As the energy transfer can be highly distance dependent, this can significantly hamper energy transfer efficiency. Especially for Dexter type energy transfer, close proximity between the organic donor and the Ln^{3+} acceptor is crucial.

Second, the photostability of the organic dye on the LnNP has only been elucidated in a few recent studies.[55,79] Efficient energy transfer from the organic chromophore to the LnNP is expected to enhance the dye stability due to the reduction in excited state lifetime. However, no comprehensive studies have been performed looking into longer time dye stability on the LnNP as would be required for commercial applications. Similarly, the actual coordination of the organic dye onto the LnNP surface is largely unexplored and future work could focus on investigating the different anchoring methods (covalent bonding, physisorption, electrostatic, etc.) to optimize dye coordination.[26]

Finally, the number of organic dyes on the LnNP remains a key issue. For most organic dyes, which do not show aggregation-induced fluorescence, an upper limit of dyes per LnNP exists for which the energy transfer and subsequent brightness enhancements are optimal. This is a direct consequence of self-quenching occurring between organic chromophores if they are spatially too close to each other on the LnNP surface, thereby preventing energy transfer. This thus does not make optimal usage of the available LnNP surface and limits the overall absorption cross section of the LnNP@organic heterostructure.

Overall, besides the practical concerns discussed in the paragraphs above, the exact discrimination between the sensitization mechanisms at play in LnNP@organic heterostructure remains challenging.[215] Studies directly looking at whether the energy transfer process is singlet- or triplet-mediated via, for example, TAS while also monitoring the distance dependence of this process, i.e., multipolar-based or exchange mediated are scarce, and to the best of our knowledge, no such study for LnNP@organics has been reported to date. This is an important topic for further future exploration so that the design of these structures can be optimized according to the energetic requirements of the dominant energy transfer mechanism(s).

B. Inorganic dyes

The number of inorganic dyes that have been reported to sensitize the luminescence of LnNPs is limited. Inorganic dyes tend to have continuous excited state energy bands from which the energy transfer is expected to occur [Fig. 11(f)]. PB is the most common inorganic dye that has been reported to interact with LnNPs. This contrasts with organic dyes where only a limited number of individual dyes can generally be coordinated onto the LnNP surface. We have coated a layer of PB on NdNPs to construct NdNP@PB heterostructures [Fig. 12(e)].[120] The broad absorption spectrum of PB has excellent spectral overlap with the NdNPs. Following coating of the PB layer, we found a five to eight times enhancement of the absorption in the spectral region around 800 nm, which was able to subsequently induce greater photothermal conversion efficiency of the NdNPs [Fig. 12(f)]. Wang *et al.* fabricated a system composed of PB-coated $NaErF_4$@$NaYF_4$@$NaNdF_4$ nanocrystals. Here, the $NaErF_4$ core was incorporated as an imaging agent. The PB coating was found to enhance the absorption of this system by ninefold at 808 nm.

However, in contrast to enhancing particle brightness through sensitization as is the case for most LnNP@organic nanohybrids, these LnNP@PB systems have almost exclusively been reported for photothermal applications. Hence, instead of energy transfer, the PB in these systems has been reported to be responsible for enhancing non-radiative decay processes in LnNPs in order to enhance heat generation. This interaction between the LnNPs and the PB inorganic dyes is thus fundamentally different as for organic dyes. The inorganic PB dye was reported to induce new CR pathways in the NdNPs, thereby resulting in more heat generation and hence enhancing the

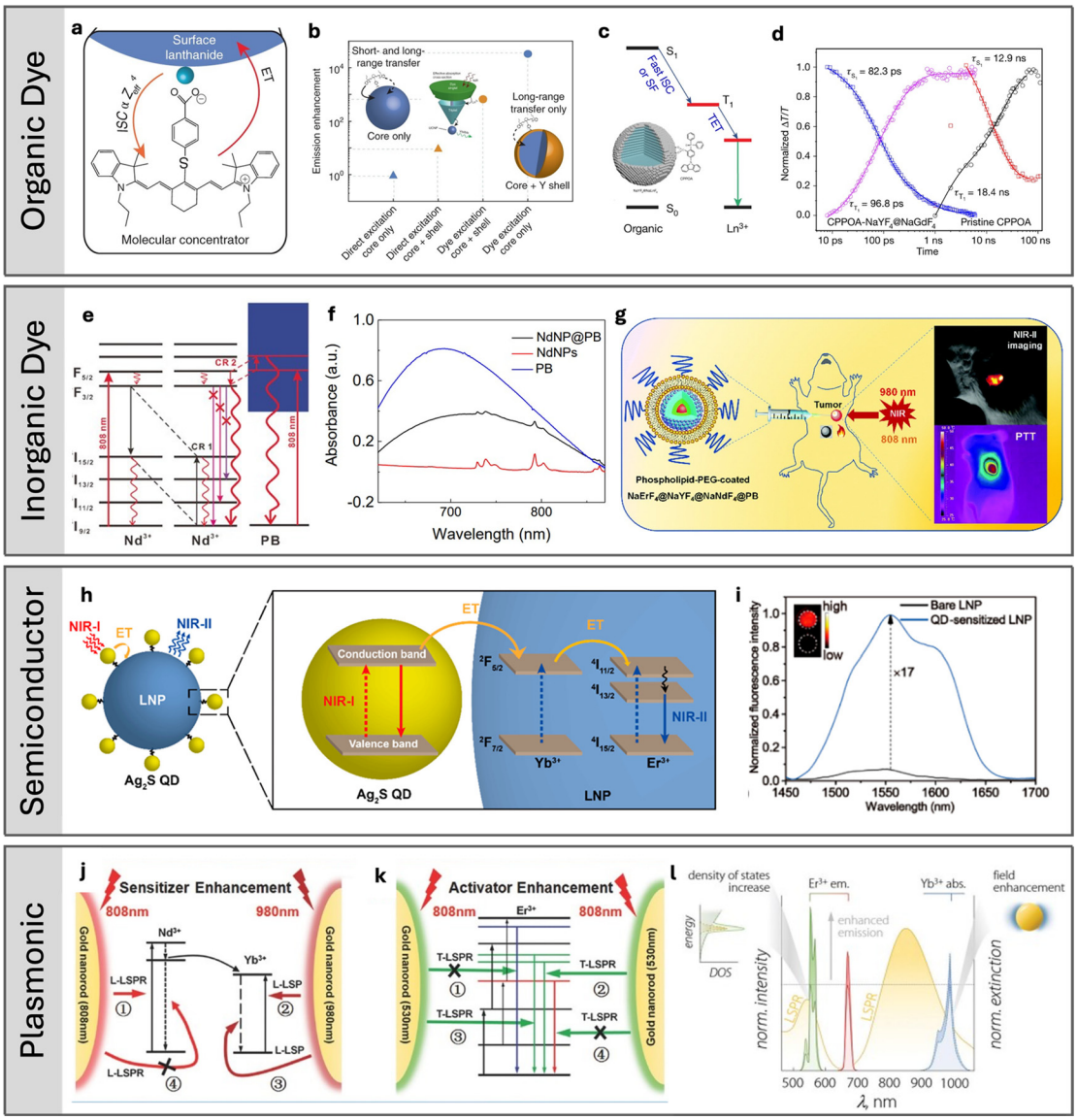

FIG. 12. (a) Magnified illustration of the interactions between IR806 and the surface of an LnNP, the heavy nucleus of the lanthanide aids in ISC from IR806 $S_1 \rightarrow T_1$ states.[34] (b) Emission enhancement from directly excited 30% Gd^{3+} LnNPs (blue triangle), directly excited 20% Gd^{3+} LnNP coated with a 1.2 nm YNP shell (orange triangle), the same CS LnNPs but dye-sensitized (orange circle), and IR806-sensitized 30% Gd^{3+} LnNPs (blue circle). Reproduced with permission from Nat. Photonics **12**, 402 (2018).[34] Copyright 2018 Springer Nature. (c) Simplified energy diagram showing triplet energy transfer (TET) from the molecular triplet state to lanthanide emitters (Ln^{3+}) following a fast ISC or singlet fission (SF) process.[35] (d) Kinetics showing the S_1 decay and T_1 growth of a solution containing pristine CPPOA molecules and of a solution of CPPOA-modified YNP@GdNPs. The ISC time decreases from 12.9 ns in the pristine CPPOA to 82.3 ps in CPPOA-modified YNP@GdNPs. Reproduced with permission from Nature **587**, 594 (2020).[35] Copyright 2020 Springer Nature. (e) Simplified diagrams of new cross-relaxation pathways between Nd^{3+} ions and PB.[120] (f) The absorption of NdNPs, PB, and NdNP@PB nanocomplex under the same concentration.[120] (g) A schematic illustration of CSS@PB nanocomposites with switched imaging and hyperthermia abilities for image-guided photothermal therapy (PTT). Reproduced with permission from Angew. Chem. Int. Ed. **58**, 8536 (2019).[120] Copyright 2019 John Wiley and Sons. (h) Schematic illustration of QD-sensitized LnNP system. Multiple Ag_2S QDs absorb NIR-I incident light and transfer excitation energy to the lanthanide ion pair (Yb^{3+}/Er^{3+}) in a single LnNP, where it is emitting the longer NIR-II wavelength.[204,241] (i) NIR-II fluorescence spectra and *in vitro* imaging of QD-sensitized LnNP and bare LnNP under 808 nm laser excitation. Reproduced with permission from Anal. Chem. **92**, 6094 (2020).[204] Copyright 2020 American Chemical Society. (j) LSPR-induced absorption enhancement for an Nd^{3+} ion upon excitation at 808 nm and for the Yb^{3+} ion upon excitation at 980 nm. The radiative decay rate of the Yb^{3+} ion is also accelerated by the LSPR overlapping the Yb^{3+} emission while that of the Nd^{3+} ion is not because of the fast phonon-mediated relaxation and energy migration to the Yb^{3+} ion.[198] (k) LSPR-induced green-emission enhancement for both Nd^{3+} and Yb^{3+} ions upon excitation at 808 nm. The blue and red emissions are not affected by the LSPR due to energy mismatch. Reproduced with permission from Adv. Funct. Mater. **27**, 1701842 (2017).[198] Copyright 2017 John Wiley and Sons. (l) Plasmon-enhancement in a Yb^{3+}/Er^{3+} upconversion system, where absorption due to local field enhancement and emission due to the Purcell effect are simultaneously enhanced. Reproduced with permission from Nanoscale Horiz. **6**, 209 (2021).[26] Copyright 2021 Royal Society of Chemistry.

photothermal conversion efficiency (60.8%) compared with NdNPs that were not decorated with PB (8.7%).

To explain this, we need to first understand the CR pathways at play in these systems. Nd^{3+} ions, as shown in Fig. 11, have ladder-like energy levels. Following excitation of a Nd^{3+} ion to one of its higher lying states, a second Nd^{3+} ion nearby in its ground state can induce a non-radiative recombination pathway through CR, where, for example, the $^4F_{3/2}$ to $^4I_{15/2}$ transition in the excited Nd^{3+} ion is accompanied by a transition from the ground state $^4I_{9/2}$ to $^4I_{15/2}$ state, after which both $^4I_{15/2}$ states can non-radiatively decay to the ground state while generating heat, giving rise to the photothermal effect. This type of CR can be controlled by tuning the lanthanide dopant concentration, with higher doping concentrations generally giving rise to more CR due to the shorter average distances between neighboring lanthanides.[120]

When coating a layer of PB onto the surface of such NdNPs, a new CR pathway is hypothesized between the PB and the NdNPs. PB is known to have continuous energy bands, and when excited upon being in contact with the NdNPs, the $^4F_{5/2}$ to $^4F_{3/2}$ non-radiative transition in the NdNPs can induce CR in the PB layer, making photons in the PB continuous excited state energy band jump from lower to higher energy. This is a much shorter CR pathway that will (i) generate more heat in the NdNPs and (ii) increase the Nd^{3+} population in the $^4F_{3/2}$ level, which can subsequently undergo the CR pathway described in the previous paragraph, thereby resulting in improved heat generation and enhanced photothermal capability in the heterostructure.[120]

Wang *et al.* produced PB-coated $NaErF_4@NaYF_4@NaNdF_4$ nanocrystals and reported a threefold enhancement of the photothermal conversion efficiency in comparison to the CSS particles without PB.[119] The ErNP core of the CSS NPs could produce luminescence at 1525 nm in the NIR-II window under 980 nm excitation. As the Er^{3+} ions are located in the NP core, high quantum yields were achieved due to suppressed surface quenching, thereby acting as a good imaging agent [Fig. 12(g)].

Like the system reported by our group,[120] excitation of the Nd^{3+} ions in the shell of the CSS nanoparticles could induce CR from the $^4F_{3/2}$ state, preventing its radiative decay and for each $^4F_{3/2}$ state produce two $^4I_{15/2}$ states that undergo rapid non-radiative decay to the ground state thereby dissipating the contained energy into heat. Again, following PB coating, a new CR from the $^4F_{5/2}$ to $^4F_{3/2}$ state was induced, thereby increasing the generation of $^4F_{3/2}$ states that can undergo the "conventional" Nd^{3+} CR and enhance heat generation.[119]

Thus, while the formation of LnNP@inorganic dye heterostructures has mostly been reported in the context of enhancing non-radiative recombination to induce heat generation in the LnNPs, it is obvious that the incorporation of inorganic dyes can induce transitions in LnNPs. Hence, energy transfer in these systems could be explored in future studies.

C. Plasmonics

Two strategies to increase the brightness of LnNPs have been addressed above. An alternative strategy to enhance their brightness is by SPR coupling.[145] A surface plasmon refers to the collective oscillation of free electrons at the interface between a dielectric material and metallic NPs. If the incident light aligns with the collective vibration frequency of the free electrons, the metal NPs have a strong absorption of the photon energy, forming a so-called LSPR that can be observed as an absorption peak in an absorption spectrum.[216]

The first example of SPR enhanced upconversion luminescence was reported by Feng *et al.* in 2009 who fabricated nanocomposites of the type Ag-nanowire-$NaYF_4$:Yb^{3+},Er^{3+} and showed that the Er^{3+} emission at 543 and 659 nm under 980 nm excitation could be enhanced by 3.7 and 2.3 times, respectively.[217] The underlying mechanism of the achieved enhancement remained elusive.

Nowadays, the consensus is that SPR coupling can enhance the LnNP brightness in three different ways: (i) through enhancing the incident light absorption [Fig. 11(h)], (ii) through enhancing energy transfer inside the LnNP, and (iii) through enhancing the Ln^{3+} emission. The essence of these enhancements is the resonance of the surface plasmon of the metal NPs with the light, resulting in an LSPR effect.[218] Which specific "brightness–enhancement" interaction is dominant depends largely on the spectral overlap between the surface plasmon resonance frequency and the absorption and emission frequencies of the LnNPs.

The first process, enhanced light absorption, is facilitated by coupling metallic NPs, which have an SPR aligned with the incident light frequency. When this condition is fulfilled, the surface plasmon restricts the incident light to the metallic NP surface, thereby enhancing the local electromagnetic field and creating "hot spots" in the vicinity of the metallic NPs.[218,219] When the local electromagnetic field (E) is enhanced, the absorption cross section (σ) of the Ln^{3+} ions in the LnNPs can directly be enhanced too when the electric field vector of the plasmon wave couples to the transition dipole in the LnNPs, which can result in enhanced light absorption by the LnNPs. This is a direct consequence of the absorption cross section being proportional to the square of the local external electric field:[218]

$$\sigma \propto \frac{|E|^2}{|E_0|^2}. \tag{12}$$

The actual luminescence intensity I of such upconversion LnNP can be estimated as follows:[218]

$$I \propto \sigma * |E|^2 * \phi_{ET} * \phi_A. \tag{13}$$

Here, ϕ_{ET} is the energy transfer efficiency and ϕ_A is the quantum yield of the emitter, i.e., activator ion. Thus when LnNPs are placed in the near vicinity of metallic NPs, the SPR effect can generate local hot spots, which can expand the incoming flux of incident light and thereby boost the absorption cross section of the LnNPs, which can subsequently result in a higher luminescence intensity of these particles.[220] Several examples of such absorption enhancements have been reported. For example, Chen *et al.* prepared Au/Ag alloyed films that were coupled with doped $NaYF_4$ films to reach upconversion luminescence enhancements of up to 180 times.[221]

Similarly, when the SPR oscillation frequency overlaps with the frequency of the emitted radiation from the LnNPs, the local state density of photons can be magnified, which has been reported to result in accelerated radiative decay rates.[222] These faster radiative transition rates of the LnNP activator ions will lead to increased luminescence, i.e., enhanced quantum yields of the emitter.[223] Fermi's golden rule describes the electronic transition rate γ to be directly proportional to the density of states:

$$\gamma = \frac{2\omega}{3\hbar\varepsilon_0}|\mu|^2\rho_{LDOS}(r,\omega), \tag{14}$$

where $\rho_{LDOS}(r,\omega)$ is the local photon density of states, h is the Planck constant, ε_0 is the vacuum dielectric constant, and μ represents the transition dipole moment associated with the electronic transition occurring at the frequency ω. The emergence of evanescent modes through plasmons leads to an increased photon state density and a higher rate of radiation attenuation. This phenomenon was known as the Purcell effect.[224] This can boost the LnNP emission and enhance their brightness. An example of this was reported by Priyam *et al.* who prepared $NaYF_4$:Yb,Er NPs that they shelled with Au metallic NPs and reported a luminescence intensity enhancement of the Er^{3+} emissions of —two to four times depending on the emission wavelength and reported the emission enhancement mechanism to be predominantly responsible for this.[225]

Finally, coupling LnNP with surface plasmons has been reported to reduce non-radiative losses primarily through improved energy transfer inside LnNPs between sensitizer and activator ions.[218] Sun *et al.* based on calculations reported a sixfold enhancement of the energy transfer when coupling Au pyramidal plasmon structures to $NaYF_4$:Yb,Er NPs.[144] Lu *et al.* later confirmed the role of the SPR effect in enhancing the energy transfer rate in an Ag nanograting (980 nm LSPR) coupled to $NaYF_4$:Yb^{3+},Er^{3+} upconversion LnNPs.[226] The researchers found that the energy transfer rate on a bare Ag film was zero. Upon comparison, they showed that the energy transfer rate of the coupled sample surpassed that of the reference sample, indicating an acceleration in the energy transfer rate. These findings confirm that the plasmon effect can enhance luminescence by accelerating the energy transfer process.

Oftentimes, two or three of the discussed enhancement mechanisms might be active simultaneously. For example, two groups reported composites of the type Au-nanorods@SiO_2@upconversion LnNPs and showed that both the absorption cross section and the emission could be simultaneously enhanced [Figs. 12(j)–12(l)].[198,227] The use of Au-nanorods allows for the effective use of both the transverse and longitudinal SPR wavelengths, where the longer longitudinal SPR wavelength was tuned to match the excitation wavelength of the sensitizer Ln^{3+} ions and the shorter transverse SPR wavelength was matched with the emission band of the activator Ln^{3+} ions. With any of these studies, it is important to keep in mind that the reported enhancement factors are highly dependent on the geometry of the plasmonic NP as well as the excitation power. The latter is especially relevant for upconversion, especially as the upconversion efficiency is a function of excitation power and hence reported enhancement factors are highly power dependent: the upconversion luminescence intensity depends quadratically on excitation power in the weak excitation limit and linearly in the strong limit.[228] This behavior is preserved in the presence of metallic NPs exhibiting SPRs, except that curves are shifted to lower power densities. Thus, it is crucial for the experimental conditions to be accurately reported so it can easily be identified whether measurements were conducted in the weak or strong excitation regime. Interestingly, based on rate equation analysis, Lu *et al.* concluded that enhancements in the strong excitation regime are primarily due to enhancements of the absorption cross section rather than emission or energy transfer enhancements. In the weak excitation regime, any three of the enhancement mechanisms were found to be able to be dominant.[228]

Furthermore, another key issue to pay attention to is the effect of the metallic plasmonic NP on the Ln^{3+} decay rate.[229] Non-radiative decay rates such as multiphonon emissions are not directly affected by the plasmonic NPs. However, if energy transfer from the LnNP to the metallic NP is possible, this can offer an alternative, in this case, non-radiative, decay pathway resulting in luminescence quenching.[218] This has experimentally been shown as the quantum yield decreases with decreasing separation between the metallic NPs and single LnNP.[230,231] Hence, in practice, a spacer such as SiO_2 is often applied between the plasmonic NPs and the LnNPs.[198]

D. Quantum dots

Since QDs are semiconductors, they have a strong broadband absorption above their bandgap. The bandgap of a QD is tunable via its size, shape, composition, and shell material.[232,233] This allows for the selection of the absorption profile that is best suited for the application at hand. Additionally, the tunability of the bandgap allows for changing the energy offset between the QD and the Ln^{3+} ion, which allows for engineering of the energy transfer rate. The donating semiconductor excited state can be localized excitonic levels, inter-bandgap levels, and charge trap states.[233,234] In here we will only discuss heterostructures where the QD and LnNP are "separated" rather than doping of semiconductor lattices with Ln^{3+} ions.

The use of QDs as sensitizer for LnNPs has been motivated partly by certain specific drawbacks of using organic dyes as sensitizers, which tend to suffer from poor stability. Compared with organic dyes, QDs possess certain superior photophysical properties, such as high quantum yields, easily tunable absorption, and especially a pronounced resistance to photobleaching.[234] While the energy transfer from QDs to LnNPs has mechanistically been largely unexplored, the reverse process has received more attention. The seminal publication reporting the energy transfer from LnNPs to QDs came from Bednarkiewicz *et al.* in 2010 who reported energy transfer from $NaYF_4$:Yb^{3+},Er^{3+} LnNPs to CdSe QDs, reporting an FRET efficiency of approximately 15%.[235] They claimed an FRET mechanism was mostly responsible for the energy transfer based on (i) the high spectral overlap between Er^{3+} emission and CdSe absorption and (ii) the decrease in donor lifetime upon the addition of CdSe. They calculated a critical R_0 distance of 1.5 nm and suggested the Er^{3+} ions on the surface to predominantly transfer energy to the CdSe QDs. A Dexter type mechanism was not discussed here but cannot be ruled out due to the long lifetimes of the Er^{3+} excited states and the wavefunction leakage of the QDs presumably allowing for sufficient wavefunction overlap.

The capability of upconverting LnNP to transfer energy to QDs has been widely demonstrated. In general, consensus seems to exist that a combination of radiative energy transfer and FRET is the dominant energy transfer mechanism in these type of systems [Fig. 11(g)].[236] The distance dependence of the rates of these processes differs and can be used to formally distinguish between the two types. Furthermore, FRET should result in quenching of the donor luminescence lifetime, which is often used to conclude that an FRET mechanism is active. Strictly speaking, however, a quenching of the luminescence lifetime does not necessarily indicate an FRET mechanism, and more studies should investigate the actual distance dependence of this multipolar energy transfer mechanism in order to design better, more efficient heterostructures of this type.

Regarding future directions, the preparation of CS structures of the type LnNP@QD or QD@LnNP might be beneficial to boost the brightness of the LnNPs. However, the lattice mismatch between the

two materials might hinder this approach from becoming widely applicable and optimization is required to successfully employ this strategy. Alternatively, coupling between pre-synthesized QDs and LnNP might prove beneficial as it allows for more straightforward fine-tuning of the properties of both moieties. The main drawback of the latter approach is the possible distance between the two types of particles not allowing for efficient energy transfer.

E. Metal–organic frameworks

Combining LnNPs with MOFs is a recent field. One of the main factors that held back this field for some time was the difficulty of fabrication methods to incorporate luminescent nanomaterials with MOFs.[237] MOFs are highly crystalline porous materials, and their open pore structure allows for the confinement of other materials inside their pores.[238]

These types of structures have so far not been reported to enhance the absorption of LnNPs. The flow of energy transfer in these systems generally occurs from the (often upconverting) LnNPs to the MOFs, and this interaction has been reported to primarily occur through an FRET type mechanism, with the LnNPs acting as an energy donor and molecular linker ligands in the MOFs framework as an energy acceptor.[238–240] These heterostructures bring LnNPs and MOFs in proximity in the nanoscale regime, thereby enabling efficient FRET. Upconversion FRET in these systems is reported to only occur within 10 nm distances, meaning that only those activator ions close to the LnNP surface can participate in FRET, while ions beyond that region are expected to be inactive. Thus, spatially confining Ln^{3+} ions near the surface of LnNPs through, for example, CS designs can boost the FRET efficiency.[238] So far using light absorbing MOFs as the chromophoric unit to sensitize Ln^{3+} ions has remained largely unexplored and could be a research direction to explore in future studies as the LnNPs inside MOFs have the potential to offer a unique materials platform.

While energy transfer is evident in many reported LnNP@chromophore heterostructures, as found from brightness enhancements, detailed energy transfer studies highlighting the mechanism via which the energy transfer proceeds are often lacking. A fair comparison between different types of sensitizers (organic dye vs inorganic dye vs PNP vs QD) has proven challenging due to the lack of consistency in reporting energy transfer efficiencies and brightness enhancements. There is a strong need for standardized procedures to determine emission enhancements as well as energy transfer efficiencies as current methods are unreliable, unclear, and difficult to compare. A more in-depth understanding of the mechanisms via which energy transfer proceeds ultimately resulting in brightness enhancements through absorption enhancements would allow for more effective heterostructure design.

IV. APPLICATION OF LANTHANIDE-BASED HETEROSTRUCTURES

A. Perovskite solar cells (PSCs)

Traditional perovskite-based solar cells exhibit limited efficiency in utilization of light beyond the visible region. Integration of LnNPs into these devices can extend this further into the NIR, harnessing more of the solar spectrum. For example, Song's group reported such a device ($LiYF_4$:Yb,Er/FTO/TiO_2/$MAPbI_3$/HTM/Au) in 2016 (Fig. 13).[242] The as-synthesized upconversion LnNPs produced red and green emission under photoexcitation of both 900–1000 and 1500–1600 nm. Therefore, the power conversion efficiency (PCE) performance of the device was improved. Subsequent works improve the NIR light harvesting using CS nanocrystals[243] and plasmonic

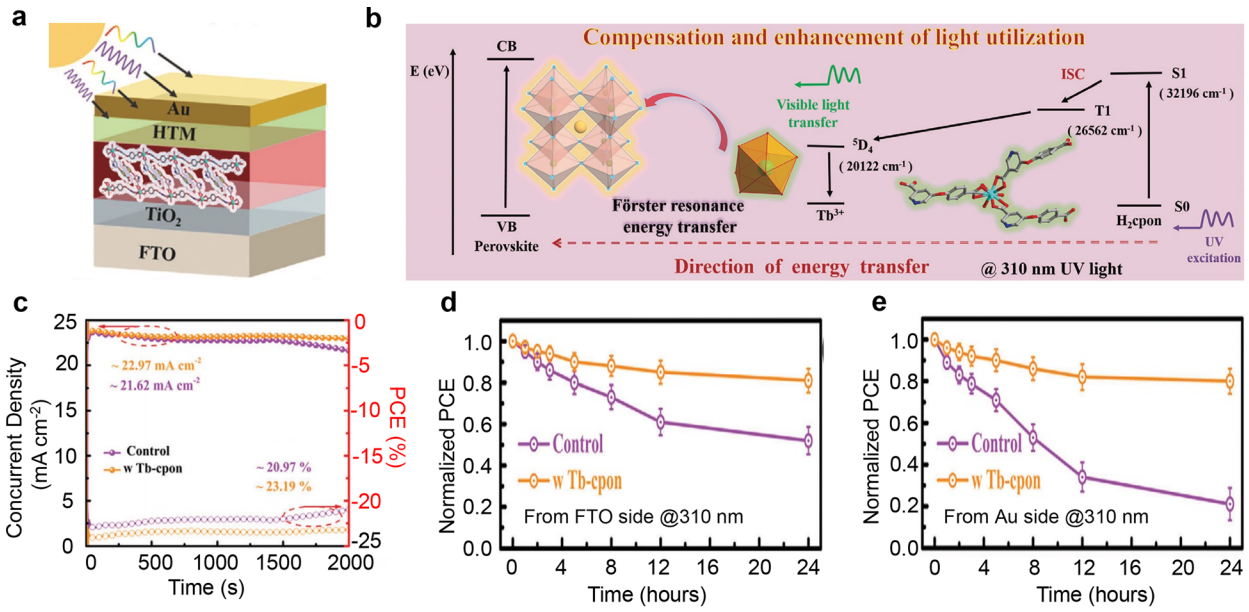

FIG. 13. (a) Schematic structure of Tb-cpon [H_2cpon stands for 5–(4-carboxy-phenoxy)-nicotinic acid)] doped PSC. (b) Energy transfer diagram between Tb-cpon and perovskite. (c) Stability of the different PSCs tracked at MPP for 2000 s. Long-tcpon under 310 nm UV light (d) from FTO side and (e) from Au side. (a)–(e) Reproduced with permission from Adv. Mater. **35**, 2306140 (2023).[244] Copyright 2023 John Wiley and Sons.

enhancement combined with dye-sensitization resulted in a record upconversion enhanced perovskite solar cell efficiency of 20.5%.[61]

B. Near-infrared photodetectors

Surface passivation, photonic crystal engineering, plasmonic/organic antennas, and the superlensing effect of dielectric optical microstructures have been explored to boost the upconversion luminescence and decrease the pumping threshold of upconversion LnNPs. For example, Liu and coworkers developed NIR photodetectors using perovskite films and $NaYF_4$:Yb,Er@$NaYF_4$@$NaYF_4$:Yb,Nd,Tm, which were capable of selective detection at 808, 980, and 1540 nm with response times around 100 ms.[152] They utilized a cascade optical field modulation strategy based on both the superlensing effect of dielectric microlens arrays and the plasmonic effect of gold nanorods to deliver upconversion enhancement of more than four orders of magnitude under weak light irradiation.

C. Bio-applications

Lanthanide-based heterostructures have been demonstrated in a variety of bio-applications, such as bioimaging,[176] bio-detection,[179,245] antibacterial,[180] phototherapy,[173,246] or drug delivery.[181,247] Early in 2015, Tang and coworkers reported upconversion LnNP@MOF nanostructures by coating $NaYF_4$:Yb,Er cores with amino-functionalized iron carboxylate MOF shells for optical and T_2-magnetic response (MR) bimodal imaging [Fig. 14(a)].[176] The LnNP@MOF was functionalized with PEG-folic acid (FA), which enabled selective uptake by the folate receptor overexpressed in HeLa cells. Owing to the excellent NIR optical property of the LnNP and the T_2-magnetic response (MR) imaging property of the MOF shell, respectively, in the nanostructures, LnNP@MOF exhibited significant targeted luminescence/MR imaging both *in vitro* and *in vivo*. Integration of lanthanide with Au, MnO_2, MOF, and QDs enables detection of biomolecules, including ROS,[179,245] pH,[248] metal ions,[249] proteins,[250] and glucose,[251], with different sensitivity and selectivity. Kuang *et al.* reported an upconversion LnNP core and a chiral NiSx NPs-decorated MOF shell for the detection of hydrogen peroxide (H_2O_2).[179] Reactive oxygen species (ROS), such as superoxide ($O_2\bullet^-$), H_2O_2, hydroxyl radicals (•OH), and hypochlorite (ClO^-), play critical roles in many physiological and pathological processes. Accurate and rapid determination of ROS levels is thus of great importance. The NiSx NPs showed a circular dichroism signal, which sensitively and selectively responded to H_2O_2 with a limit of detection three orders of magnitude lower than the H_2O_2 level in human blood plasma [Figs. 14(b) and 14(c)]. We recently reported a dye-sensitized lanthanide nanoprobe [$NaGdF_4$:Nd/ICG; indocyanine green (ICG)] for *in vivo* activatable imaging of ClO^-.[70] ICG sensitization not only delivers a fivefold NIR-II enhancement compared to the ICG-free counterpart but taking advantage of dye oxidation allows for activatable NIR-II imaging of ClO^- in a drug-induced lymphatic inflammation mouse model.

In addition, lanthanide-based heterostructures can also be utilized for bacterial inhibition,[180] phototherapy,[173,246] and drug delivery carriers.[181,247] For example, Liu and coworkers designed function-oriented CS nanostructures (LnNPs/HOF) for NIR-responsive bacterial inhibition.[180] The upconversion LnNP core excited the perylenediimide-based hydrogen-bonded organic framework (HOF)

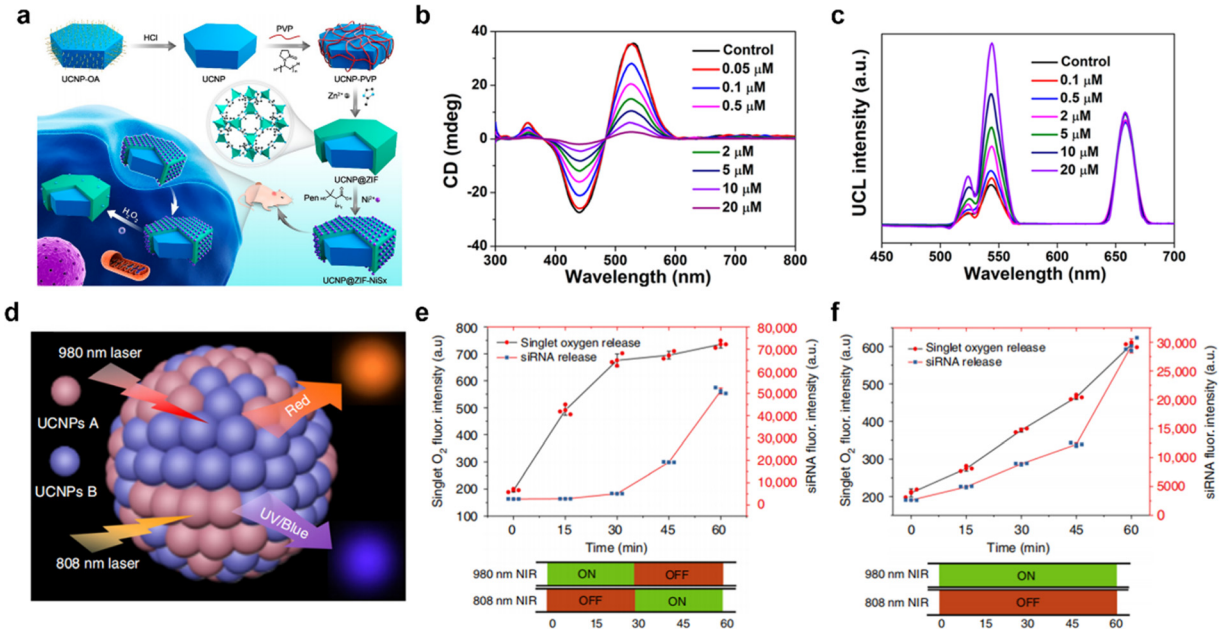

FIG. 14. (a) ROS detection using upconversion LnNP@MOF-NiSx nanoassemblies.[179] (b) CD and (c) UCL spectra of the nanoassemblies responded to different concentrations of H_2O_2 *in vitro*.[179] Reproduced with permission from J. Am. Chem. Soc. **141**, 19373 (2019).[179] Copyright 2019 American Chemical Society. (d) Schematic illustration of orthogonal excitation superballs with mixed LnNPs A and B.[247] (e) Orthogonal activation of singlet oxygen production and siRNA release from OP-SBs@azo-Psi over time.[247] (f) Non-orthogonal activation of singlet oxygen production and siRNA release from Control-SBs@azo-Psi over time.[247] Reproduced with permission from Nat. Commun. **10**, 4586 (2019). Copyright 2019 Springer Nature.

"shell" through resonance energy transfer to achieve significant photothermal effect and singlet oxygen generation. The photothermal conversion efficiency of 48.3% and strong singlet oxygen generation capabilities offered excellent NIR-responsive bacterial inhibition toward *Escherichia coli*. Zhang and coworkers further reported 808 nm-activated upconversion nanoparticles/HOF nanocomposites for NIR-II imaging-guided cancer therapy [Fig. 14(d)].[246] Specifically, 808 nm was employed to control the release of siRNA from the upconversion LnNP clusters to knockdown the unwanted genes, whereas 980 nm was employed to trigger singlet oxygen release for cancer therapy [Figs. 14(e) and 14(f)].[247] Hence, significantly higher therapeutic efficacy was achieved both in *in vitro* and *in vivo* compared to conventional, non-programmed activation.

V. PERSPECTIVE AND CONCLUSIONS

The formation of lanthanide-based heterostructures to enhance and broaden the absorption of lanthanides will greatly boost their brightness or energy conversion efficiency and enrich the functionalities. Despite the exciting advancements in the field, challenges still remain for both the synthesis and applications of lanthanide-based heterostructures. First, dedicated studies on the structure–function relationship of lanthanide-based heterostructures have yet to be explored. Considering the formation mechanism fundamentally affects their performance, detailed experiments and mechanistic studies to understand this may inspire more synthetic approaches to meet the demands of applications. Second, energy transfer pathways between lanthanides and the counterparts remain debated and dedicated distance dependence measurements are needed to elucidate the active energy transfer mechanisms. Moreover, a general protocol should be developed to properly measure the corresponding energy conversion efficiencies to allow for fair and straightforward comparison between systems. Most lanthanides feature narrow-band emissions with low intensity and their emissions can be further reduced by competing processes such as non-radiative CR and migration to surface defects. TAS that characterizes the excited state dynamics of lanthanide-based heterostructures can give deeper insights into the underlying mechanisms enhancing the lanthanide absorption and light conversion performance. Third, the stability of lanthanide-based heterostructures needs to be further investigated and improved. Factors such as oxygen, water, and sunlight may degrade their stability. This is especially important for their bio-related applications. Most of the currently developed lanthanide-based heterostructures cannot be utilized directly in biological systems without surface modification. Although approaches have been developed and improve the surface modification of lanthanide-based nanocrystals, the outcome is far from satisfactory, especially for clinical translation. The weak interaction between hydrophilic surface ligands and lanthanide ions causes the detaching of the coating from the particles and consequent aggregation. Therefore, methods to impart the lanthanide-based heterostructures with enhanced biocompatibility are worthy of more detailed studies.

In summary, this review article has classified five types of lanthanide-based heterostructures, compared the enhancement of absorption by fabricating these heterostructures, discussed the energy transfer pathways, mechanisms, and efficiencies between LnNP and the chromophore counterparts, and introduced the existing and potential applications for the heterostructures. We have also highlighted the existing misalignment and inappropriate comparison in different systems to give a clear guidance to evaluate the energy transfer dynamics and energy conversion efficiencies of the synthesized heterostructures. Overall, the fabrication of lanthanide-based heterostructures still serves as the most effective way to enhance the weak absorption of lanthanides and boost the lanthanide emission. We hope that this review will inspire more studies on lanthanide-based heterostructures with novel nanostructures and excellent energy conversion performance.

SUPPLEMENTARY MATERIAL

See the supplementary material for structures of dyes used to sensitize lanthanide-doped nanoparticles.

ACKNOWLEDGMENTS

Z.Y. acknowledges funding from UKRI Postdoctoral Individual Fellowships (Grant No. EP/X023133X/1). L.v.T. acknowledges funding from the Winton Programme for the Physics of Sustainability and from the EPSRC. A.T. acknowledges support from the EPSRC Cambridge NanoDTC (No. EP/L015978/1). R.A. acknowledges support from St. John's College Cambridge, the Rutherford Foundation of the Royal Society Te Apārangi of New Zealand, and the Winton Programme for the Physics of Sustainability. Y.Z. acknowledges funding from the National Natural Science Foundation of China (No. 22322406).

AUTHOR DECLARATIONS

Conflict of Interest

The authors have no conflicts to disclose.

Author Contributions

Alasdair Tew and Lars van Turnhout contributed equally.

Alasdair Tew: Writing – original draft (equal); Writing – review & editing (equal). **Lars van Turnhout:** Writing – original draft (equal); Writing – review & editing (equal). **Yunzhou Deng:** Writing – original draft (equal); Writing – review & editing (equal). **Rakesh Arul:** Writing – original draft (equal); Writing – review & editing (equal). **Junzhi Ye:** Writing – original draft (equal); Writing – review & editing (equal). **Tianjun Liu:** Writing – original draft (equal). **Zhao Jiang:** Writing – original draft (equal); Writing – review & editing (equal). **Linjie Dai:** Writing – original draft (equal). **Huangtianzhi Zhu:** Writing – original draft (equal); Writing – review & editing (equal). **Yan Zhang:** Writing – original draft (equal); Writing – review & editing (equal). **Akshay Rao:** Conceptualization (equal); Supervision (equal); Writing – review & editing (equal). **Zhongzheng Yu:** Conceptualization (equal); Supervision (equal); Writing – original draft (equal); Writing – review & editing (equal).

DATA AVAILABILITY

Data sharing is not applicable to this article as no new data were created or analyzed in this study.

REFERENCES

[1]Z. Yu, W. K. Chan, and T. T. Y. Tan, "Neodymium-sensitized nanoconstructs for near-infrared enabled photomedicine," Small **16**, 1905265 (2020).
[2]Y. Zhang, W. Wei, G. K. Das, and T. T. Y. Tan, "Engineering lanthanide-based materials for nanomedicine," J. Photochem. Photobiol. C **20**, 71 (2014).

[3]Z. Jiang, L. He, Z. Yang, H. Qiu, X. Chen, X. Yu, and W. Li, "Ultra-wideband-responsive photon conversion through co-sensitization in lanthanide nanocrystals," Nat. Commun. **14**, 827 (2023).
[4]L. Vijayalakshmi, K. N. Kumar, K. S. Rao, and P. Hwang, "Tunable color emission via energy transfer in co-doped Ce^{3+}/Dy^{3+}:Li_2O-LiF-B_2O_3-ZnO glasses for photonic applications," Opt. Mater. **72**, 781 (2017).
[5]J.-C. G. Bünzli and S. V. Eliseeva, in *Lanthanide Luminescence: Photophysical, Analytical and Biological Aspects*, edited by P. Hänninen, H. Härmä, P. Hänninen, and H. Härmä (Springer Science & Business Media, Berlin, Heidelberg, 2011), p. 1.
[6]N. M. Idris, M. K. Jayakumar, A. Bansal, and Y. Zhang, "Upconversion nanoparticles as versatile light nanotransducers for photoactivation applications," Chem. Soc. Rev. **44**, 1449 (2015).
[7]A. Gnach, T. Lipinski, A. Bednarkiewicz, J. Rybka, and J. A. Capobianco, "Upconverting nanoparticles: Assessing the toxicity," Chem. Soc. Rev. **44**, 1561 (2015).
[8]Z. Jiang, Z. Yang, and W. Li, "Self-luminous probe with one-step energy conversion from bioluminescence to NIR-IIb," Adv. Healthc. Mater. **12**, e2302089 (2023).
[9]W. Shao, G. Chen, A. Kuzmin, H. L. Kutscher, A. Pliss, T. Y. Ohulchanskyy, and P. N. Prasad, "Tunable narrow band emissions from dye-sensitized core/shell/shell nanocrystals in the second near-infrared biological window," J. Am. Chem. Soc. **138**, 16192 (2016).
[10]J. Huang, J. Li, X. Zhang, W. Zhang, Z. Yu, B. Ling, X. Yang, and Y. Zhang, "Artificial atomic vacancies tailor near-infrared II excited multiplexing upconversion in core-shell lanthanide nanoparticles," Nano Lett. **20**, 5236 (2020).
[11]Y. Fan, P. Wang, Y. Lu, R. Wang, L. Zhou, X. Zheng, X. Li, J. A. Piper, and F. Zhang, "Lifetime-engineered NIR-II nanoparticles unlock multiplexed in vivo imaging," Nat. Nanotechnol. **13**, 941 (2018).
[12]Y. Zhong, Z. Ma, F. Wang, X. Wang, Y. Yang, Y. Liu, X. Zhao, J. Li, H. Du, M. Zhang, Q. Cui, S. Zhu, Q. Sun, H. Wan, Y. Tian, Q. Liu, W. Wang, K. C. Garcia, and H. Dai, "In vivo molecular imaging for immunotherapy using ultra-bright near-infrared-IIb rare-earth nanoparticles," Nat. Biotechnol. **37**, 1322 (2019).
[13]Z. Jiang, L. He, X. Yu, Z. Yang, W. Wu, X. Wang, R. Mao, D. Cui, X. Chen, and W. Li, "Antiangiogenesis combined with inhibition of the hypoxia pathway facilitates low-dose, X-ray-induced photodynamic therapy," ACS Nano **15**, 11112 (2021).
[14]J. Li, J. Huang, Y. Ao, S. Li, Y. Miao, Z. Yu, L. Zhu, X. Lan, Y. Zhu, Y. Zhang, and X. Yang, "Synergizing upconversion nanophotosensitizers with hyperbaric oxygen to remodel the extracellular matrix for enhanced photodynamic cancer therapy," ACS Appl. Mater. Interfaces **10**, 22985 (2018).
[15]Z. Yu, Y. Y. Chun, J. Xue, J. Z. Y. Tan, W. K. Chan, W. Cai, Y. Zhang, and T. T. Y. Tan, "Balancing the thickness of sensitizing and inert layers in neodymium-sensitized tetralayer nanoconstructs for optimal ultraviolet upconversion and near-infrared cross-linked hydrogel tissue sealants," Biomater. Sci. **8**, 2878 (2020).
[16]Y. Zhang, W. Zhang, K. Zeng, Y. Ao, M. Wang, Z. Yu, F. Qi, W. Yu, H. Mao, L. Tao, C. Zhang, T. T. Y. Tan, X. Yang, K. Pu, and S. Gao, "Upconversion nanoparticles-based multiplex protein activation to neuron ablation for locomotion regulation," Small **16**, e1906797 (2020).
[17]Y. Ao, K. Zeng, B. Yu, Y. Miao, W. Hung, Z. Yu, Y. Xue, T. T. Y. Tan, T. Xu, M. Zhen, X. Yang, Y. Zhang, and S. Gao, "An upconversion nanoparticle enables near infrared-optogenetic manipulation of the *Caenorhabditis elegans* motor circuit," ACS Nano **13**, 3373 (2019).
[18]Y. Chen, J. Zhang, X. Liu, S. Wang, J. Tao, Y. Huang, W. Wu, Y. Li, K. Zhou, X. Wei, S. Chen, X. Li, X. Xu, L. Cardon, Z. Qian, and M. Gou, "Noninvasive in vivo 3D bioprinting," Sci. Adv. **6**, eaba7406 (2020).
[19]Y. Zhang, Z. Yu, J. Li, Y. Ao, J. Xue, Z. Zeng, X. Yang, and T. T. Y. Tan, "Ultrasmall-superbright neodymium-upconversion nanoparticles via energy migration manipulation and lattice modification: 808 nm-activated drug release," ACS Nano **11**, 2846 (2017).
[20]C. Lee, E. Z. Xu, Y. Liu, A. Teitelboim, K. Yao, A. Fernandez-Bravo, A. M. Kotulska, S. H. Nam, Y. D. Suh, A. Bednarkiewicz, B. E. Cohen, E. M. Chan, and P. J. Schuck, "Giant nonlinear optical responses from photon-avalanching nanoparticles," Nature **589**, 230 (2021).
[21]S. Cui, L. Tao, W. K. Chan, D. Zhou, Z. Yu, and W. Xu, "Tunable concentration-dependent upconversion and downconversion luminescence in $NaYF_4$:Yb^{3+}, Er^{3+}@$NaYF_4$:Yb^{3+}, Nd^{3+} core-shell nanocrystals for a dual-mode anti-counterfeiting imaging application," Opt. Lett. **47**, 2814 (2022).
[22]Z. Yu, C. K. Lim, W. K. Chan, Y. Chen, W. Shao, Y. Zhang, P. N. Prasad, and T. T. Y. Tan, "Dye-sensitized lanthanide-doped upconversion nanoparticles for water detection in organic solvents," ACS Appl. Nano Mater. **4**, 14069 (2021).
[23]X. Chen, L. Jin, W. Kong, T. Sun, W. Zhang, X. Liu, J. Fan, S. F. Yu, and F. Wang, "Confining energy migration in upconversion nanoparticles towards deep ultraviolet lasing," Nat. Commun. **7**, 10304 (2016).
[24]L. Jin, X. Chen, Y. Wu, X. Ai, X. Yang, S. Xiao, and Q. Song, "Dual-wavelength switchable single-mode lasing from a lanthanide-doped resonator," Nat. Commun. **13**, 1727 (2022).
[25]W. Wei, G. Chen, A. Baev, G. S. He, W. Shao, J. Damasco, and P. N. Prasad, "Alleviating luminescence concentration quenching in upconversion nanoparticles through organic dye sensitization," J. Am. Chem. Soc. **138**, 15130 (2016).
[26]R. Marin, D. Jaque, and A. Benayas, "Switching to the brighter lane: Pathways to boost the absorption of lanthanide-doped nanoparticles," Nanoscale Horiz. **6**, 209 (2021).
[27]W. Q. Zou, C. Visser, J. A. Maduro, M. S. Pshenichnikov, and J. C. Hummelen, "Broadband dye-sensitized upconversion of near-infrared light," Nat. Photonics **6**, 560 (2012).
[28]W. Shao, C. K. Lim, Q. Li, M. T. Swihart, and P. N. Prasad, "Dramatic enhancement of quantum cutting in lanthanide-doped nanocrystals photosensitized with an aggregation-induced enhanced emission dye," Nano Lett. **18**, 4922 (2018).
[29]C. Tan, X. Li, Z. Li, S. Lu, F. Wang, Y. Liu, F. Wen, R. Li, D. Tu, Z. Chen, and X. Chen, "Near-infrared-responsive nanoplatforms integrating dye-sensitized upconversion and heavy-atom effect for enhanced photodynamic therapy efficacy," Nano Today **54**, 102089 (2024).
[30]Y. Zhu, X. Luo, Z. Yu, S. Wen, G. Bao, L. Zhang, C. Zhang, and Y. Xian, "Dye-sensitized rare-earth-doped nanoprobe for simultaneously enhanced NIR-II imaging and precise treatment of bacterial infection," Acta Biomater. **170**, 532 (2023).
[31]M. Kaur, S. L. Maurizio, G. A. Mandl, and J. A. Capobianco, "Achieving photostability in dye-sensitized upconverting nanoparticles and their use in Fenton type photocatalysis," Nanoscale **15**, 13583 (2023).
[32]A. N. Carneiro Neto, R. T. Moura, and O. L. Malta, "On the mechanisms of non-radiative energy transfer between lanthanide ions: Centrosymmetric systems," J. Lumin. **210**, 342 (2019).
[33]S. S. Skourtis, C. Liu, P. Antoniou, A. M. Virshup, and D. N. Beratan, "Dexter energy transfer pathways," Proc. Natl. Acad. Sci. U. S. A. **113**, 8115 (2016).
[34]D. J. Garfield, N. J. Borys, S. M. Hamed, N. A. Torquato, C. A. Tajon, B. Tian, B. Shevitski, E. S. Barnard, Y. D. Suh, S. Aloni, J. B. Neaton, E. M. Chan, B. E. Cohen, and P. J. Schuck, "Enrichment of molecular antenna triplets amplifies upconverting nanoparticle emission," Nat. Photonics **12**, 402 (2018).
[35]S. Han, R. Deng, Q. Gu, L. Ni, U. Huynh, J. Zhang, Z. Yi, B. Zhao, H. Tamura, A. Pershin, H. Xu, Z. Huang, S. Ahmad, M. Abdi-Jalebi, A. Sadhanala, M. L. Tang, A. Bakulin, D. Beljonne, X. Liu, and A. Rao, "Lanthanide-doped inorganic nanoparticles turn molecular triplet excitons bright," Nature **587**, 594 (2020).
[36]G. Y. Chen, W. Shao, R. R. Valiev, T. Y. Ohulchanskyy, G. S. He, H. Agren, and P. N. Prasad, "Efficient broadband upconversion of near-infrared light in dye-sensitized core/shell nanocrystals," Adv. Opt. Mater. **4**, 1760 (2016).
[37]H. B. Nasrabadi, E. Madirov, R. Popescu, L. Stacková, P. Stacko, P. Klán, B. S. Richards, D. Hudry, and A. Turshatov, "Coordination mechanism of cyanine dyes on the surface of core@active shell β-$NaGdF_4$:Yb^{3+},Er^{3+} nanocrystals and its role in enhancing upconversion luminescence," J. Mater. Chem. C **9**, 16313 (2021).
[38]S. I. Weissman, "Intramolecular energy transfer the fluorescence of complexes of europium," J. Chem. Phys. **10**, 214 (1942).
[39]M. Kleinerman, "Energy migration in lanthanide chelates," J. Chem. Phys. **51**, 2370 (1969).
[40]M. Yin, W. Zhang, S. Xia, and J. C. Krupa, "Luminescence of nanometric scale Y_2SiO_5:Eu^{3+}," J. Lumin. **68**, 335 (1996).

[41]S. Heer, O. Lehmann, M. Haase, and H. U. Gudel, "Blue, green, and red upconversion emission from lanthanide-doped $LuPO_4$ and $YbPO_4$ nanocrystals in a transparent colloidal solution," Angew. Chem. Int. Ed. **42**, 3179 (2003).
[42]J. Zhang, C. M. Shade, D. A. Chengelis, and S. Petoud, "A strategy to protect and sensitize near-infrared luminescent Nd^{3+} and Yb^{3+}: Organic tropolonate ligands for the sensitization of Ln^{3+}-doped $NaYF_4$ nanocrystals," J. Am. Chem. Soc. **129**, 14834 (2007).
[43]J. Zuo, D. Sun, L. Tu, Y. Wu, Y. Cao, B. Xue, Y. Zhang, Y. Chang, X. Liu, X. Kong, W. J. Buma, E. J. Meijer, and H. Zhang, "Precisely tailoring upconversion dynamics via energy migration in core-shell nanostructures," Angew. Chem. Int. Ed. **57**, 3054 (2018).
[44]R. T. Wegh, H. Donker, K. D. Oskam, and A. Meijerink, "Visible quantum cutting in $LiGdF_4$:Eu^{3+} through downconversion," Science **283**, 663 (1999).
[45]Z. Wang and A. Meijerink, "Dye-sensitized downconversion," J. Phys. Chem. Lett. **9**, 1522 (2018).
[46]F. Auzel, "Upconversion and anti-Stokes processes with f and d ions in solids," Chem. Rev. **104**, 139 (2004).
[47]P. Kim, C. Li, R. E. Riman, and J. Watkins, "Refractive index tuning of hybrid materials for highly transmissive luminescent lanthanide particle-polymer composites," ACS Appl. Mater. Interfaces **10**, 9038 (2018).
[48]A. Knebel, A. Bavykina, S. J. Datta, L. Sundermann, L. Garzon-Tovar, Y. Lebedev, S. Durini, R. Ahmad, S. M. Kozlov, G. Shterk, M. Karunakaran, I. D. Carja, D. Simic, I. Weilert, M. Klüppel, U. Giese, L. Cavallo, M. Rueping, M. Eddaoudi, J. Caro, and J. Gascon, "Solution processable metal–organic frameworks for mixed matrix membranes using porous liquids," Nat. Mater. **19**, 1346 (2020).
[49]J. Zhang, P. D. Badger, S. J. Geib, and S. Petoud, "Sensitization of near-infrared-emitting lanthanide cations in solution by tropolonate ligands," Angew. Chem. Int. Ed. **44**, 2508 (2005).
[50]K.-L. Wong, J.-C. G. Bünzli, and P. A. Tanner, "Quantum yield and brightness," J. Lumin. **224**, 117256 (2020).
[51]M. Kaiser, C. Wurth, M. Kraft, I. Hyppanen, T. Soukka, and U. Resch-Genger, "Power-dependent upconversion quantum yield of $NaYF_4$:Yb^{3+},Er^{3+} nano- and micrometer-sized particles—Measurements and simulations," Nanoscale **9**, 10051 (2017).
[52]Y. Wang, L. P. Tu, J. W. Zhao, Y. J. Sun, X. G. Kong, and H. Zhang, "Upconversion luminescence of β-$NaYF_4$:Yb^{3+},Er^{3+}@β-$NaYF_4$ core/shell nanoparticles: Excitation power density and surface dependence," J. Phys. Chem. C **113**, 7164 (2009).
[53]C. M. S. Jones, A. Gakamsky, and J. Marques-Hueso, "The upconversion quantum yield (UCQY): A review to standardize the measurement methodology, improve comparability, and define efficiency standards," Sci. Technol. Adv. Mater. **22**, 810 (2021).
[54]J. Hu, B. Zhao, R. Wen, X. Zhang, Y. Zhang, D. S. Kohane, and Q. Liu, "Squaraine dye-sensitized upconversion with enhanced stability and minimized aggregation-caused quenching," Nano Lett. **23**, 5209 (2023).
[55]X. Wang, C. Jiang, Z. Wang, B. E. Cohen, E. M. Chan, and G. Chen, "Triplet-induced singlet oxygen photobleaches near-infrared dye-sensitized upconversion nanosystems," Nano Lett. **23**, 7001 (2023).
[56]X. Wang, M. Li, X. Zheng, B. Sun, Y. Wang, J. Xu, T. Han, S. Ma, S. Zhu, and S. Zhang, "Dye-triplet-sensitized downshifting nanoprobes with ratiometric dual-NIR-IIb emission for accurate in vivo detection," Anal. Chem. **95**, 15264 (2023).
[57]C. L. Wang, H. X. Lin, X. G. Ge, J. Mu, L. C. Su, X. Zhang, M. Niu, H. H. Yang, and J. B. Song, "Dye-sensitized downconversion nanoprobes with emission beyond 1500 nm for ratiometric visualization of cancer redox state," Adv. Funct. Mater. **31**, 2009942 (2021).
[58]T. Liang, Z. Li, P. Wang, F. Zhao, J. Liu, and Z. Liu, "Breaking through the signal-to-background limit of upconversion nanoprobes using a target-modulated sensitizing switch," J. Am. Chem. Soc. **140**, 14696 (2018).
[59]X. Wu, Y. Zhang, K. Takle, O. Bilsel, Z. Li, H. Lee, Z. Zhang, D. Li, W. Fan, C. Duan, E. M. Chan, C. Lois, Y. Xiang, and G. Han, "Dye-sensitized core/active shell upconversion nanoparticles for optogenetics and bioimaging applications," ACS Nano **10**, 1060 (2016).
[60]R. Meng, Z. He, X. Luo, C. Zhang, M. Chen, H. Lu, and Y. Yang, "Wide spectral response perovskite solar cells mixed with $NaGdF_4$:Yb^{3+},Er^{3+}@$NaGdF_4$:Eu^{3+} core-shell rare earth nanoparticles," Opt. Mater. **119**, 111326 (2021).
[61]W. Bi, Y. Wu, C. Chen, D. Zhou, Z. Song, D. Li, G. Chen, Q. Dai, Y. Zhu, and H. Song, "Dye sensitization and local surface plasmon resonance-enhanced upconversion luminescence for efficient perovskite solar cells," ACS Appl. Mater. Interfaces **12**, 24737 (2020).
[62]Q. Y. Guo, J. H. Wu, Y. Q. Yang, X. P. Liu, J. B. Jia, J. Dong, Z. Lan, J. M. Lin, M. L. Huang, Y. L. Wei, and Y. F. Huang, "High performance perovskite solar cells based on β-$NaYF_4$:Yb^{3+}/Er^{3+}/Sc^{3+}@$NaYF_4$ core-shell upconversion nanoparticles," J. Power Sources **426**, 178 (2019).
[63]E. Hemmer, A. Benayas, F. Legare, and F. Vetrone, "Exploiting the biological windows: Current perspectives on fluorescent bioprobes emitting above 1000 nm," Nanoscale Horiz. **1**, 168 (2016).
[64]G. Chen, J. Damasco, H. Qiu, W. Shao, T. Y. Ohulchanskyy, R. R. Valiev, X. Wu, G. Han, Y. Wang, C. Yang, H. Agren, and P. N. Prasad, "Energy-cascaded upconversion in an organic dye-sensitized core/shell fluoride nanocrystal," Nano Lett. **15**, 7400 (2015).
[65]A. Dong, X. Ye, J. Chen, Y. Kang, T. Gordon, J. M. Kikkawa, and C. B. Murray, "A generalized ligand-exchange strategy enabling sequential surface functionalization of colloidal nanocrystals," J. Am. Chem. Soc. **133**, 998 (2011).
[66]X. D. Wang and G. Y. Chen, "A strategy for prompt phase transfer of upconverting nanoparticles through surface oleate-mediated supramolecular assembly of amino-β-cyclodextrin," Front. Chem. **7**, 161 (2019).
[67]P. Zhang, J. Ke, D. Tu, J. Li, Y. Pei, L. Wang, X. Shang, T. Guan, S. Lu, Z. Chen, and X. Chen, "Enhancing dye-triplet-sensitized upconversion emission through the heavy-atom effect in $CsLu_2F_7$:Yb/Er nanoprobes," Angew. Chem. Int. Ed. **61**, e202112125 (2022).
[68]F. Zhao, J. Hu, D. Guan, J. Liu, X. Zhang, H. Ling, Y. Zhang, and Q. Liu, "Boosting dye-sensitized luminescence by enhanced short-range triplet energy transfer," Adv. Mater. **35**, e2304907 (2023).
[69]J. Liu, P. Geiregat, L. Pilia, R. Van Deun, and F. Artizzu, "Molecular size matters: Ultrafast dye singlet sensitization pathways to bright nanoparticle emission," Adv. Opt. Mater. **9**, 2001678 (2021).
[70]J. Huang, X. Zhang, S. Li, F. Qu, B. Huang, R. Cui, Y. Liu, W. Hu, X. Yang, and Y. Zhang, "Activatable lanthanide nanoprobes with dye-sensitized second near-infrared luminescence for in vivo inflammation imaging," Anal. Chem. **95**, 3761 (2023).
[71]Z. Q. Liang, Z. Y. Zou, X. Yan, X. B. Zhang, D. D. Song, C. Q. Ye, X. M. Wang, and X. T. Tao, "Conjugate and non-conjugate controls of a sensitizer to enhance dye-sensitized upconversion luminescence," J. Mater. Chem. C **10**, 2205 (2022).
[72]A. A. Abdel-Shafi and D. R. Worrall, "Mechanism of the excited singlet and triplet states quenching by molecular oxygen in acetonitrile," J. Photochem. Photobiol. A: Chem. **172**, 170 (2005).
[73]X. Wu, H. Lee, O. Bilsel, Y. Zhang, Z. Li, T. Chen, Y. Liu, C. Duan, J. Shen, A. Punjabi, and G. Han, "Tailoring dye-sensitized upconversion nanoparticle excitation bands towards excitation wavelength selective imaging," Nanoscale **7**, 18424 (2015).
[74]Q. Liu, X. Zou, Y. Shi, B. Shen, C. Cao, S. Cheng, W. Feng, and F. Li, "An efficient dye-sensitized NIR emissive lanthanide nanomaterial and its application in fluorescence-guided peritumoral lymph node dissection," Nanoscale **10**, 12573 (2018).
[75]X. Y. Zhao, M. F. Wang, Z. W. Cai, D. Y. Xia, L. Zhao, Q. W. Song, Y. R. Qin, and W. Wei, "Optimizing the performance of dye-sensitized upconversion nanoparticles," Dyes Pigment. **192**, 109428 (2021).
[76]M. Z. Zhou, X. Y. Wang, X. L. Tian, L. T. Ren, W. W. Li, and Q. Q. Su, "Downshifting luminescence amplification by multi-phase energy harvesting," Chem. Eng. J. **475**, 146433 (2023).
[77]B. Xue, D. Wang, L. Tu, D. Sun, P. Jing, Y. Chang, Y. Zhang, X. Liu, J. Zuo, J. Song, J. Qu, E. J. Meijer, H. Zhang, and X. Kong, "Ultrastrong absorption meets ultraweak absorption: Unraveling the energy-dissipative routes for dye-sensitized upconversion luminescence," J. Phys. Chem. Lett. **9**, 4625 (2018).
[78]J. L. Hu, D. M. Guan, B. J. Zhao, Y. X. Zhang, X. C. Qiu, Y. X. Zhang, and Q. Liu, "Ytterbium-enriched outmost shell for enhanced upconversion single molecule imaging and interfacial triplet energy transfer," Adv. Opt. Mater. **10**, 2101763 (2022).
[79]M. Kaur, G. A. Mandl, S. L. Maurizio, G. Tessitore, and J. A. Capobianco, "On the photostability and luminescence of dye-sensitized upconverting nanoparticles using modified IR820 dyes," Nanoscale Adv. **4**, 608 (2022).

[80]X. B. Zhang, Z. Q. Liang, X. Yan, M. M. Li, C. Q. Ye, X. M. Wang, and X. T. Tao, "The effect of triethylamine on dye-sensitized upconversion luminescence and its application in nanoprobes and photostability," Phys. Chem. Chem. Phys. **25**, 12401 (2023).
[81]G. Bao, S. Wen, W. Wang, J. Zhou, S. Zha, Y. Liu, K. L. Wong, and D. Jin, "Enhancing hybrid upconversion nanosystems via synergistic effects of moiety engineered NIR dyes," Nano Lett. **21**, 9862 (2021).
[82]Y. Ji, F. Lu, Y. F. Tang, W. Qian, Q. L. Fan, and W. Huang, "Tandem energy upconversion in a conjugated polymer-sensitized core/shell nanocrystal," Inorg. Chem. Commun. **111**, 107640 (2020).
[83]C. D. LaBoda and C. L. Dwyer, "Upconverting nanoparticle relays for resonance energy transfer networks," Adv. Funct. Mater. **26**, 2866 (2016).
[84]D. Yin, Y. Liu, J. Tang, F. Zhao, Z. Chen, T. Zhang, X. Zhang, N. Chang, C. Wu, D. Chen, and M. Wu, "Huge enhancement of upconversion luminescence by broadband dye sensitization of core/shell nanocrystals," Dalton Trans. **45**, 13392 (2016).
[85]T. Liang, Q. R. Wang, Z. Li, P. P. Wang, J. J. Wu, M. M. Zuo, and Z. H. Liu, "Removing the obstacle of dye-sensitized upconversion luminescence in aqueous phase to achieve high-contrast deep imaging in vivo," Adv. Funct. Mater. **30**, 1910765 (2020).
[86]Q. Wang, T. Liang, J. Wu, Z. Li, and Z. Liu, "Dye-sensitized rare earth-doped nanoparticles with boosted NIR-IIb emission for dynamic imaging of vascular network-related disorders," ACS Appl. Mater. Interfaces **13**, 29303 (2021).
[87]X. Zou, X. Zhou, C. Cao, W. Lu, W. Yuan, Q. Liu, W. Feng, and F. Li, "Dye-sensitized upconversion nanocomposites for ratiometric semi-quantitative detection of hypochlorite in vivo," Nanoscale **11**, 2959 (2019).
[88]S. Wang, L. Liu, Y. Fan, A. M. El-Toni, M. S. Alhoshan, D. Li, and F. Zhang, "In vivo high-resolution ratiometric fluorescence imaging of inflammation using NIR-II nanoprobes with 1550 nm emission," Nano Lett. **19**, 2418 (2019).
[89]L. He, Y. Li, Q. Zeng, X. Li, H. Liang, and T. Zhang, "A dye-quenched/sensitized switching upconversion nanoprobe for high-contrast mapping of the pH-related tumor microenvironment," Nanoscale **15**, 16727 (2023).
[90]Y. Zhao, S. Gu, S. Xu, and L. Wang, "Selective ligand sensitization of lanthanide nanoparticles for multilevel information encryption with excellent durability," Anal. Chem. **93**, 14317 (2021).
[91]J. Goetz, A. Nonat, A. Diallo, M. Sy, I. Sera, A. Lecointre, C. Lefevre, C. F. Chan, K. L. Wong, and L. J. Charbonniere, "Ultrabright lanthanide nanoparticles," ChemPlusChem **81**, 526 (2016).
[92]J. Liu, R. V. Deun, L. Pilia, P. Geiregat, and F. Artizzu, "Controlling energy transfer routes in dye-sensitized lanthanide-based nanoparticles for enhanced emission," SPIE Conf. Proc. **11277**, 11277OE (2020).
[93]K. Xu, C. Lin, M.-F. Qin, Z. Yuan, Y. Tao, S.-S. Bao, R. Chen, X. Xie, and L.-M. Zheng, "Amplifying photoluminescence of lanthanide-doped nanoparticles by iridium phosphonate complex," ACS Mater. Lett. **5**, 854 (2023).
[94]Q. Duan, F. Qin, Z. Zhang, and W. Cao, "Quantum cutting mechanism in $NaYF_4$:Tb^{3+}, Yb^{3+}," Opt. Lett. **37**, 521 (2012).
[95]X. Zhang, W. Chen, X. Xie, Y. Li, D. Chen, Z. Chao, C. Liu, H. Ma, Y. Liu, and H. Ju, "Boosting luminance energy transfer efficiency in upconversion nanoparticles with an energy-concentrating zone," Angew. Chem. Int. Ed. **58**, 12117 (2019).
[96]X. Zou, M. Xu, W. Yuan, Q. Wang, Y. Shi, W. Feng, and F. Li, "A water-dispersible dye-sensitized upconversion nanocomposite modified with phosphatidylcholine for lymphatic imaging," Chem. Commun. **52**, 13389 (2016).
[97]C. Yao, P. Wang, L. Zhou, R. Wang, X. Li, D. Zhao, and F. Zhang, "Highly biocompatible zwitterionic phospholipids coated upconversion nanoparticles for efficient bioimaging," Anal. Chem. **86**, 9749 (2014).
[98]J. Xu, A. Gulzar, Y. Liu, H. Bi, S. Gai, B. Liu, D. Yang, F. He, and P. Yang, "Integration of IR-808 sensitized upconversion nanostructure and MoS_2 nanosheet for 808 nm NIR light triggered phototherapy and bioimaging," Small **13**, 1701841 (2017).
[99]Q. Shao, X. Li, P. Hua, G. Zhang, Y. Dong, and J. Jiang, "Enhancing the upconversion luminescence and photothermal conversion properties of approximately 800 nm excitable core/shell nanoparticles by dye molecule sensitization," J. Colloid Interface Sci. **486**, 121 (2017).
[100]S. L. Lin, Z. R. Chen, and C. A. Chang, "Nd^{3+} sensitized core-shell-shell nanocomposites loaded with IR806 dye for photothermal therapy and up-conversion luminescence imaging by a single wavelength NIR light irradiation," Nanotheranostics **2**, 243 (2018).
[101]D. Wang, D. P. Wang, A. Kuzmin, A. Pliss, W. Shao, J. Xia, J. L. Qu, and P. N. Prasad, "ICG-sensitized $NaYF_4$:Er nanostructure for theranostics," Adv. Opt. Mater. **6**, 1701142 (2018).
[102]Y. Wei, S. Liu, C. Pan, Z. Yang, Y. Liu, J. Yong, and L. Quan, "Molecular antenna-sensitized upconversion nanoparticle for temperature monitored precision photothermal therapy," Int. J. Nanomed. **15**, 1409 (2020).
[103]J. Lee, B. Yoo, H. Lee, G. D. Cha, H. S. Lee, Y. Cho, S. Y. Kim, H. Seo, W. Lee, D. Son, M. Kang, H. M. Kim, Y. I. Park, T. Hyeon, and D. H. Kim, "Ultra-wideband multi-dye-sensitized upconverting nanoparticles for information security application," Adv. Mater. **29**, 1603169 (2017).
[104]H. Chen, X. Yang, Y. Liu, and L. Wang, "Turn-on detection of glutathione S-transferase based on luminescence resonance energy transfer between near-infrared to near-infrared core-shell upconversion nanoparticles and organic dye," Anal. Bioanal. Chem. **412**, 5843 (2020).
[105]X. Zou, Y. Liu, X. Zhu, M. Chen, L. Yao, W. Feng, and F. Li, "An Nd^{3+}-sensitized upconversion nanophosphor modified with a cyanine dye for the ratiometric upconversion luminescence bioimaging of hypochlorite," Nanoscale **7**, 4105 (2015).
[106]W. Wang, M. Zhao, L. Wang, and H. Chen, "Core-shell upconversion nanoparticles of type $NaGdF_4$:Yb,Er@$NaGdF_4$:Nd,Yb and sensitized with a NIR dye are a viable probe for luminescence determination of the fraction of water in organic solvents," Mikrochim. Acta **186**, 630 (2019).
[107]J. Xu, P. Yang, M. Sun, H. Bi, B. Liu, D. Yang, S. Gai, F. He, and J. Lin, "Highly emissive dye-sensitized upconversion nanostructure for dual-photosensitizer photodynamic therapy and bioimaging," ACS Nano **11**, 4133 (2017).
[108]Z. Li, J. Wu, Q. Wang, T. Liang, J. Ge, P. Wang, and Z. Liu, "A universal strategy to construct lanthanide-doped nanoparticles-based activable NIR-II luminescence probe for bioimaging," iScience **23**, 100962 (2020).
[109]Y. Q. Ma, Z. Wang, Y. X. Wang, Z. H. Liu, Y. K. Wang, and R. C. Lv, "Coumarin derivative dye sensitized $NaYGdF_4$:Yb,Er nanoparticles with enhanced NIR II luminescence for bio-vascular imaging," J. Rare Earths **41**, 1843 (2023).
[110]S. Han, Z. Yi, J. Zhang, Q. Gu, L. Liang, X. Qin, J. Xu, Y. Wu, H. Xu, A. Rao, and X. Liu, "Photon upconversion through triplet exciton-mediated energy relay," Nat. Commun. **12**, 3704 (2021).
[111]*Principles of Fluorescence Spectroscopy*, edited by J. R. Lakowicz (Springer US, Boston, MA, 2006), p. 443.
[112]H. Xu, S. Han, R. Deng, Q. Su, Y. Wei, Y. Tang, X. Qin, and X. Liu, "Anomalous upconversion amplification induced by surface reconstruction in lanthanide sublattices," Nat. Photonics **15**, 732 (2021).
[113]Y. Zhang, Y. Jia, and S. Zhu, *NIR-II Cyanine@albumin Fluorophore for Deep Tissue Imaging and Imaging-Guided Surgery* (Wiley, 2023).
[114]T. Chen, L. Zheng, J. Yuan, Z. An, R. Chen, Y. Tao, H. Li, X. Xie, and W. Huang, "Understanding the control of singlet-triplet splitting for organic exciton manipulating: A combined theoretical and experimental approach," Sci. Rep. **5**, 10923 (2015).
[115]D. M. E. Freeman, A. J. Musser, J. M. Frost, H. L. Stern, A. K. Forster, K. J. Fallon, A. G. Rapidis, F. Cacialli, I. McCulloch, T. M. Clarke, R. H. Friend, and H. Bronstein, "Synthesis and exciton dynamics of donor-orthogonal acceptor conjugated polymers: Reducing the singlet-triplet energy gap," J. Am. Chem. Soc. **139**, 11073 (2017).
[116]P. B. Green, O. S. Lecina, P. P. Albertini, A. Loiudice, and R. Buonsanti, "Colloidal-ALD-grown metal oxide shells enable the synthesis of photoactive ligand/nanocrystal composite materials," J. Am. Chem. Soc. **145**, 8189 (2023).
[117]T. D. Pollard, "A guide to simple and informative binding assays," Mol. Biol. Cell. **21**, 4061 (2010).
[118]S. Sudheendran Swayamprabha, D. K. Dubey, Shahnawaz, R. A. K. Yadav, M. R. Nagar, A. Sharma, F. C. Tung, and J. H. Jou, "Approaches for long lifetime organic light emitting diodes," Adv. Sci. **8**, 2002254 (2020).
[119]X. Wang, H. Li, F. Li, X. Han, and G. Chen, "Prussian blue-coated lanthanide-doped core/shell/shell nanocrystals for NIR-II image-guided photothermal therapy," Nanoscale **11**, 22079 (2019).
[120]Z. Yu, W. Hu, H. Zhao, X. Miao, Y. Guan, W. Cai, Z. Zeng, Q. Fan, and T. T. Y. Tan, "Generating new cross-relaxation pathways by coating Prussian blue

on $NaNdF_4$ to fabricate enhanced photothermal agents," Angew. Chem. Int. Ed. **58**, 8536 (2019).
[121]W. L. Barnes, S. A. R. Horsley, and W. L. Vos, "Classical antennas, quantum emitters, and densities of optical states," J. Opt. **22**, 073501 (2020).
[122]J. J. Baumberg, J. Aizpurua, M. H. Mikkelsen, and D. R. Smith, "Extreme nanophotonics from ultrathin metallic gaps," Nat. Mater. **18**, 668 (2019).
[123]K. J. Vahala, "Optical microcavities," Nature **424**, 839 (2003).
[124]P. Lalanne, W. Yan, K. Vynck, C. Sauvan, and J. P. Hugonin, "Light interaction with photonic and plasmonic resonances," Laser Photonics Rev. **12**, 1700113 (2018).
[125]A. Pasquazi, M. Peccianti, L. Razzari, D. J. Moss, S. Coen, M. Erkintalo, Y. K. Chembo, T. Hansson, S. Wabnitz, P. Del'Haye, X. X. Xue, A. M. Weiner, and R. Morandotti, "Micro-combs: A novel generation of optical sources," Phys. Rep. Rev. Sec. Phys. Lett. **729**, 1 (2018).
[126]E. Le Ru and P. Etchegoin, *Principles of Surface-Enhanced Raman Spectroscopy: And Related Plasmonic Effects* (Elsevier, 2008).
[127]S. Karaveli, A. J. Weinstein, and R. Zia, "Direct modulation of lanthanide emission at sub-lifetime scales," Nano Lett. **13**, 2264 (2013).
[128]L. Yang, S. Wang, M. Shen, J. Xie, and H. X. Tang, "Controlling single rare earth ion emission in an electro-optical nanocavity," Nat. Commun. **14**, 1718 (2023).
[129]J. M. Kindem, A. Ruskuc, J. G. Bartholomew, J. Rochman, Y. Q. Huan, and A. Faraon, "Control and single-shot readout of an ion embedded in a nanophotonic cavity," Nature **580**, 201 (2020).
[130]J. Rochman, T. Xie, J. G. Bartholomew, K. C. Schwab, and A. Faraon, "Microwave-to-optical transduction with erbium ions coupled to planar photonic and superconducting resonators," Nat. Commun. **14**, 1153 (2023).
[131]K. Drexhage, "Influence of a dielectric interface on fluorescence decay time," J. Lumin. **1–2**, 693 (1970).
[132]R. Arul, K. Menghrajani, M. S. Rider, R. Chikkaraddy, W. L. Barnes, and J. J. Baumberg, "Raman probing the local ultrastrong coupling of vibrational plasmon polaritons on metallic gratings," Phys. Rev. Lett. **131**, 126902 (2023).
[133]W. Luo, F. Xu, A. H. Li, and Z. J. Sun, "Resonant control and enhancement of upconversion luminescence of $NaYF_4$:Yb,Er nanoparticles on metal gratings," Adv. Opt. Mater. **10**, 2102668 (2022).
[134]B. de Nijs, R. W. Bowman, L. O. Herrmann, F. Benz, S. J. Barrow, J. Mertens, D. O. Sigle, R. Chikkaraddy, A. Eiden, A. Ferrari, O. A. Scherman, and J. J. Baumberg, "Unfolding the contents of sub-nm plasmonic gaps using normalising plasmon resonance spectroscopy," Faraday Discuss. **178**, 185 (2015).
[135]D. B. Grys, M. Niihori, R. Arul, S. M. Sibug-Torres, E. W. Wyatt, B. de Nijs, and J. J. Baumberg, "Controlling atomic-scale restructuring and cleaning of gold nanogap multilayers for surface-enhanced Raman scattering sensing," ACS Sens. **8**, 2879 (2023).
[136]R. Chikkaraddy, R. Arul, L. A. Jakob, and J. J. Baumberg, "Single-molecule mid-infrared spectroscopy and detection through vibrationally assisted luminescence," Nat. Photonics **17**, 865 (2023).
[137]R. Arul, D. B. Grys, R. Chikkaraddy, N. S. Mueller, A. Xomalis, E. Miele, T. G. Euser, and J. J. Baumberg, "Giant mid-IR resonant coupling to molecular vibrations in sub-nm gaps of plasmonic multilayer metafilms," Light Sci. Appl. **11**, 281 (2022).
[138]E. Elliott, K. Bedingfield, J. Huang, S. Hu, B. de Nijs, A. Demetriadou, and J. J. Baumberg, "Fingerprinting the hidden facets of plasmonic nanocavities," ACS Photonics **9**, 2643 (2022).
[139]Y. Lei, Y. Li, and Z. Jin, "Photon energy loss and management in perovskite solar cells," Energy Rev. **1**, 100003 (2022).
[140]Z. Huang, X. Li, M. Mahboub, K. M. Hanson, V. M. Nichols, H. Le, M. L. Tang, and C. J. Bardeen, "Hybrid molecule-nanocrystal photon upconversion across the visible and near-infrared," Nano Lett. **15**, 5552 (2015).
[141]B. J. Ainslie, "A review of the fabrication and properties of erbium-doped fibers for optical amplifiers," J. Lightwave Technol. **9**, 220 (1991).
[142]P. D. Dragic, M. Cavillon, and J. Ballato, "Materials for optical fiber lasers: A review," Appl. Phys. Rev. **5**, 041301 (2018).
[143]Y. Wu, J. Xu, E. T. Poh, L. Liang, H. Liu, J. K. W. Yang, C. W. Qiu, R. A. L. Vallee, and X. Liu, "Upconversion superburst with sub-2 μs lifetime," Nat. Nanotechnol. **14**, 1110 (2019).
[144]Q. C. Sun, H. Mundoor, J. C. Ribot, V. Singh, I. I. Smalyukh, and P. Nagpal, "Plasmon-enhanced energy transfer for improved upconversion of infrared radiation in doped-lanthanide nanocrystals," Nano Lett. **14**, 101 (2014).
[145]W. Park, D. Lu, and S. Ahn, "Plasmon enhancement of luminescence upconversion," Chem. Soc. Rev. **44**, 2940 (2015).
[146]Z. Yin, H. Li, W. Xu, S. Cui, D. Zhou, X. Chen, Y. Zhu, G. Qin, and H. Song, "Local field modulation induced three-order upconversion enhancement: Combining surface plasmon effect and photonic crystal effect," Adv. Mater. **28**, 2518 (2016).
[147]A. Fernandez-Bravo, D. Wang, E. S. Barnard, A. Teitelboim, C. Tajon, J. Guan, G. C. Schatz, B. E. Cohen, E. M. Chan, P. J. Schuck, and T. W. Odom, "Ultralow-threshold, continuous-wave upconverting lasing from subwavelength plasmons," Nat. Mater. **18**, 1172 (2019).
[148]M. Kataria, K. Yadav, A. Nain, H. I. Lin, H. W. Hu, C. R. Paul Inbaraj, T. J. Chang, Y. M. Liao, H. Y. Cheng, K. H. Lin, H. T. Chang, F. G. Tseng, W. H. Wang, and Y. F. Chen, "Self-sufficient and highly efficient gold sandwich upconversion nanocomposite lasers for stretchable and bio-applications," ACS Appl. Mater. Interfaces **12**, 19840 (2020).
[149]X. Chen, T. Sun, and F. Wang, "Lanthanide-based luminescent materials for waveguide and lasing," Chem. Asian J. **15**, 21 (2020).
[150]Y. Meng, D. Huang, H. Li, X. Feng, F. Li, Q. Liang, T. Ma, J. Han, J. Tang, G. Chen, and X.-W. Chen, "Bright single-nanocrystal upconversion at sub 0.5 W cm^{-2} irradiance via coupling to single nanocavity mode," Nat. Photonics **17**, 73 (2022).
[151]Y. Xue, C. Ding, Y. Rong, Q. Ma, C. Pan, E. Wu, B. Wu, and H. Zeng, "Tuning plasmonic enhancement of single nanocrystal upconversion luminescence by varying gold nanorod diameter," Small **13**, 28783235 (2017).
[152]Y. Ji, W. Xu, N. Ding, H. Yang, H. Song, Q. Liu, H. Agren, J. Widengren, and H. Liu, "Huge upconversion luminescence enhancement by a cascade optical field modulation strategy facilitating selective multispectral narrow-band near-infrared photodetection," Light Sci. Appl. **9**, 184 (2020).
[153]M. C. T. Nguyen, H. Q. Nguyen, H. Kang, M. Goddati, S. Y. Lee, K. J. Yee, and J. Lee, "Metal plasmon-enhanced lanthanide fluorescent nanoparticles for monitoring aqueous copper ions," Mater. Today Nano **24**, 100380 (2023).
[154]Z. Wang, L. Li, S. Zhan, and S. Wu, "Plasmonic near field assistant highly sensitive detection of hypochlorite by lanthanide co-doped core/shell upconversion probe," J. Solid State Chem. **315**, 123456 (2022).
[155]Z. Chu, T. Tian, Z. Tao, J. Yang, B. Chen, H. Chen, W. Wang, P. Yin, X. Xia, H. Wang, and H. Qian, "Upconversion nanoparticles@$AgBiS_2$ core-shell nanoparticles with cancer-cell-specific cytotoxicity for combined photothermal and photodynamic therapy of cancers," Bioact. Mater. **17**, 71 (2022).
[156]J. K. Swabeck, S. Fischer, N. D. Bronstein, and A. P. Alivisatos, "Broadband sensitization of lanthanide emission with indium phosphide quantum dots for visible to near-infrared downshifting," J. Am. Chem. Soc. **140**, 9120 (2018).
[157]L. Dai, J. Ye, and N. C. Greenham, "Thermalization and relaxation mediated by phonon management in tin-lead perovskites," Light Sci. Appl. **12**, 208 (2023).
[158]L. C. Schmidt, A. Pertegas, S. Gonzalez-Carrero, O. Malinkiewicz, S. Agouram, G. Minguez Espallargas, H. J. Bolink, R. E. Galian, and J. Perez-Prieto, "Nontemplate synthesis of $CH_3NH_3PbBr_3$ perovskite nanoparticles," J. Am. Chem. Soc. **136**, 850 (2014).
[159]L. Protesescu, S. Yakunin, M. I. Bodnarchuk, F. Krieg, R. Caputo, C. H. Hendon, R. X. Yang, A. Walsh, and M. V. Kovalenko, "Nanocrystals of cesium lead halide perovskites ($CsPbX_3$, X = Cl, Br, and I): Novel optoelectronic materials showing bright emission with wide color gamut," Nano Lett. **15**, 3692 (2015).
[160]D. Zhou, L. Tao, Z. Yu, J. Jiao, and W. Xu, "Efficient chromium ion passivated $CsPbCl_3$:Mn perovskite quantum dots for photon energy conversion in perovskite solar cells," J. Mater. Chem. C **8**, 12323 (2020).
[161]W. K. Chan, J. Chen, D. Zhou, J. Ye, R. J. Vazquez, C. Zhou, G. C. Bazan, A. Rao, Z. Yu, and T. T. Y. Tan, "Hybrid organic-inorganic perovskite superstructures for ultrapure green emissions," Nanomaterials **13**(5), 815 (2023).
[162]W. K. Chan, D. Zhou, Z. Yu, and T. T. Y. Tan, "Mechanistic studies of $CsPbBr_3$ superstructure formation," J. Mater. Chem. C **9**, 14699 (2021).
[163]W. Zheng, P. Huang, Z. Gong, D. Tu, J. Xu, Q. Zou, R. Li, W. You, J. G. Bunzli, and X. Chen, "Near-infrared-triggered photon upconversion tuning in all-inorganic cesium lead halide perovskite quantum dots," Nat. Commun. **9**, 3462 (2018).
[164]I. Cherniukh, G. Rainò, T. Stöferle, M. Burian, A. Travesset, D. Naumenko, H. Amenitsch, R. Erni, R. F. Mahrt, M. I. Bodnarchuk, and M. V. Kovalenko,

"Perovskite-type superlattices from lead halide perovskite nanocubes," Nature **593**, 535 (2021).
[165]L. Francés-Soriano, S. Gonzalez-Carrero, E. Navarro-Raga, R. E. Galian, M. González-Béjar, and J. Pérez-Prieto, "Efficient cementing of $CH_3NH_3PbBr_3$ nanoparticles to upconversion nanoparticles visualized by confocal microscopy," Adv. Funct. Mater. **26**, 5131 (2016).
[166]N. Estebanez, A. Cortés-Villena, J. Ferrera-González, M. González-Béjar, R. E. Galian, S. González-Carrero, and J. Pérez-Prieto, "Linear coassembly of upconversion and perovskite nanoparticles: Sensitized upconversion emission of perovskites by lanthanide-doped nanoparticles," Adv. Funct. Mater. **30**, 2003766 (2020).
[167]L. Xie, Z. Hong, J. Zan, Q. Wu, Z. Yang, X. Chen, X. Ou, X. Song, Y. He, J. Li, Q. Chen, and H. Yang, "Broadband detection of X-ray, ultraviolet, and near-infrared photons using solution-processed perovskite-lanthanide nanotransducers," Adv. Mater. **33**, e2101852 (2021).
[168]L. Ruan and Y. Zhang, "NIR-excitable heterostructured upconversion perovskite nanodots with improved stability," Nat. Commun. **12**, 219 (2021).
[169]H. Xiao, B. Liu, L. Qiu, G. Li, G. Zhang, D. Huang, Y. Zhao, C. Yang, F. Jiang, P. Dang, H. Lian, Z. Cheng, and J. Lin, "Core-shell structured upconversion/lead-free perovskite nanoparticles for anticounterfeiting applications," Angew. Chem. Int. Ed. **61**, e202115136 (2022).
[170]W. K. Chan, Z. Yu, D. Zhou, J. Ye, A. Tew, L. v Turnhout, A. Rao, and T. Tan, *Overcoming Lattice Mismatch for Heterostructures* (Springer, 2023).
[171]Z. Wang, B. Liu, Q. Sun, L. Feng, F. He, P. Yang, S. Gai, Z. Quan, and J. Lin, "Upconverted metal-organic framework Janus architecture for near-infrared and ultrasound co-enhanced high performance tumor therapy," ACS Nano **15**, 12342 (2021).
[172]Y. Shao, B. Liu, Z. Di, G. Zhang, L. D. Sun, L. Li, and C. H. Yan, "Engineering of upconverted metal-organic frameworks for near-infrared light-triggered combinational photodynamic/chemo-/immunotherapy against hypoxic tumors," J. Am. Chem. Soc. **142**, 3939 (2020).
[173]Y. Li, Z. Di, J. Gao, P. Cheng, C. Di, G. Zhang, B. Liu, X. Shi, L. D. Sun, L. Li, and C. H. Yan, "Heterodimers made of upconversion nanoparticles and metal-organic frameworks," J. Am. Chem. Soc. **139**, 13804 (2017).
[174]C. Liu, B. Liu, J. Zhao, Z. Di, D. Chen, Z. Gu, L. Li, and Y. Zhao, "Nd^{3+}-sensitized upconversion metal-organic frameworks for mitochondria-targeted amplified photodynamic therapy," Angew. Chem. Int. Ed. **59**, 2634 (2020).
[175]Z. Shi, K. Zhang, S. Zada, C. Zhang, X. Meng, Z. Yang, and H. Dong, "Upconversion nanoparticle-induced multimode photodynamic therapy based on a metal-organic framework/titanium dioxide nanocomposite," ACS Appl. Mater. Interfaces **12**, 12600 (2020).
[176]Y. Li, J. Tang, L. He, Y. Liu, Y. Liu, C. Chen, and Z. Tang, "Core-shell upconversion nanoparticle@metal-organic framework nanoprobes for luminescent/magnetic dual-mode targeted imaging," Adv. Mater. **27**, 4075 (2015).
[177]D. Li, S. H. Yu, and H. L. Jiang, "From UV to near-infrared light-responsive metal-organic framework composites: Plasmon and upconversion enhanced photocatalysis," Adv. Mater. **30**, e1707377 (2018).
[178]W. F. Guo, L. L. Tan, Q. Li, J. M. Li, and L. Shang, "Upconversion nanorods anchored metal-organic frameworks via hierarchical and dynamic assembly for synergistic therapy," Nano Res. **15**, 7533 (2022).
[179]C. Hao, X. Wu, M. Sun, H. Zhang, A. Yuan, L. Xu, C. Xu, and H. Kuang, "Chiral core-shell upconversion nanoparticle@MOF nanoassemblies for quantification and bioimaging of reactive oxygen species in vivo," J. Am. Chem. Soc. **141**, 19373 (2019).
[180]B. T. Liu, X. H. Pan, D. Y. Zhang, R. Wang, J. Y. Chen, H. R. Fang, and T. F. Liu, "Construction of function-oriented core-shell nanostructures in hydrogen-bonded organic frameworks for near-infrared-responsive bacterial inhibition," Angew. Chem. Int. Ed. **60**, 25701 (2021).
[181]X. Zhao, S. He, B. Li, B. Liu, Y. Shi, W. Cong, F. Gao, J. Li, F. Wang, K. Liu, C. Sheng, J. Su, and H. G. Hu, "DUCNP@Mn-MOF/FOE as a highly selective and bioavailable drug delivery system for synergistic combination cancer therapy," Nano Lett. **23**, 863 (2023).
[182]W. Bao, M. Liu, J. Meng, S. Liu, S. Wang, R. Jia, Y. Wang, G. Ma, W. Wei, and Z. Tian, "MOFs-based nanoagent enables dual mitochondrial damage in synergistic antitumor therapy via oxidative stress and calcium overload," Nat. Commun. **12**, 6399 (2021).
[183]L. He, Q. Ni, J. Mu, W. Fan, L. Liu, Z. Wang, L. Li, W. Tang, Y. Liu, Y. Cheng, L. Tang, Z. Yang, Y. Liu, J. Zou, W. Yang, O. Jacobson, F. Zhang, P. Huang, and X. Chen, "Solvent-assisted self-assembly of a metal-organic framework based biocatalyst for cascade reaction driven photodynamic therapy," J. Am. Chem. Soc. **142**, 6822 (2020).
[184]Q. X. Wang, Y. F. Yang, X. F. Yang, Y. Pan, L. D. Sun, W. Y. Zhang, Y. L. Shao, J. Shen, J. Lin, L. L. Li, and C. H. Yan, "Upconverted/downshifted $NaLnF_4$ and metal-organic framework heterostructures boosting NIR-II imaging-guided photodynamic immunotherapy toward tumors," Nano Today **43**, 101439 (2022).
[185]J. Wu, Q. Lu, X. Fu, H. Xu, P. Wan, H. Fu, J. Ding, J. Zhang, and Q. Mei, "ZIF-8 encapsulated upconversion nanoprobes to evaluate pH variations in food spoilage," Mikrochim. Acta **189**, 87 (2022).
[186]X. H. Wei, G. D. Zhao, P. F. Feng, Y. Kou, and Y. Tang, "Core-shell lanthanide-doped nanoparticles@Eu-MOF nanocomposites for anticounterfeiting applications," ACS Appl. Nano Mater. **5**, 1161 (2022).
[187]Z. Li, X. Qiao, G. He, X. Sun, D. Feng, L. Hu, H. Xu, H.-B. Xu, S. Ma, and J. Tian, "Core-satellite metal-organic framework upconversion nanoparticle superstructures via electrostatic self-assembly for efficient photodynamic theranostics," Nano Res. **13**, 3377 (2020).
[188]A. R. Hong, J. S. Han, G. Kang, H. Ko, and H. S. Jang, "Bright blue, green, and red luminescence from dye-sensitized core@shell upconversion nanophosphors under 800 nm near-infrared light," Mater. (Basel) **13**, 5338 (2020).
[189]F. Ren, H. Liu, H. Zhang, Z. Jiang, B. Xia, C. Genevois, T. He, M. Allix, Q. Sun, Z. Li, and M. Gao, "Engineering NIR-IIb fluorescence of Er-based lanthanide nanoparticles for through-skull targeted imaging and imaging-guided surgery of orthotopic glioma," Nano Today **34**, 100905 (2020).
[190]M. I. Saleh, I. D. Panas, F. Frenzel, C. Wurth, B. Ruhle, Y. L. Slominskii, A. Demchenko, and U. Resch-Genger, "Sensitization of upconverting nanoparticles with a NIR-emissive cyanine dye using a micellar encapsulation approach," Methods Appl. Fluoresc. **7**, 014003 (2019).
[191]J. Liu, F. Artizzu, M. Zeng, L. Pilia, P. Geiregat, and R. Van Deun, "Dye-sensitized Er^{3+}-doped CaF_2 nanoparticles for enhanced near-infrared emission at 1.5 μm," Photonics Res. **9**, 2037–2045 (2021).
[192]J. Liu, A. M. Kaczmarek, F. Artizzu, and R. Van Deun, "Ultraefficient cascade energy transfer in dye-sensitized core/shell fluoride nanoparticles," ACS Photonics **6**, 659 (2019).
[193]V. V. Utochnikova, A. S. Kalyakina, L. S. Lepnev, and N. P. Kuzmina, "Luminescence enhancement of nanosized ytterbium and europium fluorides by surface complex formation with aromatic carboxylates," J. Lumin. **170**, 633 (2016).
[194]N. Gauthier, O. Raccurt, D. Imbert, and M. Mazzanti, "Efficient sensitization of Ln^{3+}-doped $NaYF_4$ nanocrystals with organic ligands," J. Nanopart. Res. **15**, 1723 (2013).
[195]L. J. Charbonnière, J.-L. Rehspringer, R. Ziessel, and Y. Zimmermann, "Highly luminescent water-soluble lanthanide nanoparticles through surface coating sensitization," New J. Chem. **32**, 1055 (2008).
[196]Y. Qin, Z. Dong, D. Zhou, Y. Yang, X. Xu, and J. Qiu, "Modification on populating paths of β-$NaYF_4$:Nd/Yb Ho@SiO_2@Ag core/double-shell nanocomposites with plasmon enhanced upconversion emission," Opt. Mater. Express **6**, 1942 (2016).
[197]P. Kannan, F. Abdul Rahim, R. Chen, X. Teng, L. Huang, H. Sun, and D. H. Kim, "Au nanorod decoration on $NaYF_4$:Yb/Tm nanoparticles for enhanced emission and wavelength-dependent biomolecular sensing," ACS Appl. Mater. Interfaces **5**, 3508 (2013).
[198]F. Kang, J. He, T. Sun, Z. Y. Bao, F. Wang, and D. Y. Lei, "Plasmonic dual-enhancement and precise color tuning of gold nanorod@SiO_2 coupled core–shell–shell upconversion nanocrystals," Adv. Funct. Mater. **27**, 1701842 (2017).
[199]L. Sudheendra, V. Ortalan, S. Dey, N. D. Browning, and I. M. Kennedy, "Plasmonic enhanced emissions from cubic $NaYF_4$:Yb:Er/Tm nanophosphors," Chem. Mater. **23**, 2987 (2011).
[200]P. Kannan, F. A. Rahim, X. Teng, R. Chen, H. D. Sun, L. Huang, and D. H. Kim, "Enhanced emission of $NaYF_4$:Yb,Er/Tm nanoparticles by selective growth of Au and Ag nanoshells," RSC Adv. **3**, 7718 (2013).
[201]D. Yin, C. Wang, J. Ouyang, X. Zhang, Z. Jiao, Y. Feng, K. Song, B. Liu, X. Cao, L. Zhang, Y. Han, and M. Wu, "Synthesis of a novel core-shell

nanocomposite Ag@SiO_2@Lu_2O_3:Gd/Yb/Er for large enhancing upconversion luminescence and bioimaging," ACS Appl. Mater. Interfaces **6**, 18480 (2014).
[202]A. Das, C. Mao, S. Cho, K. Kim, and W. Park, "Over 1000-fold enhancement of upconversion luminescence using water-dispersible metal-insulator-metal nanostructures," Nat. Commun. **9**, 4828 (2018).
[203]T. Hinamoto, T. Higashiura, H. Sugimoto, and M. Fujii, "Elongated metal nanocap with two magnetic dipole resonances and its application for upconversion enhancement," J. Phys. Chem. C **123**, 25809 (2019).
[204]W. Zhang, T. Chen, L. Su, X. Ge, X. Chen, J. Song, and H. Yang, "Quantum dot-based sensitization system for boosted photon absorption and enhanced second near-infrared luminescence of lanthanide-doped nanoparticle," Anal. Chem. **92**, 6094 (2020).
[205]D. Song, S. Y. Chi, X. Li, C. X. Wang, Z. Li, and Z. Liu, "Upconversion system with quantum dots as sensitizer: Improved photoluminescence and PDT efficiency," ACS Appl. Mater. Interfaces **11**, 41100 (2019).
[206]G. C. Bao, S. H. Wen, G. G. Lin, J. L. Yuan, J. Lin, K. L. Wong, J. C. G. Bünzli, and D. Y. Jin, "Learning from lanthanide complexes: The development of dye-lanthanide nanoparticles and their biomedical applications," Coord. Chem. Rev. **429**, 213642 (2021).
[207]H. Zhu, Q. Li, W. Zhu, and F. Huang, "Pillararenes as versatile building blocks for fluorescent materials," Accounts Mater. Res. **3**, 658 (2022).
[208]H. Zhu, J. Liu, Y. Wu, L. Wang, H. Zhang, Q. Li, H. Wang, H. Xing, J. L. Sessler, and F. Huang, "Substrate-responsive pillar[5]arene-based organic room-temperature phosphorescence," J. Am. Chem. Soc. **145**, 11130 (2023).
[209]M. Kasha, "Characterization of electronic transitions in complex molecules," Discuss. Faraday Soc. **9**, 14 (1950).
[210]J.-C. G. Bünzli, "On the design of highly luminescent lanthanide complexes," Coord. Chem. Rev. **293–294**, 19–47 (2015).
[211]T. Förster, "Transfer mechanisms of electronic excitation energy," Radiat. Res. Suppl. **2**, 326–339 (1960).
[212]D. L. Dexter, "A theory of sensitized luminescence in solids," J. Chem. Phys. **21**, 836 (1953).
[213]A. R. Clapp, I. L. Medintz, J. M. Mauro, B. R. Fisher, M. G. Bawendi, and H. Mattoussi, "Fluorescence resonance energy transfer between quantum dot donors and dye-labeled protein acceptors," J. Am. Chem. Soc. **126**, 301 (2004).
[214]J. Wang and R. Deng, "Energy transfer in dye-coupled lanthanide-doped nanoparticles: From design to application," Chem. Asian J. **13**, 614 (2018).
[215]H. Z. Lu, Y. Peng, H. Q. Ye, X. J. Cui, J. X. Hu, H. Gu, A. N. Khlobystov, M. A. Green, P. J. Blower, P. B. Wyatt, W. P. Gillin, and I. Hernández, "Sensitization, energy transfer and infra-red emission decay modulation in Yb^{3+}-doped $NaYF_4$ nanoparticles with visible light through a perfluoroanthraquinone chromophore," Sci. Rep. **7**, 5066 (2017).
[216]C. Ayala-Orozco, J. G. Liu, M. W. Knight, Y. Wang, J. K. Day, P. Nordlander, and N. J. Halas, "Fluorescence enhancement of molecules inside a gold nanomatryoshka," Nano Lett. **14**, 2926 (2014).
[217]W. Feng, L.-D. Sun, and C.-H. Yan, "Ag nanowires enhanced upconversion emission of $NaYF_4$:Yb, Er nanocrystals via a direct assembly method," Chem. Commun. **29**, 4393–4395 (2009).
[218]T. T. Liu, X. M. Liu, Y. S. Feng, and C. J. Yao, "Advances in plasmonic enhanced luminenscence of upconversion nanoparticles," Mater. Today Chem. **34**, 101788 (2023).
[219]W. Deng, F. Xie, H. T. M. C. M. Baltar, and E. M. Goldys, "Metal-enhanced fluorescence in the life sciences: Here, now and beyond," Phys. Chem. Chem. Phys. **15**, 15695 (2013).
[220]H. Peng, S. Li, J. Xing, F. Yang, and A. Wu, "Surface plasmon resonance of Au/Ag metals for the photoluminescence enhancement of lanthanide ion Ln^{3+} doped upconversion nanoparticles in bioimaging," J. Mater. Chem. B **11**, 5238 (2023).
[221]X. Chen, W. Xu, L. Zhang, X. Bai, S. Cui, D. Zhou, Z. Yin, H. Song, and D. H. Kim, "Large upconversion enhancement in the "Islands" Au–Ag Alloy/$NaYF_4$:Yb^{3+}, Tm^{3+}/Er^{3+} composite films, and fingerprint identification," Adv. Funct. Mater. **25**, 5462 (2015).
[222]S. Han, R. Deng, X. Xie, and X. Liu, "Enhancing luminescence in lanthanide-doped upconversion nanoparticles," Angew. Chem. Int. Ed. **53**, 11702 (2014).
[223]P. Xu, Q. Li, T. Li, W. Y. Rao, Y. Z. Wang, S. Lan, and L. J. Wu, "Enhancing the surface-state emission in trap-rich CdS nanocrystals by silver nanoparticles," Plasmonics **9**, 1039 (2014).
[224]E. M. Purcell, H. C. Torrey, and R. V. Pound, "Resonance absorption by nuclear magnetic moments in a solid," Phys. Rev. **69**, 37 (1946).
[225]A. Priyam, N. M. Idris, and Y. Zhang, "Gold nanoshell coated $NaYF_4$ nanoparticles for simultaneously enhanced upconversion fluorescence and dark-field imaging," J. Mater. Chem. **22**, 960 (2012).
[226]D. Lu, C. Mao, S. K. Cho, S. Ahn, and W. Park, "Experimental demonstration of plasmon enhanced energy transfer rate in $NaYF_4$:Yb^{3+},Er^{3+} upconversion nanoparticles," Sci. Rep. **6**, 18894 (2016).
[227]J. He, W. Zheng, F. Ligmajer, C. F. Chan, Z. Bao, K. L. Wong, X. Chen, J. Hao, J. Dai, S. F. Yu, and D. Y. Lei, "Plasmonic enhancement and polarization dependence of nonlinear upconversion emissions from single gold nanorod@SiO_2@CaF_2:Yb^{3+},Er^{3+} hybrid core-shell-satellite nanostructures," Light Sci. Appl. **6**, e16217 (2017).
[228]D. Lu, S. K. Cho, S. Ahn, L. Brun, C. J. Summers, and W. Park, "Plasmon enhancement mechanism for the upconversion processes in $NaYF_4$:Yb^{3+},Er^{3+} nanoparticles: Maxwell versus Forster," ACS Nano **8**, 7780 (2014).
[229]M. Khan and H. Idriss, "Advances in plasmon-enhanced upconversion luminescence phenomena and their possible effect on light harvesting for energy applications," Wiley Interdiscip. Rev. Energy Environ. **6**, e254 (2017).
[230]P. Anger, P. Bharadwaj, and L. Novotny, "Enhancement and quenching of single-molecule fluorescence," Phys. Rev. Lett. **96**, 113002 (2006).
[231]S. Rohani, M. Quintanilla, S. Tuccio, F. De Angelis, E. Cantelar, A. O. Govorov, L. Razzari, and F. Vetrone, "Enhanced luminescence, collective heating, and nanothermometry in an ensemble system composed of lanthanide-doped upconverting nanoparticles and gold nanorods," Adv. Opt. Mater. **3**, 1606 (2015).
[232]A. P. Alivisatos, "Semiconductor clusters, nanocrystals, and quantum dots," Science **271**, 933 (1996).
[233]P. Reiss, M. Protiere, and L. Li, "Core/shell semiconductor nanocrystals," Small **5**, 154 (2009).
[234]U. Resch-Genger, M. Grabolle, S. Cavaliere-Jaricot, R. Nitschke, and T. Nann, "Quantum dots versus organic dyes as fluorescent labels," Nat. Methods **5**, 763 (2008).
[235]A. Bednarkiewicz, M. Nyk, M. Samoc, and W. Strek, "Up-conversion FRET from Er^{3+}/Yb^{3+}:$NaYF_4$ nanophosphor to CdSe quantum dots," J. Phys. Chem. C **114**, 17535 (2010).
[236]R. Marin, L. Labrador-Paéz, A. Skripka, P. Haro-González, A. Benayas, P. Canton, D. Jaque, and F. Vetrone, "Upconverting nanoparticle to quantum dot Forster resonance energy transfer: Increasing the efficiency through donor design," ACS Photonics **5**, 2261 (2018).
[237]Z. Yuan, L. Zhang, S. Li, W. Zhang, M. Lu, Y. Pan, X. Xie, L. Huang, and W. Huang, "Paving metal-organic frameworks with upconversion nanoparticles via self-assembly," J. Am. Chem. Soc. **140**, 15507 (2018).
[238]J. R. Du, T. Jia, J. H. Zhang, and G. Y. Chen, "Heterostructures combining upconversion nanoparticles and metal-organic framework: Fundamental, classification, and theranostic applications," Adv. Opt. Mater. **11**, 2202122 (2023).
[239]Q. Liu, B. Wu, M. Li, Y. Huang, and L. Li, "Heterostructures made of upconversion nanoparticles and metal–organic frameworks for biomedical applications," Adv. Sci. **9**, 2103911 (2022).
[240]Y. Li, J. Liu, Z. Wang, J. Jin, Y. Liu, C. Chen, and Z. Tang, "Optimizing energy transfer in nanostructures enables in vivo cancer lesion tracking via near-infrared excited hypoxia imaging," Adv. Mater. **32**, e1907718 (2020).
[241]Z. Yu, W. K. Chan, Y. Zhang, and T. T. Y. Tan, "Near-infrared-II activated inorganic photothermal nanomedicines," Biomaterials **269**, 120459 (2021).
[242]X. Chen, W. Xu, H. Song, C. Chen, H. Xia, Y. Zhu, D. Zhou, S. Cui, Q. Dai, and J. Zhang, "Highly efficient $LiYF_4$:Yb^{3+}, Er^{3+} upconversion single crystal under solar cell spectrum excitation and photovoltaic application," ACS Appl. Mater. Interfaces **8**, 9071 (2016).
[243]M. Que, W. Que, X. Yin, P. Chen, Y. Yang, J. Hu, B. Yu, and Y. Du, "Enhanced conversion efficiency in perovskite solar cells by effectively utilizing near infrared light," Nanoscale **8**, 14432 (2016).
[244]W. Wang, J. Zhang, K. Lin, J. Wang, X. Zhang, B. Hu, Y. Dong, D. Xia, and Y. Yang, "Lanthanide 3D supramolecular framework boosts stable perovskite solar cells with high UV utilization," Adv. Mater. **35**, e2306140 (2023).
[245]Y. Zhan, P. Yu, X. Wang, Y. Xie, H. Zhang, and F. Zhang, "Activatable NIR-II lanthanides-polymetallic oxomolybdate hybrid nanosensors for monitoring chemotherapy induced enteritis," Adv. Funct. Mater. **33**, 2301683 (2023).

[246]Y. Liang, R. An, P. Du, P. Lei, and H. Zhang, "NIR-activated upconversion nanoparticles/hydrogen-bonded organic framework nanocomposites for NIR-II imaging-guided cancer therapy," Nano Today **48**, 101751 (2023).
[247]Z. Zhang, M. K. G. Jayakumar, X. Zheng, S. Shikha, Y. Zhang, A. Bansal, D. J. J. Poon, P. L. Chu, E. L. L. Yeo, M. L. K. Chua, S. K. Chee, and Y. Zhang, "Upconversion superballs for programmable photoactivation of therapeutics," Nat. Commun. **10**, 4586 (2019).
[248]L. Yan, Y. N. Chang, W. Yin, X. Liu, D. Xiao, G. Xing, L. Zhao, Z. Gu, and Y. Zhao, "Biocompatible and flexible graphene oxide/upconversion nanoparticle hybrid film for optical pH sensing," Phys. Chem. Chem. Phys. **16**, 1576 (2014).
[249]S. Xu, S. Xu, Y. Zhu, W. Xu, P. Zhou, C. Zhou, B. Dong, and H. Song, "A novel upconversion, fluorescence resonance energy transfer biosensor (FRET) for sensitive detection of lead ions in human serum," Nanoscale **6**, 12573 (2014).
[250]T. Hao, X. Wu, L. Xu, L. Liu, W. Ma, H. Kuang, and C. Xu, "Ultrasensitive detection of prostate-specific antigen and thrombin based on gold-upconversion nanoparticle assembled pyramids," Small **13**, 1603944 (2017).
[251]J. Yuan, Y. Cen, X. J. Kong, S. Wu, C. L. Liu, R. Q. Yu, and X. Chu, "MnO_2-nanosheet-modified upconversion nanosystem for sensitive turn-on fluorescence detection of H_2O_2 and glucose in blood," ACS Appl. Mater. Interfaces **7**, 10548 (2015).